U.S.NRC
United States Nuclear Regulatory Commission
Protecting People and the Environment

NUREG/CR-7222

Tsunami Hazard Assessment Based on Wave Generation, Propagation, and Inundation Modeling for the U.S. East Coast

Office of Nuclear Regulatory Research

AVAILABILITY OF REFERENCE MATERIALS IN NRC PUBLICATIONS

NRC Reference Material

As of November 1999, you may electronically access NUREG-series publications and other NRC records at NRC's Library at www.nrc.gov/reading-rm.html. Publicly released records include, to name a few, NUREG-series publications; *Federal Register* notices; applicant, licensee, and vendor documents and correspondence; NRC correspondence and internal memoranda; bulletins and information notices; inspection and investigative reports; licensee event reports; and Commission papers and their attachments.

NRC publications in the NUREG series, NRC regulations, and Title 10, "Energy," in the *Code of Federal Regulations* may also be purchased from one of these two sources.

1. **The Superintendent of Documents**
   U.S. Government Publishing Office
   Mail Stop IDCC
   Washington, DC 20402-0001
   Internet: bookstore.gpo.gov
   Telephone: (202) 512-1800
   Fax: (202) 512-2104

2. **The National Technical Information Service**
   5301 Shawnee Rd., Alexandria, VA 22312-0002
   www.ntis.gov
   1-800-553-6847 or, locally, (703) 605-6000

A single copy of each NRC draft report for comment is available free, to the extent of supply, upon written request as follows:

Address: **U.S. Nuclear Regulatory Commission**
Office of Administration
Publications Branch
Washington, DC 20555-0001
E-mail: distribution.resource@nrc.gov
Facsimile: (301) 415-2289

Some publications in the NUREG series that are posted at NRC's Web site address www.nrc.gov/reading-rm/doc-collections/nuregs are updated periodically and may differ from the last printed version. Although references to material found on a Web site bear the date the material was accessed, the material available on the date cited may subsequently be removed from the site.

Non-NRC Reference Material

Documents available from public and special technical libraries include all open literature items, such as books, journal articles, transactions, *Federal Register* notices, Federal and State legislation, and congressional reports. Such documents as theses, dissertations, foreign reports and translations, and non-NRC conference proceedings may be purchased from their sponsoring organization.

Copies of industry codes and standards used in a substantive manner in the NRC regulatory process are maintained at—

The NRC Technical Library
Two White Flint North
11545 Rockville Pike
Rockville, MD 20852-2738

These standards are available in the library for reference use by the public. Codes and standards are usually copyrighted and may be purchased from the originating organization or, if they are American National Standards, from—

American National Standards Institute
11 West 42nd Street
New York, NY 10036-8002
www.ansi.org
(212) 642-4900

Legally binding regulatory requirements are stated only in laws; NRC regulations; licenses, including technical specifications; or orders, not in NUREG-series publications. The views expressed in contractorprepared publications in this series are not necessarily those of the NRC.

The NUREG series comprises (1) technical and administrative reports and books prepared by the staff (NUREG–XXXX) or agency contractors (NUREG/CR–XXXX), (2) proceedings of conferences (NUREG/CP–XXXX), (3) reports resulting from international agreements (NUREG/IA–XXXX), (4) brochures (NUREG/BR–XXXX), and (5) compilations of legal decisions and orders of the Commission and Atomic and Safety Licensing Boards and of Directors' decisions under Section 2.206 of NRC's regulations (NUREG–0750).

U.S.NRC
United States Nuclear Regulatory Commission
Protecting People and the Environment

NUREG/CR-7222

Tsunami Hazard Assessment Based on Wave Generation, Propagation, and Inundation Modeling for the U.S. East Coast

Manuscript Completed: April 2016
Date Published: July 2016

Prepared by: Vasily Titov, Christopher W. Moore,
Mick Spillane, Yong Wei, Edison Gica, and Hongqiang Zhou

Pacific Marine Environmental Laboratory
Office of Oceanic and Atmospheric Research
National Oceanic and Atmospheric Administration
7600 Sand Point Way, N.E., Seattle, WA

Rasool Anooshehpoor, NRC Project Manager

NRC Job Code Number N6401

Office of Nuclear Regulatory Research

ABSTRACT

This report describes a comprehensive study of tsunami hazard assessment for the Atlantic coast of the United States (U.S.) based on potential tsunami scenarios.

The study makes use of the Pacific Marine Environmental Laboratory (PMEL) pre-computed database of over a thousand synthetic tsunami sources to identify potentially hazardous tsunami events for the eastern U.S. coastline, in particular the area of Virginia Beach, Virginia. The historical Lisbon 1755 tsunami event is used to validate the simulations by comparing the computed results with the evidence of tsunami impact along the Caribbean arc.

As a result of this investigation, a segment of the Caribbean seismic arc located north of Puerto Rico between the U.S. Virgin Islands and Hispaniola and known as the Puerto Rico Trench, is identified as the most hazardous tsunami source for the U.S. eastern coastline. For potential seismic events of magnitudes between M_{w} 8.6 and M_{w} 8.9 the modeled run-up heights are between 3.5 and 5 m in Virginia Beach. In addition to the seismically generated tsunami hazard, the impact of potential tsunamis generated by the possible future collapse of the flank of the Cumbre Vieja volcano in La Palma (Canary Islands), and by the Currituck landslide on the Atlantic continental shelf of the U.S. are also investigated. For the landslide events, the Eulerian-Lagrangian hydrocode, iSALE is used to compute the generated landslide and the solution is coupled to three different tsunami simulation models. Special attention is paid to wave dispersion effects by comparing results from these three different simulations using the shallow water wave equations, the weakly non-linear Boussinesq equations, and the strongly-nonlinear Boussinesq equations. The Method of Splitting Tsunamis (MOST) code is used to compute the non-dispersive shallow water wave solution with numerical dispersion adjusted to match that prescribed by linear theory in deep water.

The results of this study show that dispersive effects tend to be weak when the tsunami propagates over shallow areas of the continental shelf, with good agreement between simulations computed with MOST and with the dispersive Boussinesq-type models.

FOREWORD

Subsequent to the 2004 and 2005 series of tsunamis in southeastern Asia, the U. S. Nuclear Regulatory Commission (NRC) conducted an in-depth review of past tsunami evaluations and guidelines for the Atlantic and Gulf coast nuclear power plants (NPPs). Although the NRC staff concluded that these coastal NPPs are adequately protected, the 2004 Indian Ocean tsunami raised the level of concern for an extreme tsunami-initiated event, which could potentially exceed the dimensions of all of the recorded events taken into consideration in the design basis for those NPPs. NRC's previous tsunami design guidelines for these coastal facilities considered historical tsunami records but did not explicitly characterize design-basis tsunamigenic sources including earthquakes, submarine landslides, and other potential sources for the Atlantic and Gulf coasts.

Consequently, NRC sponsored a series of research projects at the National Oceanic and Atmospheric Administration (NOAA) and the U.S. Geologic Survey (USGS) to further the staff's understanding of tsunamis and their potential sources so that quantitative tsunami wave criteria can be available to assess the tsunami hazards for any prospective Atlantic and Gulf coast NPP site.

This NUREG/CR describes a comprehensive study of tsunami hazard assessment for the Atlantic coast of the U.S. based on potential tsunami scenarios. The study makes use of the Pacific Marine Environmental Laboratory's (PMEL) pre-computed database of over a thousand synthetic tsunami sources to identify potentially hazardous tsunami events for the eastern U.S. coastline. The historical Lisbon 1755 tsunami event is used to validate the simulations by comparing the computed results with the evidence of tsunami impact along the Caribbean arc.

This report and the results from related tsunami projects should provide the NRC staff with the means and criteria to assess evaluations and analyses provided by the licensees on their tsunami design for nuclear facilities. This information will permit the NRC staff to: (1) confirm that adequate levels of safety are maintained; (2) improve the effectiveness and efficiency of the review processes; and (3) support the staff's technical decisions in a reasonably conservative and realistic manner and, thereby, increase public confidence in the staff's actions.

TABLE OF CONTENTS

LIST OF FIGURES

LIST OF TABLES

EXECUTIVE SUMMARY

This NUREG/CR provides modeling results from the impact of severe tsunami events on the U.S. eastern seaboard based on potential seismic and landslide sources. This report consists of five chapters. Chapter 1 is the introduction. Chapter 2 identifies potential seismic tsunami sources in the Atlantic that could affect the U. S. East Coast. Chapter 3 uses propagation and inundation numerical techniques to model tsunami hazards from the 1755 Lisbon Earthquake, and from potential earthquakes in the Caribbean Sea and South Sandwich Islands. Chapter 4 investigates the effects on the U. S. Atlantic coast of a tsunami generated by the hypothetical collapse of the Cumbre Vieja volcano on Isla La Palma in the Canary Islands. Chapter 5 simulates the tsunamis generated by potential landslides on the continental slope and their effect on the U. S. eastern coast.

Seafloor deformations during earthquakes account for the majority of tsunamis worldwide. Since the damaging tsunamis are generally associated with large seismic events ($M_w > 7.5$) on faults that are at least 100 km in length, the likely seismic source regions in this study are divided into rectangular sub-faults, 50 km wide and 100 km long. Each sub-fault has a slip of one meter with a purely reverse faulting mechanism for maximum vertical seafloor deformation. Thus, assuming a crustal rigidity of 4.0×10^{11} dyne/cm^2, an earthquake associated with a unit sub-fault will have a moment magnitude of 7.5. Larger tsunamigenic earthquakes are then constructed from a linear combination of sub-faults that are properly scaled. The database at the National Oceanic and Atmospheric Administration (NOAA) Center for Tsunami Research (NCTR) has pre-computed tsunami-propagation solutions to unit sub-faults in many known subduction zones, including the Caribbean and South Sandwich Islands. It also has a series of source scenarios for the eastern Atlantic Ocean, designed to represent possible source mechanisms for the 1755 Lisbon Earthquake.

In the Caribbean, the greatest potential threat for seismically generated tsunamis is associated with the subducting plate boundary on the ocean side of the island arc of the Greater and Lesser Antilles, between Hispaniola in the north and Trinidad in the south. Another stretch of subducting boundary lies in the vicinity of Panama. Numerous other fault lines, north of Venezuela, in the vicinity of the Cayman Islands, and south of Puerto Rico pose further potential hazards. In contrast, the threat posed by East Atlantic sources is not well understood. The 1755 Lisbon earthquake and the associated tsunami have been documented on several Caribbean islands, but there are no reports from the sparsely populated U.S. mainland at the time. In the absence of extended and clearly delineated subduction zones in the eastern Atlantic, this study relies on several potential sources posited in the literature on the 1755 event, and on collaborative works with the U. S. Geologic Survey (USGS) and in Portugal.

This study also investigates the possible effect on the U.S. Atlantic coast of a tsunami generated by the hypothetical collapse of the Cumbre Vieja volcano located on the Isla La Palma in the Canary Islands. This research aims to help the NRC evaluate tsunami hazards for nuclear power plants, and to significantly add to the current state of science with respect to East Coast and Gulf of Mexico tsunami hazard assessment. The development and testing of the new landslide hydrocode within the NOAA modeling approach will allow the application of this well-benchmarked numerical technique to both evaluate the possible impact of a Canary Islands' eruption on the coastal United States, and to use field data to investigate landslide locations at the continental slope.

The inundation locations in this report, Myrtle Beach, Daytona Beach, and Virginia Beach, were chosen because they are near the latitude of La Palma or because of their proximity to Currituck, one of the largest landslides along the North American Atlantic offshore margin. These locations show little inundation due to wave amplitude attenuation over the shelf. However, other U.S. East Coast locations might show a much higher level of impact because the shelf is significantly narrower in other regions, particularly at Cape Hatteras, as it tends to lie in the path of high-amplitude waves from La Palma and Currituck, and because the shelf is at its narrowest at this location.

For the La Palma simulation, wave amplitudes at Myrtle Beach of less than 1 m were not as high as the 1 to 2 m height at Daytona Beach because of the directionality of the propagating wave, and possibly due to blocking by Bermuda Island. The incoming waves are short, less than 1 km, and steep, with amplitudes off-shelf of almost 2 m, rising to a peak amplitude of about 2 m off Myrtle Beach and about 4 m off Daytona Beach, at the location of the shelf break. However, these amplitudes drop quickly as the waves cross the shelf.

The results of this study show that the East Atlantic earthquake sources result in minor tsunami impact at the U.S. East Coast, with a maximum wave amplitude of 1.5 m at Virginia Beach. However, tsunami threat from Caribbean earthquakes may be high at many locations along the U.S. Atlantic coast, with wave heights approaching 4.6 m for a M_w 8.8 event. Coastal impact from these sources exhibits considerable focusing and defocusing associated with the fine spatial structure of the continental shelf in the North, and with the more gradual continental slope in the South. Enhanced (or decreased) inshore impact is not overly sensitive to source location, so sites like Cape Fear stand out as a high-impact site for all scenarios. Unlike the distribution of observed run-up in the historical tsunami catalog, in which several states along the East Coast do not appear, the threat to all states on the eastern seaboard is significant for the large rare event scenarios investigated.

ACKNOWLEDGMENTS

The research described in this NUREG/CR was sponsored by the United States Nuclear Regulatory Commission (U.S. NRC), Office of Regulatory Research. Annie Kammerer and Rasool Anooshehpoor provided guidance during this project and during preparation of this NUREG/CR. The authors acknowledge the work of researchers of the NOAA Pacific Marine Environmental Laboratory (PMEL) that was used for this report (PMEL Contribution number 4424). This research was partially funded by the Joint Institute for the Study of the Atmosphere and Ocean (JISAO) under NOAA Cooperative Agreement NA10OAR4320148 (2010-2015) and NA15OAR4320063 (2015-2020), JISAO Contribution No. 2500. The authors also acknowledge the NRC technical review team that provided invaluable comments and suggestions for improvement of the report presentation. In particular, we would like to thank Henry Jones, with the NRO, Yong Li with the NRR, Tianqing Cao with the NMSS, and Nathan Siu with the RES.

ABBREVIATIONS AND ACRONYMNS

ALE	Arbitrary Lagrangian-Eulerian
BPR	Bottom Pressure Recorders
FB	Fully nonlinear Boussinesq
GB	Geological Boussinesq
ComMIT	Community Model Interface for Tsunami
DEM	Digital Elevation Model
ETOPO1	Earth Topography (1 arc-minute digital dataset)
FEMA	Federal Emergency Management Agency
GPS	Global Positioning System
iSALE	Impact Simplified Arbitrary Lagrangian-Eulerian
MHW	Mean High Water
MOST	Method of Splitting Tsunamis
NCTR	NOAA Center for Tsunami Research
NGDC	National Geophysical Data Center
NOAA	National Oceanic and Atmospheric Administration
NMSS	Office of Nuclear Material Safety and Safeguards
NRC	Nuclear Regulatory Commission
NRR	Office of Nuclear Reactor Regulation
NRO	Office of New Reactors
PMEL	Pacific Marine Environmental Laboratory
RES	Office of Nuclear Regulatory Research
SIFT	Short-term Inundation Forecast Tool
SIM	Standby Inundation Model
TWC	Tsunami Warning Centers
USGS	United States Geological Survey

1. INTRODUCTION

Tsunami, named for a Japanese word meaning “harbor wave”, is the term used for a class of waves impacting coastal communities. These generally originate in response to vertical movement of the seafloor caused by an earthquake or by the displacement of water by landslide, either submarine or sub-aerial. Sea level fluctuations associated with the astronomical tides, or with storm surge due to meteorological events are not included, though the term “meteo-tsunami” is applied to tsunami-like waves that can be generated by the passage of weather fronts. Various terms related to tsunamis are defined in the glossary to this report. While there is some evidence that meteo-tsunamis have occurred off the East Coast of the U.S., their frequency and severity are less than in regions such as the Adriatic Sea and the Balearic Islands and are therefore not considered in this report.

Over the past decade there has been ample evidence of the devastating impact of tsunamis in terms of loss of life and damage to infrastructure. The massive casualties in nations surrounding the Indian Ocean caused by waves generated by the December 26, 2004 earthquake off Sumatra demonstrated the need for early detection, adequate warning systems, and public education; the death toll could have been far less had evacuation to high ground, or to suitable vertical structures, been possible. Infrastructure in place is less amenable to protective measures and, in light of the immediate and long-term impact to Japan resulting from the 2011 Tohoku tsunami, hardening of existing structures and careful design for future construction in the coastal environment must be a strong imperative.

1.1 Tsunami Generation, Detection and Modeling

Both the 2004 and 2011 events mentioned above originated in massive subduction zone earthquakes that raised or lowered extensive areas of the sea floor. Huge volumes of water are displaced during such events, with a correspondingly large amount of energy that spreads outward from the source region as tsunami waves. The waves can impact local coasts (the near-field) or propagate to remote ones (the far-field) across thousands of kilometers of ocean. Most tsunamis are generated in this way and, fortunately, with timely measurement close to the area of generation the spreading wave trains can be accurately modeled. This is the basis of the SIFT (Short-term Inundation Forecasting of Tsunamis) system. SIFT is a tsunami forecast system that integrates tsunami observations in the deep ocean with numerical models to provide an estimate of tsunami wave arrival and amplitude at specific coastal locations while a tsunami propagates across an ocean basin. SIFT was developed at NOAA’s Pacific Marine Environmental Lab (PMEL) and is currently in operational use at Tsunami Warning Centers (TWC) in Hawaii and Alaska. These facilities were established in response to the impact on Hawaii and the Pacific Rim by tsunamis originating off Alaska and Chile in the 1960s. Initially, warnings were promulgated whenever a large submarine earthquake was detected by seismometers. Without validation of the presence of tsunami waves, and prediction of their complex energy patterns, reliance on seismic information alone carries the risk of unnecessary evacuation and the associated expense and loss of public confidence that would entail.

Forecasting was greatly improved by the development of instruments to accurately detect and measure tsunamis in deep water and numerical methods to model their dynamics. A global array of tsunameters, bottom pressure recorders (BPR) that telemeter their observations via satellite in near-real time, are triggered automatically by waves having the tsunami “signature” or by TWC operators. In the case of seismically-generated tsunamis, the SIFT system uses statistical methods to compute which linear combination of pre-computed scenarios best matches the observations. Predictions, based on the composite propagation solution, identify

areas at risk or, quite often, permit cancellation of the early warnings. For those threatened communities where more highly-resolved inundation forecast models are available, the propagation solution provides the input and these fast-running models can often provide several hours of warning to inform the far-field emergency response. For coastal communities in the near-field the earliest waves may arrive in advance of the most accurate model predictions but the several-hour duration of a severe tsunami event, for which the leading wave may not be the most damaging, gives value to a credible though somewhat delayed "forecast".

Occasionally a tsunami detector is triggered when there is no evidence of a causative seismic event. This might be the case where a submarine landslide has occurred or, perhaps, a meteo-tsunami. Such a triggering is currently a reason for an "alert" as the modeling of such events is an area of ongoing research and is not yet integrated into the SIFT forecast system. Among the difficulties are those of identifying in near-real time the extent and speeds of movement of the debris in a landslide, and the more complex and time-consuming computations required to model an event, even were these parameters well known. Compared to the Pacific Ocean, in the Atlantic context, the rarity of major seismically generated tsunamis, as evidenced by the 1929 Grand Banks landslide that severely impacted Newfoundland, and in the Gulf of Mexico, adds weight to the landslide issue. In this report some case studies are described as examples of near-field events: the observed Lituya Bay event in Alaska permits model validation, and the prehistoric Currituck submarine landslide, offshore of North Carolina, whose volume can be estimated from seafloor profiling. A far-field landslide scenario that has gained attention is the possible flank collapse of La Palma, an island of the Canaries off northwest Africa. Unlike tsunamis caused by large subduction zone earthquakes, which have such long wavelengths, compared to even deep ocean depths, so as to behave as easily-modeled shallow-water waves during their trans-oceanic propagation phase, the massive waves likely to be generated in a flank collapse would have much shorter length scales. Energy at different scales is said to disperse, different wave components travelling at different speeds, so that their far-field impact may be much less even when the waves regrow on encountering shoaling topography. Rather than a single 3-D model that would include the dynamics of the landslide debris, its coupling to the water column, dispersive trans-ocean propagation, then inundation of the U.S. coastline, this report effectively substitutes a model of the landslide generation phase for the seismic generation of standard tsunami modeling, then employs the propagation and inundation methodologies of the latter to estimate far-field coastal impact. Further efforts in landslide modeling are the subject of a future report to the NRC.

1.1.1 The Scope of this Report

The SIFT forecast methodology, described earlier, is a well-proven operational tool for predicting localized impacts at sites for which inundation forecast models are available. At the time of writing 75 such models exist including 14 for the eastern U.S. mainland from Bar Harbor, Maine, to Key West, Florida (Figure 1.1). Several others represent communities in Puerto Rico and the Virgin Islands. Site selection was not based on the presence of nuclear power plants nor other specific infrastructure but, rather, by the availability of coastal tide gauges. Accurate prediction of inundation is achieved with a set of nested grids of increasingly fine resolution that capture the passage of tsunami waves from the deep water, where horizontal grids spaced at about 20 km are adequate, to the scales of a few tens of meters relevant to coastal impact. Fine-scale bathymetry, needed to develop the inundation models, is compiled as a Digital Elevation Model (DEM) by the National Geophysical Data Center (NGDC). Each inundation model requires several months of effort in design and testing. A reference version of the model (RM) employs finely resolved bathymetry necessitating short time steps in the numerical solution. Several hours of computing time may be needed to model a tsunami event or simulation. A forecast version (FM) of the site, with somewhat coarser grids and longer time

steps, is designed for operational use. During the design phase the model predictions are compared to verify that the FM reproduces the salient features of the RM but executes within the time constraints appropriate to an actual emergency. The stability of both models, for a broad range of potential events is established and, where possible, the FM is validated by comparing its predictions with historical observations.

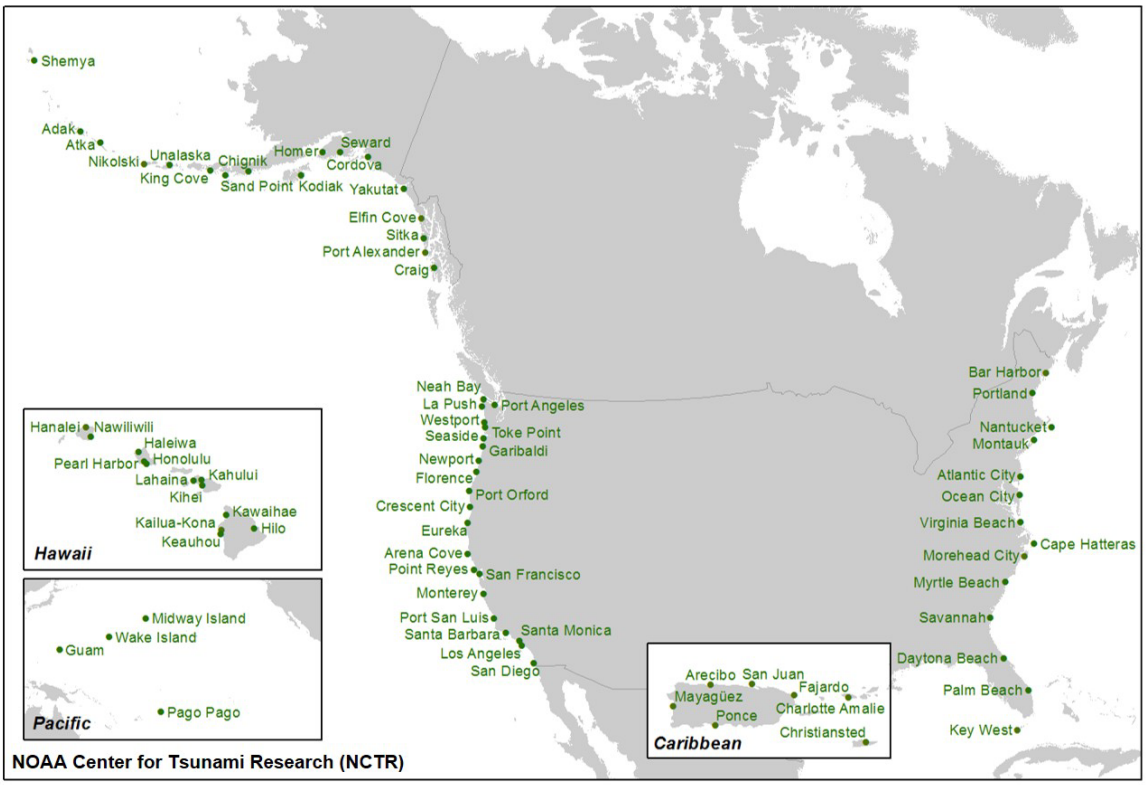

Figure 1.1: Locations of forecast inundation models (NCTR, 2012).

Given the short history, in geological terms, of historical observation, numerical simulation, based on such models, permits evaluation of the potential impact to a site from hypothetical events spanning a wide range of source locations and magnitudes. The complex pattern of tsunami energy propagation within an ocean basin can result in more severe impacts for certain wave directionalities. Likewise, our limited ability to place an upper limit on source magnitude suggests that as broad a range of source scenarios as possible be considered when planning for critical infrastructure.

Within the time constraints of this project, and in the absence of sufficiently fine scale bathymetry for the entire U.S. East and Gulf of Mexico coasts, it is not possible to provide the level of detail needed for an 'a priori' determination of the suitability or otherwise, from a tsunami threat standpoint, for the entire coast. Instead, for this report, the methodologies available for site evaluation are presented.

In Chapter 2, some broad-brush conclusions for tsunamis directly generated by earthquake are presented. These rely on the Propagation Database of source scenarios available as a component of the SIFT operational forecast system. Significant seismic sources lie outside the Gulf of Mexico and constricted access through the Florida and Yucatan Straits limit the impact of tsunamis generated in the Atlantic and Caribbean. Each database scenario is most reliable in deep water and its coarse resolution limits its applicability to the shelf. A more finely resolved

model grid spanning the entire eastern seaboard is constructed and a selection of sources throughout the Atlantic reveal the potential for bathymetric features on the shelf to focus or spread tsunami energy. The results from this model do not extend all the way to the shoreline and have been truncated at the 12 m isobath.

In Chapter 3, by employing some existing forecast models, namely Mayaguez, Ponce, and San Juan, all in Puerto Rico, as well as Virginia Beach, Virginia, we explore the impact at the shoreline and the inundation that might result from selected tsunami scenarios generated by direct seismic action.

Landslides, submarine or subaerial and perhaps triggered by a seismic event, pose an additional tsunami threat to coastal communities and infrastructure. They are discussed in the remainder of the report and some of the numerical methods to model them are illustrated using case studies. Remote landslides, for which U.S. shores are in the far-field, also hold the potential for tsunami impact. Flank collapse of volcanic islands in the eastern Atlantic might generate huge waves locally but modeling the generation and transoceanic propagation of such waves is far more demanding of computer resources than the shallow water wave dynamics appropriate to seismically generated tsunamis.

In Chapter 4 a composite approach is employed, with a generation region based on landslide physics coupled to a shallow water treatment of the transoceanic passage of the waves exiting that region, and a nested model representation of the far-field inundation. The local tsunami impacts that might result from a major flank collapse at La Palma Island is explored by coupling landslide and propagation models with the inundation models developed for the NOAA forecast system.

Chapter 5 looks at the local effects of a major slide along the continental break. In 1929 a submarine landslide caused severe local impact on Newfoundland. Unstable sediments along the Atlantic and Gulf coasts of the U.S. have the potential for future impact. The Currituck Slide, which is believed to have taken place between 24,000 and 50,000 years ago off the Carolinas is used as an exemplar. Though ancient, its scale can be estimated from seabed surveys and volume and mobility analysis give good guidance for initial conditions for this event. Its position relative to the Virginia Beach forecast model is perfectly situated to perform a detailed, well-constrained inundation analysis.

2. REGIONAL (U.S. EAST COAST) TSUNAMI HAZARD

2.1 Introduction

The primary goal of this research is to assist the Nuclear Regulatory Commission (NRC) in assessing the potential for tsunami impact along the U.S. Atlantic coast by identifying potential tsunamigenic sources and providing tools for deterministic assessment of tsunami propagation and costal inundation. In this chapter, the component of the hazard directly caused by submarine earthquakes is addressed. Such events may, by deforming the seafloor over large areas, displace huge volumes of water generating waves that radiate to nearby shores and across entire ocean basins as tsunami waves. The 2004 Sumatra and 2011 Tohoku tsunamis are examples involving such direct seismic forcing. Earthquakes may indirectly generate tsunamis by triggering submarine landslides. An example of this mechanism is the 1929 Newfoundland tsunami. Both modes may operate in concert -- an event off New Guinea in 1992 generated waves that were far in excess of what might be expected based on the magnitude of the accompanying earthquake.

NOAA's tsunami forecast methodology, employed operationally at the TWC, does not explicitly separate the generation modes. Instead, it employs direct measurement of the tsunami waves at one or more sites of an array of bottom pressure sensors. The observations, telemetered in near real time via satellite, are ingested by the SIFT where statistical "inversion" against a database of pre-computed tsunami propagation scenarios identifies the linear combination that best matches the observed wave train(s). The resulting basin-wide composite solution quantifies the threat, and a set of fine-resolution models, designed to run quickly in real time, are invoked to predict the tsunami impact to coastal communities. This information informs the emergency response, in many cases leading to cancellation of what previously might have included unnecessary evacuations. The system has proved its worth on numerous occasions in recent years.

In addition to their role in the SIFT forecast system the pre-computed tsunami scenarios of the propagation database (Gica et al., 2008), and the MOST numerical model it employs, are well-suited to the goals of this chapter. Validated through its success in real-time modeling of actual seismically-generated tsunamis, it can be applied to risk assessment in the Atlantic Ocean where the historical record of tsunami observations is sparse; however, the match to the task in hand is not perfect. Full forecast and risk assessment capability is limited to the 75 communities (14 on the U.S. East Coast) for which detailed local forecast models have been prepared. An illustration of a fully-modeled community – Virginia Beach, Virginia – is provided in Chapter 3.

For a broader view of tsunami impact along the entire U.S. East Coast a higher resolution grid is introduced. While not extending all the way to the shoreline, this grid allows the deep-water scenarios of the propagation database (and other customized sources) to be extended to the near-shore environment. The distribution of maximum tsunami height offshore, and in to the 12-meter depth contour, identifies topographic features in the coastal environment that tend to focus or disperse tsunami energy.

2.2 Seismic Tsunami Sources in the Atlantic

Potential sources of tsunamis, of concern to the eastern seaboard of the United States, have been discussed by ten Brink et al. (2008) in a report to the NRC. Included are three main source areas where direct seismic events may generate large tsunamis. These are, in order of decreasing potential impact, the Puerto Rico Trench, the complex of faults in the Gulf of Cadiz (source of the Lisbon tsunami in 1755), and the South Sandwich subduction zone in the south Atlantic.

In Figure 2.1 the layout of source scenarios (also called "unit sources") of the propagation database is presented for the Caribbean and adjacent north Atlantic. Recognizing that damaging tsunamis are generally associated with large seismic events (M_w > 7.5) on faults that are at least 100 km in length, rectangular sub-faults measuring 100 km long by 50 km wide are selected to cover potential source regions (black rectangles). For each unit source, the Okada (1985) algorithm is used to compute the seafloor deformation that would result from a one-meter slip of the rectangular sub-fault. Realistic earthquake strike, dip, and depth values are employed based on global datasets such as Bird (2003) or Coffin et al. (1998) and guidance from the United States Geological Survey (Kirby et al., 2005). The dynamics of tsunami propagation in the open ocean is linear, permitting the propagation solutions of individual unit sources to be scaled up or down and combined with those of neighboring unit sources to represent larger events. Figure 2.1 illustrates a composite source, C51, north of Puerto Rico, identified as the most hazardous tsunami scenario in the Caribbean for the U.S. East Coast (see Section 3.3.3). The solutions for ten adjacent unit sources, colored gray (centered on the source pair designated "51a" and "51b" in the propagation database) are scaled up to represent a uniformly distributed slip of 10 m. In combination, a synthetic source scenario representing a magnitude M_w 8.8 event results.

The distribution of tsunami energy from the synthetic C51 scenario is shown in Figure 2.1. Color-coded at each location is the maximum wave height in the 24-hour period following the "event." The main "beam" of energy is directed northward, normal to the source line, with wave amplitude initially decaying with distance from the source (due to geometric spreading) before re-growing as the continental rise and slope is encountered. There are side-lobes and significant variation along the shelf edge as the tsunami waves react with the bathymetry.

Waves also penetrate into the Caribbean but are attenuated in the inter-island passes. Conversely, in the North Atlantic and along the eastern seaboard of the U.S., tsunami impact from sources within the Caribbean is reduced. The constricted Yucatan Channel and Florida Strait, and the shallows surrounding the Bahamas, protect the coastlines of the Gulf of Mexico from seismically-generated tsunami impact, even from the closest sources of the Cayman Trench, the Gulf of Honduras (between Cuba and Mexico) and north of Hispaniola. Therefore, further discussion in this chapter is limited to the eastern seaboard from Florida to Maine. Synthetic sources, similar to C51, each comprised of ten unit sources but centered at adjacent columns 47 to 55, are employed as representative of the major tsunami threat to the U.S. eastern seaboard by seismic activity in the western Atlantic.

Another feature of the unit sources of the propagation database, and composite scenarios such as C51 based on them, is evident in Figure 2.1; the predictions do not extend to the shoreline. This is due to the somewhat coarse resolution employed for numerical modeling of tsunami wave propagation in the deep ocean. The resolution is appropriate to their intended use – to produce accurate prediction at the deep-water tsunami detection sites and to provide boundary conditions for more highly resolved models (Section 2.3) of the continental shelf and nearshore environment. Figure 2.1 illustrates the added steps needed to provide accurate estimates of

inundation and tsunami wave height and currents near the coast with Nantucket Island as an example. The inset shows a snapshot of the innermost of a nested set of three model grids.

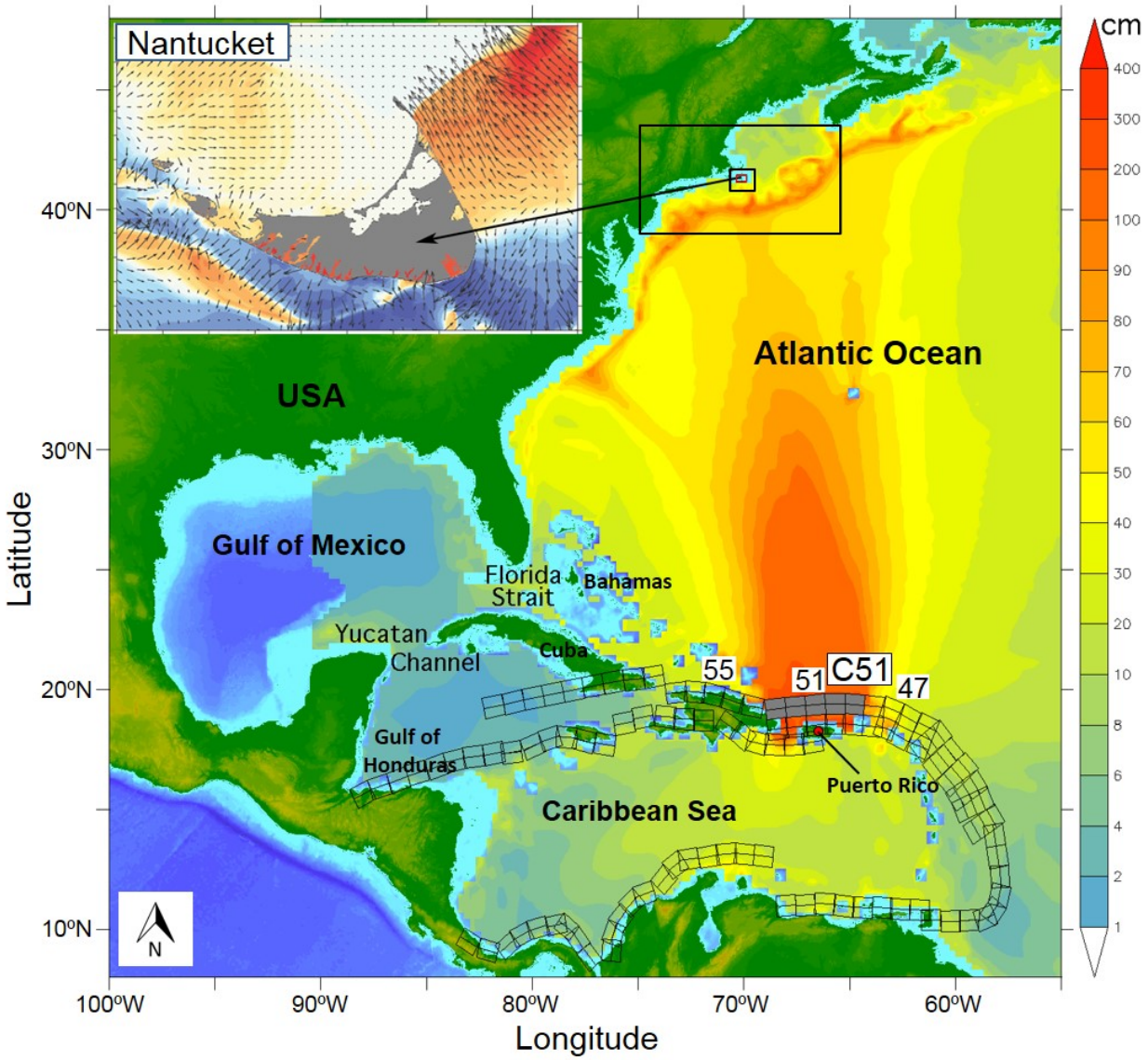

Figure 2.1: A composite synthetic source scenario (C51) for a tsunami originating in the Puerto Rico trench north of Puerto Rico. Based on the linear combination of ten unit sources (gray area centered at unit source number 51) from the propagation data-base, the results apply to the deep ocean but cannot adequately represent waves on the shelf, or coastal inundation. The inset panel illustrates how the solution can be extended to shore with a nested set of models of increasingly fine spatial resolution for Nantucket Island.

Figure 2.2 illustrates source representations for the eastern and southern Atlantic. Unit sources are available for the well-defined South Sandwich subduction zone (lower panels). For the complex fault distribution in the Gulf of Cadiz, south and west of Cape St. Vincent (upper panels), unit sources have not been defined and scenarios based on several proposed sources

of the 1755 Lisbon tsunami are employed. The origin of this event is a matter of ongoing research.

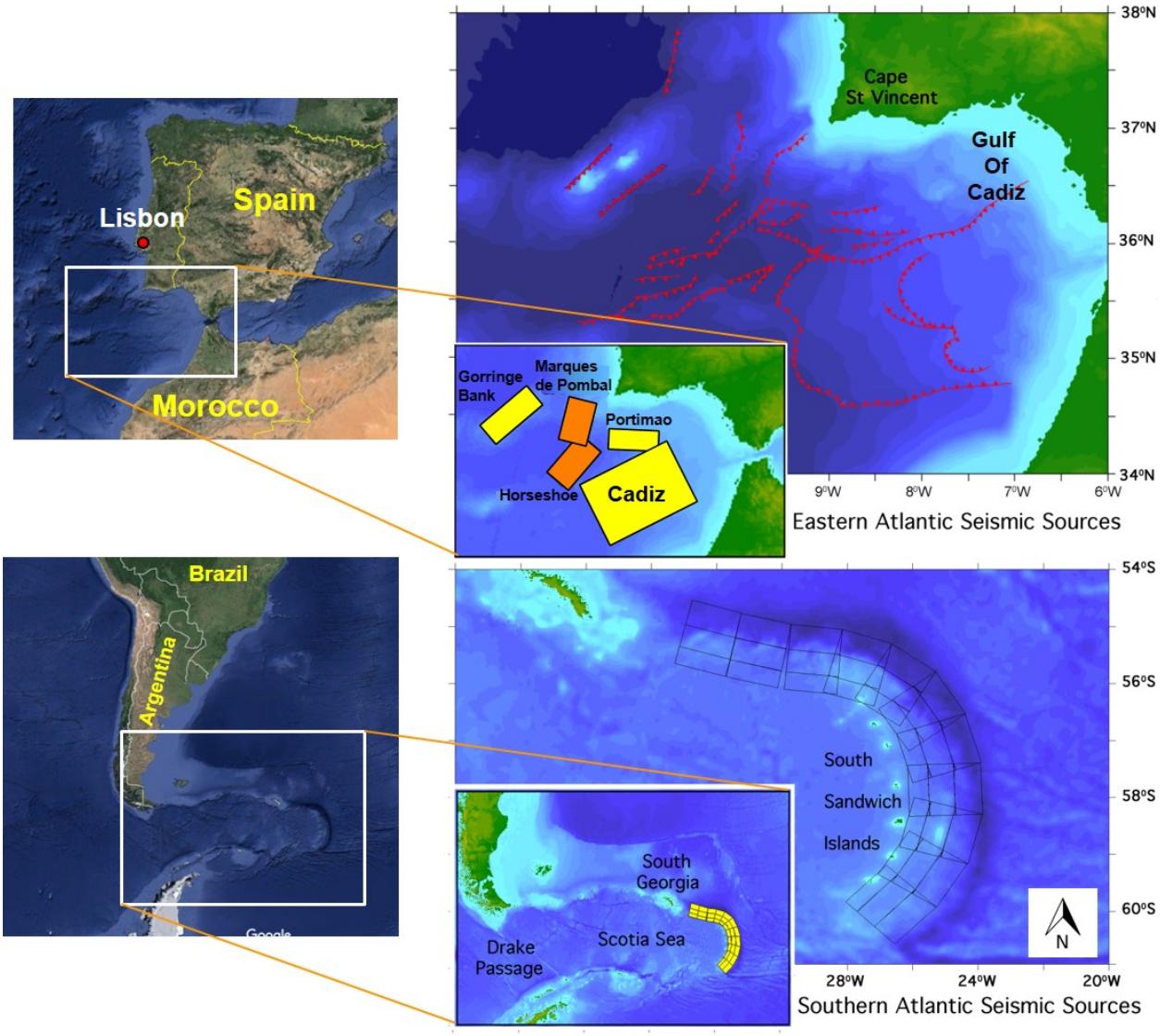

Figure 2.2: Other potential sources of seismically-generated tsunamis in the Atlantic Ocean. Upper panels: the complex distribution of faults in the Gulf of Cadiz and some proposed sources for the 1755 Lisbon tsunami. Lower panels: the well-defined subduction zone near the South Sandwich island arc and its unit source representation in the propagation database.

2.3 Grid Resolution and Model Extent

As noted above, the unit source models of the propagation database (Gica et al., 2008), and basin-wide custom models such as those representing the Lisbon 1755 scenarios, are relatively coarse in spatial resolution. The resolution that the MOST model employs to represent the bathymetry is 4 arc-minutes (approx. 7 km). Although this resolution is adequate for tsunami wave propagation in deep seas, it is too coarse for the steep continental shelf edge. Furthermore, in tsunami simulations using the seismic unit sources, the MOST model settings

employed preclude coastal inundation. As illustrated in Figure 2.1, the coarse resolution is appropriate for usage in the SIFT forecast system for a quick and approximate estimate of coastal inundation. However, when detailed predictions of flooding and inshore tsunami wave height and current at a given community are needed, a set of nested model grids with increasing spatial resolution is needed to accurately represent the bathymetry around that location. An example of nested grids is shown in Figure 2.1 as a series of rectangles converging on the island of Nantucket, with the innermost rectangle shown in the inset panel. The inundation extent at Nantucket is then assessed by additional MOST runs utilizing the propagation solution as input at the boundary of the outermost rectangle.

The design and testing of high-resolution community models is quite demanding of computing resources and thus may not be appropriate to include the entire eastern seaboard. In order to determine the appropriate grid size, tsunami wave height at a specific community – Virginia Beach, Virginia – due to the seismic source C51 is studied here to illustrate the full modeling potential. In this section, a higher resolution regional model is selected to extend the deep-water solution onto the shelf. Figure 2.3 illustrates the tsunami height at Site 1 (Virginia Beach) and Site 2 based on the grid sizes. The left hand panel shows the extent of the regional model finally chosen (Grid C). In the upper right panel, the time series of tsunami-wave height prediction from the propagation solution (4-arcminute resolution, in the absence of high-resolution Grid C) to scenario C51 at "Site 1" is drawn in red. The blue curve is the prediction for the same location when the propagation solution is applied as a boundary condition to the high-resolution (30 arc-second) regional model (Grid C). Clearly, the coarser propagation model underestimates the amplitude and distorts the timing for this on-shelf location.

The full regional model domain shown in Figure 2.3 is quite demanding in computer resources, both in run-time and storage of the results. In order to explore whether the extent of the grid could be reduced without significantly affecting the results, Grid C was replaced with two smaller grids, Grid A and Grid B. The lower right panel of Figure 2.3 shows the time series for "Site 2" in the Gulf of Maine when these sub-regional grids are forced at their boundaries by the C51 scenario from the propagation model grid (4 arc-minute). The differences are substantial and so, to avoid the uncertainties associated with the placement of sub-regional "tiles" for the entire coast, it was decided to employ the full regional "Grid C" despite the demanding computational resources.

The resolution of the regional model bathymetry (Grid C) underlying the results presented in the remainder of this chapter is 30 arc-seconds. With a time step appropriate to the greatest depths of the grid (imposed by the Courant-Friedrichs-Levy condition for model stability) the MOST model accurately represents the progression of waves onto the continental shelf. The resolution is not adequate to represent a complex shoreline of headlands and inlets. The results presented in Section 2.4.3 are extracted at the 12-meter depth contour. Green's Law[1] (e.g., Jay, 1991; Synolakis, 1991) is used in some situations to extrapolate nearshore estimates to the shoreline, for example a water depth of 1 m. Its use relies on questionable assumptions that do not fully take into account nearshore bathymetry, Green's Law scaling (simply applying a factor 1.86 in our case) would add no new information and is not applied to our results.

[1] Green's law is a classic linear theory that describes the increase in the tsunami height as it approaches the shallow coastal waters.

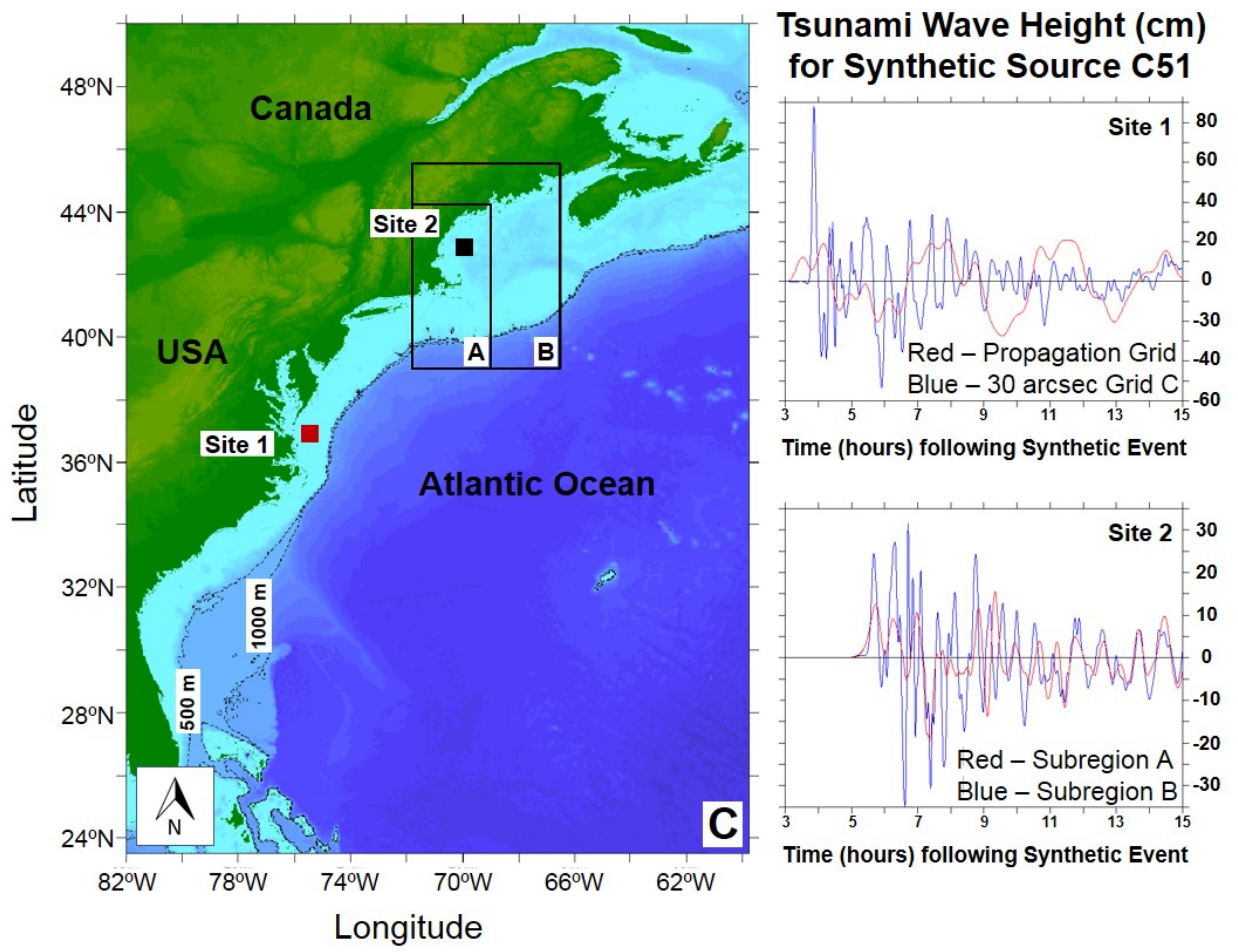

Figure 2.3: **The 30 arc-second regional bathymetry (Grid C) chosen to represent tsunami impact on the U.S. East Coast. The 500 m and 1000 m depth contours are drawn to highlight the variability in shelf width and profile. Tiling with sub-regional grids (such as A or B) was considered as an alternative to the single regional grid but that option was rejected. The right hand panels model time series for the C51 scenario are drawn for two continental shelf locations to emphasize the need for a high resolution grid spanning the entire region. At Site 1 the propagation database model solution (red) underestimates the amplitude and distorts the timing of the shelf response. At Site 2 the predicted response is sensitive to the extent of shelf included in the sub-regional grid.**

2.4 Results from the Source Scenarios

We now proceed to present the results from the source scenarios – eight in the western Atlantic representing the Puerto Rico Trench between the Virgin Islands and Hispaniola, and four for the eastern Atlantic chosen from proposed sources for the 1755 Lisbon tsunami. Scenarios representative of the southern Atlantic are not included. Their remoteness renders their likely impact on the U.S. East Coast to a level comparable to sources interior to the Caribbean, or external sources whose main beam is directed to the east. The western Atlantic sources each model a magnitude 8.8 event with evenly distributed slip over a 500 by 100 km fault plane as shown on Figure 2.1. The eastern Atlantic sources have varying geometries as detailed in Section 2.4.2.

2.4.1 Western Atlantic Scenarios

Each scenario, simulated using the MOST numerical model, results in a time history of tsunami wave amplitude (plus depth-averaged zonal and meridional speeds) in each grid cell. To summarize the impact of a tsunami, one convenient representation is the maximum wave amplitude plot, a color-coded chart of the largest amplitude encountered at each point during the simulated event. In Figure 2.4 and Figure 2.5, the maximum amplitude plots are drawn for each of the eight Caribbean scenarios. Because the response of the shelf varies markedly between scenarios, the results are normalized and drawn with a common color scale to facilitate the identification of common features. To indicate the level of severity of each scenario, the overall maximum for each case is noted in the upper left corner of each panel together with an identifier based on the center elements in the propagation database.

Comparing the panels of Figure 2.4 and Figure 2.5, the overall maximum amplitude occurs for scenario C49, the most eastern scenario considered. The computed offshore maximum occurs, however, mainly along Nova Scotia and the Grand Banks. With the exception of prominent headlands, such as Cape Fear, which frequently displays enhanced amplitudes, the U.S. mainland experiences lower impacts. As the center of the source region moves westward U.S. the normalized impact becomes more concentrated in the U.S. coastal waters, though at a lower absolute amplitude. Certain recurrent features become more evident with prominent capes experiencing greater impact due to focusing, and points inshore of submarine canyons, most notably Hudson Canyon, benefiting from defocusing of the tsunami waves. Points such as the New Jersey shore and Long Island, however, receive some of the defocused energy resulting in greater impact than might otherwise be expected.

2.4.2 Eastern Atlantic Scenarios

Although the region near Cape St. Vincent and the Gulf of Cadiz has been the source of tsunamigenic earthquakes over the past few centuries, there is little evidence of any tsunami impact on the U.S. mainland. The major event of 1755, which produced a devastating tsunami in Lisbon and was detected at several Caribbean islands, Ireland, and England, was not reported at any of the colonial settlements of the present-day U.S. mainland. Since the exact location of this event is not well known, the pattern of detection and non-detection has been used to discriminate between candidate sources in studies of this major event. Despite the lack of historic record of tsunami hazard on the U.S. East Coast from earthquake sources in eastern Atlantic, the seismicity of the area near the Strait of Gibraltar makes it desirable to evaluate the tsunami hazard associated with a large, rare seismic event in that region. Although there have been several studies (ten Brink et al., 2008), debate is ongoing as to the source mechanism of

the 1755 Lisbon earthquake. To provide a range of scenarios for potential future impacts to the U.S. East Coast from the eastern Atlantic, four seismic sources that have been proposed in Baptista and Matias (2007) are employed here. These are the Cadiz Wedge (139 km by 200 km, M_w 8.6), Gorringe Bank (120 km by 60 km, M_w 8.1), Portimao Bank (102 km by 50 km, M_w 8.0), and a composite Horseshoe/Marques de Pombal source (combined area 13,580 km^2, Mw 8.4), as illustrated in Figure 2.2.

Solutions for these four source configurations show similar patterns of focusing and spreading. Among the four, the most serious impact on the U.S. comes from the Cadiz source and its maximum amplitude pattern is shown in Figure 2.6. (In Section 3.2.3, a fifth potential source for the 1755 event, considered by Baptista (2003), poses even more serious tsunami hazard on the U.S. East Coast and the Caribbean region than the Cadiz source.) Despite being about a factor of two thirds weaker than the least of the Caribbean scenarios reported earlier, the pattern has certain similarities with those seen in Figure 2.4 and Figure 2.5. Major headlands, such as Cape Cod, Cape Hatteras, and Cape Fear, receive enhanced impact as do stretches of coast adjacent to defocusing features like the Hudson Canyon. Stretches of the Florida coast have significant impacts, partly as the result of focusing features on the more gradually shelving continental break. The southern tip of Florida receives major shielding from the Bahamas, both for the eastern Atlantic and Caribbean sources. The location of Daytona, Florida, is indicated in Figure 2.6 as this area is highlighted in a subsequent graphic.

2.4.3 The Inshore Impact

Images such as those in Figure 2.4, Figure 2.5 and Figure 2.6, while identifying common features in the continental shelf response to remote forcing, do not easily provide quantitative values for use in risk assessment near the shoreline. For this purpose, a closely spaced set of inshore points that approximate the 12 m isobath and have a nominal spacing of 5 km, was selected for sub-sampling of the model output. The time series at these points are used to extract useful statistics on the inshore response, that is, the amplitude and timing of the first and largest peak and trough impacting the shore. Such results can be conveniently represented in various forms. In Figure 2.7, the maximum wave amplitude along the 12 m isobath for the C51 scenario is presented as a color-coded strip alongshore, which conveniently retains the geographic context even without the annotations. The details of the strip are, however, difficult to read except in high-quality graphics. Alternatively, Figure 2.8 illustrates the same information but in more detail as a plot of alongshore distance versus wave amplitude. This plot captures the fine structure of the coastal response but requires annotation in order to associate the prominent features with specific geographic features or communities. Results from a similar study carried out by ten Brink et al. (2008) were in general agreement with those of the current study. Although their model used a rough approximation for tsunami run-up assumed to be 3 times that of the tsunami amplitude at 250 m isobaths based on Green's Law, the results were consistent with those of the current study. That is, the greatest tsunami hazards along the U.S. East Coast are associated with the seismic sources along the subduction zone north of Puerto Rico.

To provide a sense of common features in the inshore response over the set of scenarios investigated, a third form of presentation can be effective. In Figure 2.9, the normalized alongshore structure of all 12 scenarios are combined. Alternating pink highlights for the annotations allow groupings by state and province to be emphasized. In addition to the common features mentioned earlier, Figure 2.9 illustrates that the response to eastern Atlantic sources is greatest along the north Florida coast. In 1755, this region was apparently less populated than the regions further north and south. The Spanish colony of St. Augustine was in

its latter days as a fortification, so the lack of tsunami wave reports may be reasonable, Virginia Key, also populated at the time, was protected by the Bahamas. Today's vast increase in coastal population and infrastructure, including barrier islands, would be significantly more vulnerable to tsunamis originating in the east Atlantic. Figure 2.10 illustrates this point using the Cadiz Wedge scenario for the 1755 event. This generates waves of almost one meter on the central Florida coast, but much lower for the Carolinas and New England.

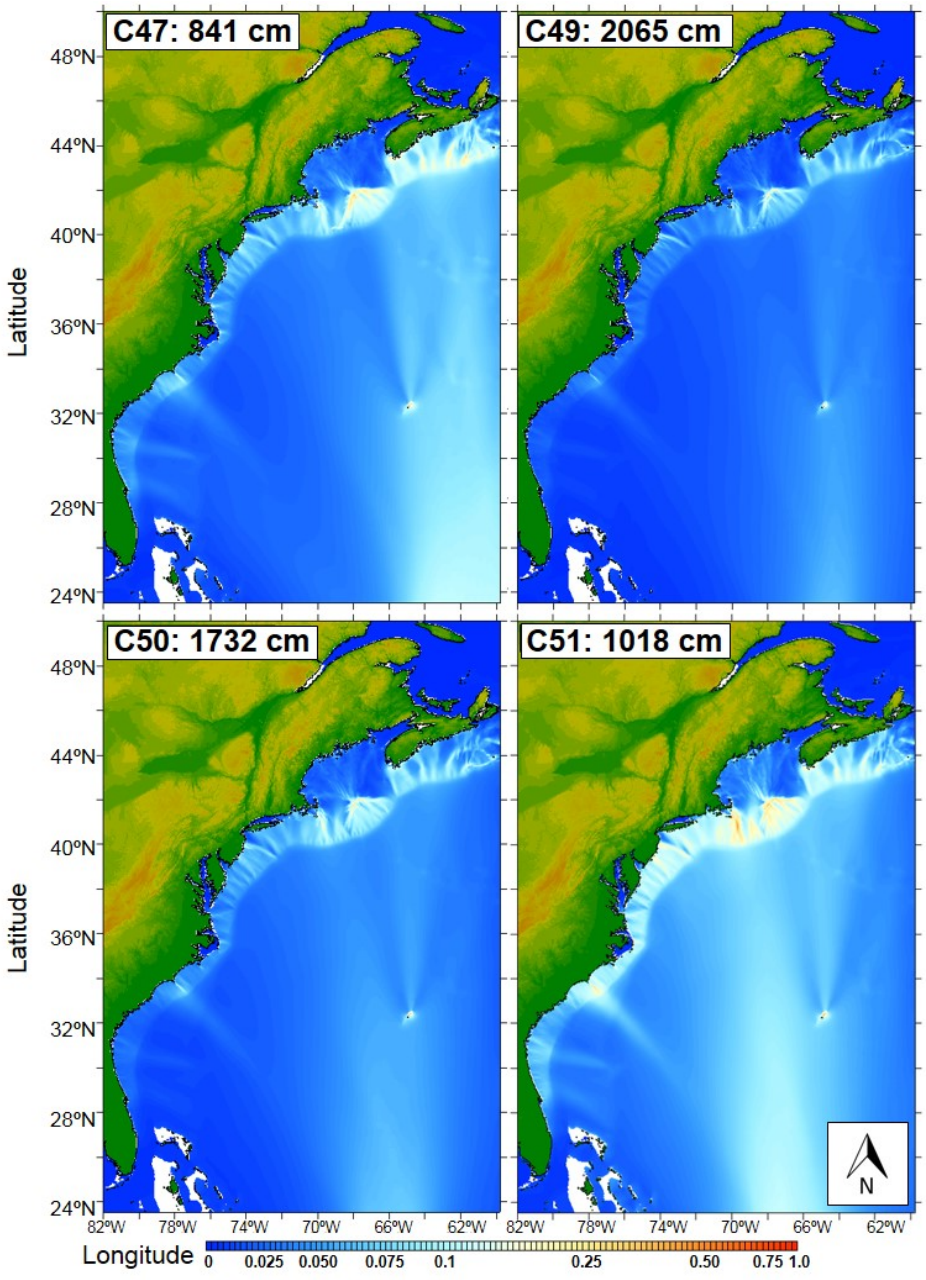

Figure 2.4: Maximum tsunami amplitude charts for Caribbean scenarios C47, C49, C50, and C51. To facilitate comparison amongst these, and the scenarios displayed in Figure 2.5 and Figure 2.6, the contoured results are normalized. Individual maxima are labeled in the upper left of each panel.

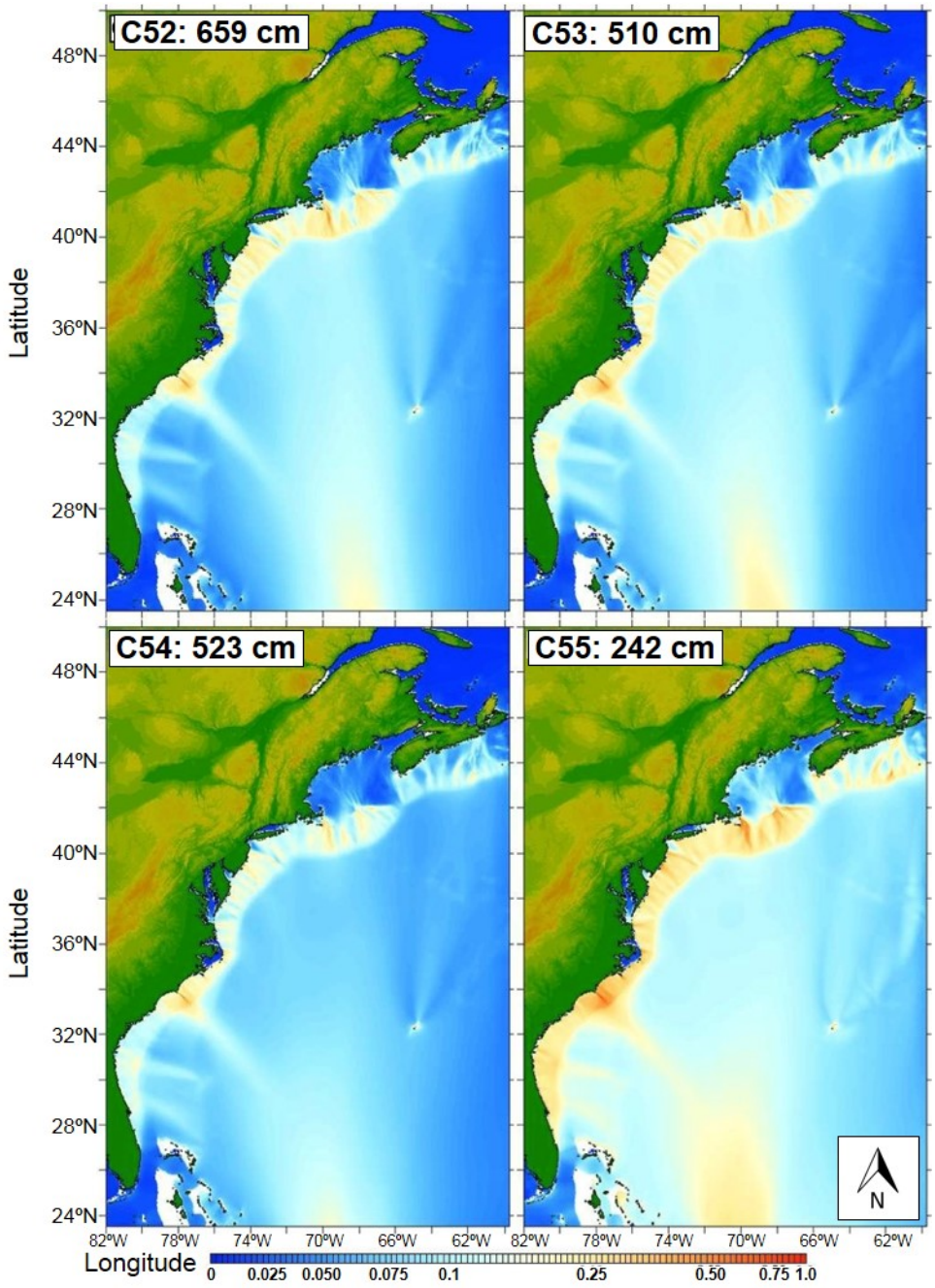

Figure 2.5: **Maximum tsunami amplitude charts for Caribbean scenarios C52, C53, C54, and C55. To facilitate comparison the contoured results are normalized. Individual maxima are labeled in the upper left of each panel.**

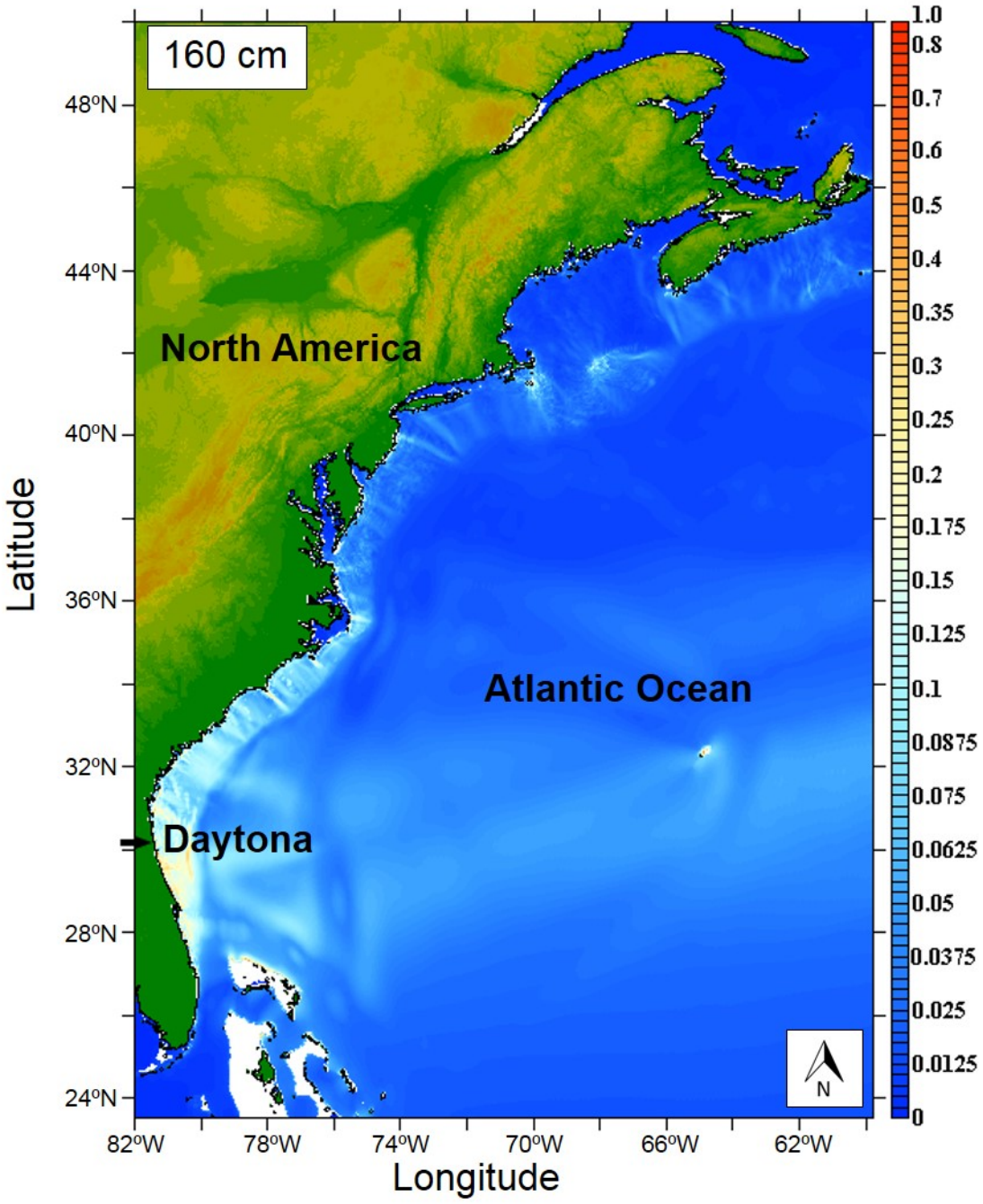

Figure 2.6: **Maximum tsunami amplitude chart for the Cadiz Wedge scenario which has the largest impact of the four eastern Atlantic cases considered. The maximum amplitude is labeled in the upper left corner and the location of Daytona, Florida is marked.**

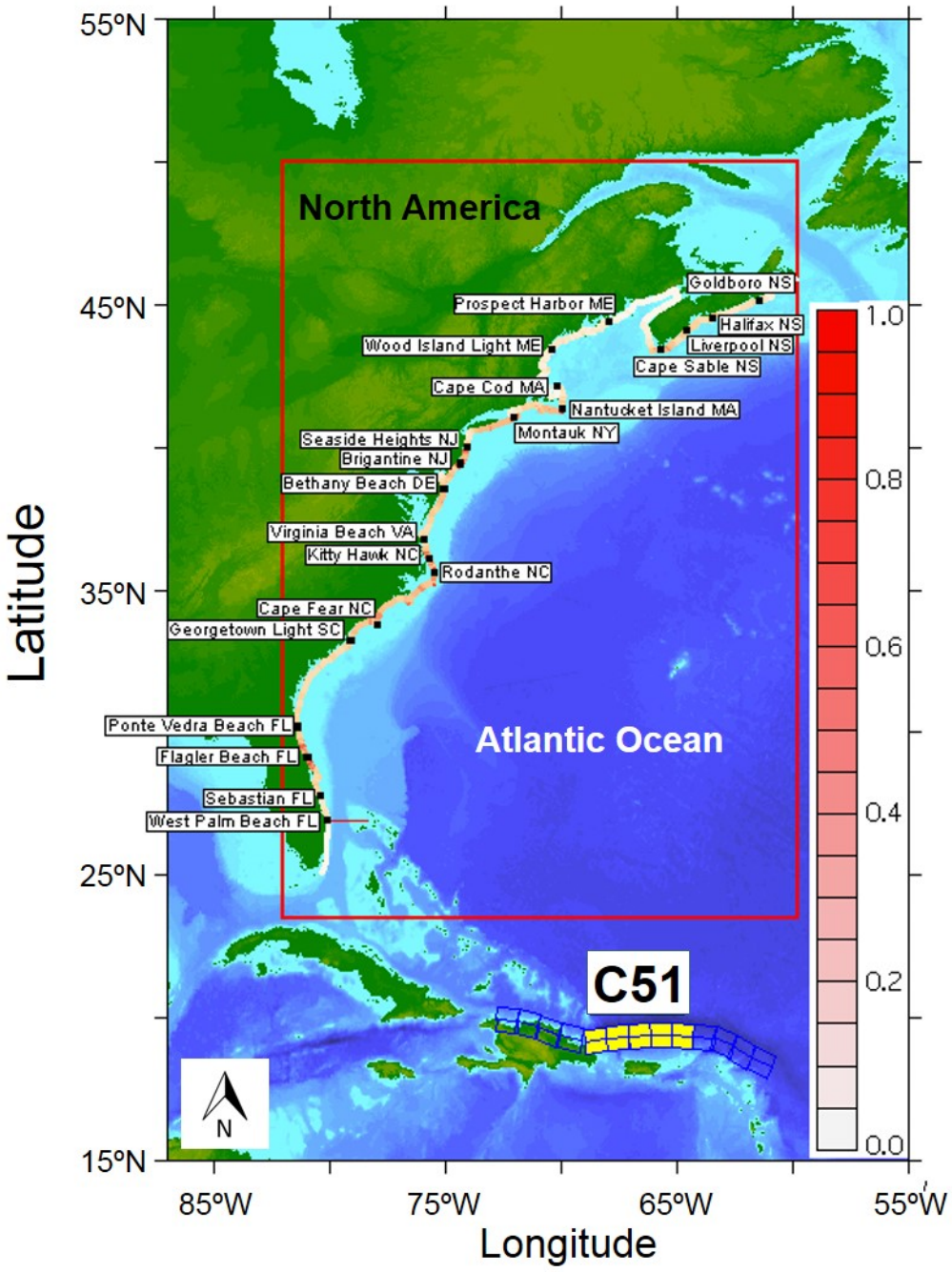

Figure 2.7: **Normalized inshore response to the C51 scenario along the 12-meter isobath with a nominal spacing of 5 km. This form, while facilitating the association of impact features with the geography, requires high-quality graphics and does not readily provide quantitative information.**

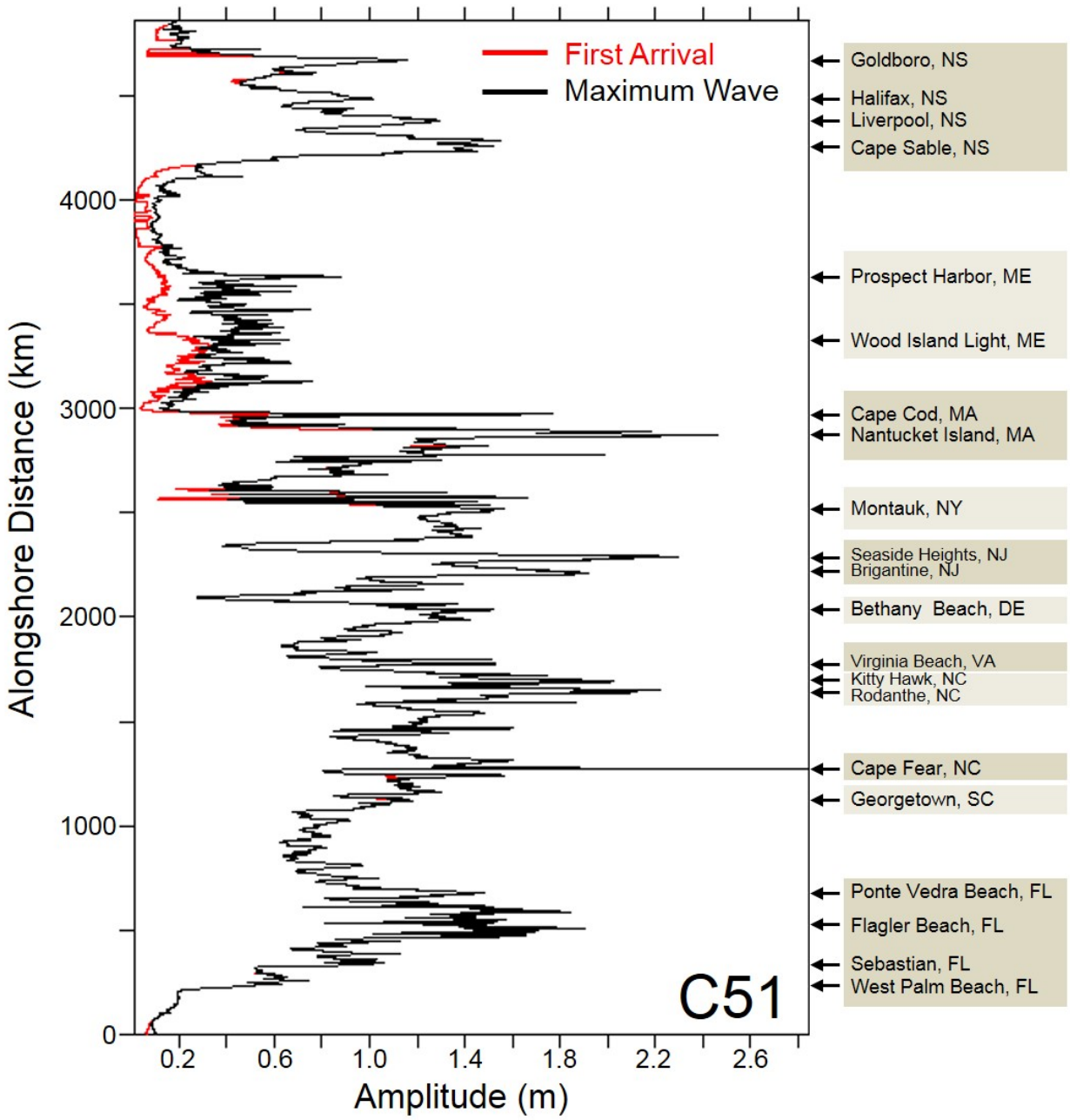

Figure 2.8: **Impact for the C51 scenario along the 12-meter depth contour. The amplitude of the earliest arriving and overall maximum wave are shown as distinct curves where they differ. The results are sampled at 5 km intervals from Florida to Nova Scotia and prominent features are labeled geographically.**

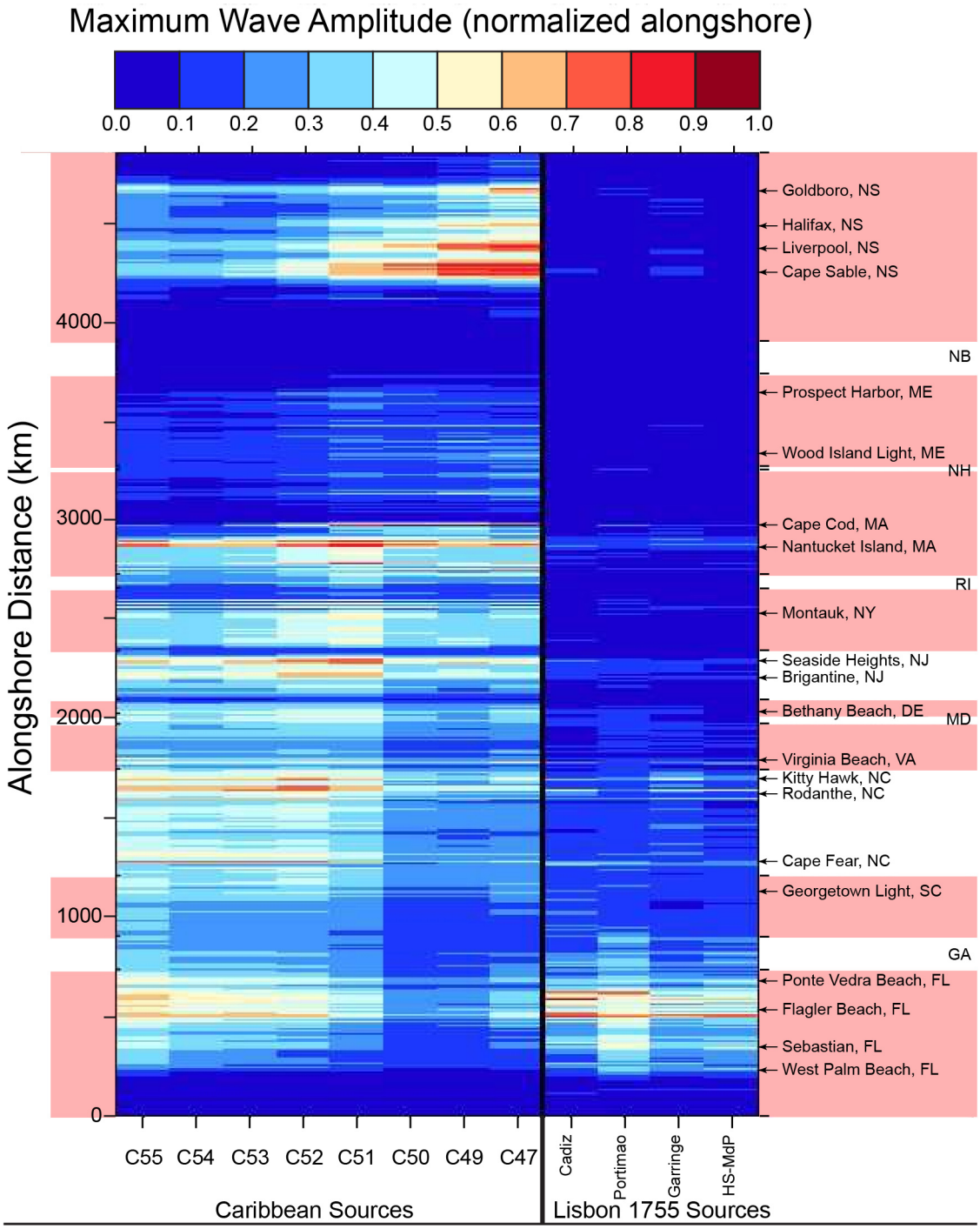

Figure 2.9: **Summary plot illustrating commonalities in the inshore response (at the 12 m isobath) to all tsunami scenarios investigated. Each vertical strip represents the maximum wave amplitude, normalized alongshore, for the scenario indicated. A geographic context is provided in the annotations to the right which are grouped by state and province.**

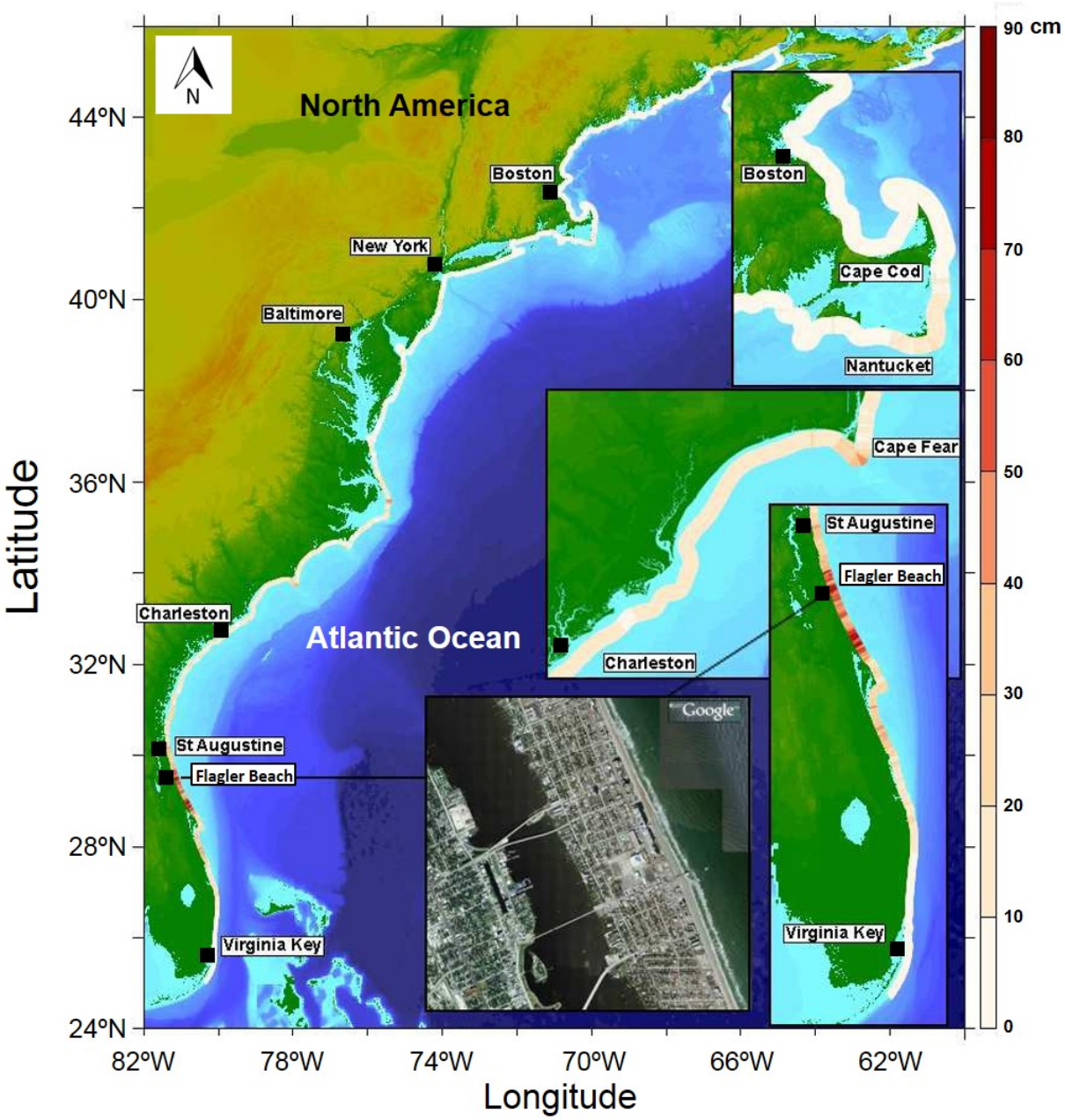

Figure 2.10: Possible inshore impact of the 1755 Lisbon tsunami represented by the Cadiz scenario. Several population centers at the time are indicated (Flagler Beach, Florida; Cape Fear, North Carolina; Cape Cod, Massachusetts). The distribution of wave amplitude may explain the lack of reported observations. The inset panel of current habitation reflects today's increased vulnerability to tsunami impact.

2.4.4 Distribution by State of Significant Impact

Using the catalog of tsunami run-up and death reports, Dunbar and Weaver (2008) have summarized by state the historical impact of tsunamis on the eastern U.S. Their analysis (based on tsunami run-up) includes the statistics for Puerto Rico and the U.S. Virgin Islands,

which were not considered in our treatment of severe tsunami scenarios. The tsunami catalog includes few major events. However, the current analysis of large rare events provides a means of supplementing the catalog-based distribution. For this purpose, the simulated inshore amplitude estimates (at 5 km intervals along the 12 m isobath) were binned by state into the size categories employed by Dunbar and Weaver (2008). A bin is incremented if any of the inshore points associated with the state meets the criterion. The bin-count sums to 12 when all scenarios are considered and to 8 for Caribbean scenarios only. None of the scenario results exceeded the 3-meter threshold, although some amplification is to be expected between 12-meter depth and the shoreline.

The results presented in Figure 2.11, contrast the scenario-based results with the run-up catalog results adapted from Table 3.1 of the Dunbar and Weaver (2008) study. The category for events of "undetermined origin" was dropped and no scenarios fell above the 3.0 m threshold:

Low	$0.0\ \text{m} \leq \text{Run-up} < 0.5\ \text{m}$
Medium	$0.5\ \text{m} \leq \text{Run-up} < 1.0\ \text{m}$
High	$1.0\ \text{m} \leq \text{Run-up} < 3.0\ \text{m}$

The primary conclusion from this admittedly limited analysis is that the threat from severe events is more widely distributed along the eastern seaboard than the sparse observational record available to the Dunbar and Weaver (2008) analysis might suggest.

2.5 Conclusion

This chapter provides some interim results from the ongoing study of the impact of severe tsunami events on the U.S. eastern seaboard. Waves generated directly by seismic activity by rare large events in the western and eastern Atlantic have the potential to cause significant impacts. The greatest hazard is likely to be associated with sources centered between the U.S. Virgin Islands and Hispaniola, though some sources in the eastern Atlantic may also be significant. The results from this report are consistent with ten Brink et al. (2008) study for the NRC. Simulations by ten Brink et al. (2008) were generated using the COMCOT (Cornell Multi-grid Coupled Tsunami Model) numerical code (Liu et al., 1998).

The coastal impacts reported exhibit considerable fine-scale structure in the alongshore variability due to the focusing and defocusing associated with bathymetry. Enhanced (or decreased) inshore impact is not overly sensitive to source location, so sites like Cape Fear stand out as a high-impact site for all scenarios. Unlike the distribution of observed run-up in the historical tsunami catalog, in which several states do not appear, the threat to all states on the eastern seaboard is significant for the scenarios investigated. This mismatch is due to the almost complete absence of observed large tsunamis in the historical record for the Atlantic Ocean basin. Given the potential for devastation these rare events pose, and the fine-scale structure in coastal impact evident in the results presented here, it is important that further studies employ high-resolution bathymetry and explore a broad suite of synthetic scenarios.

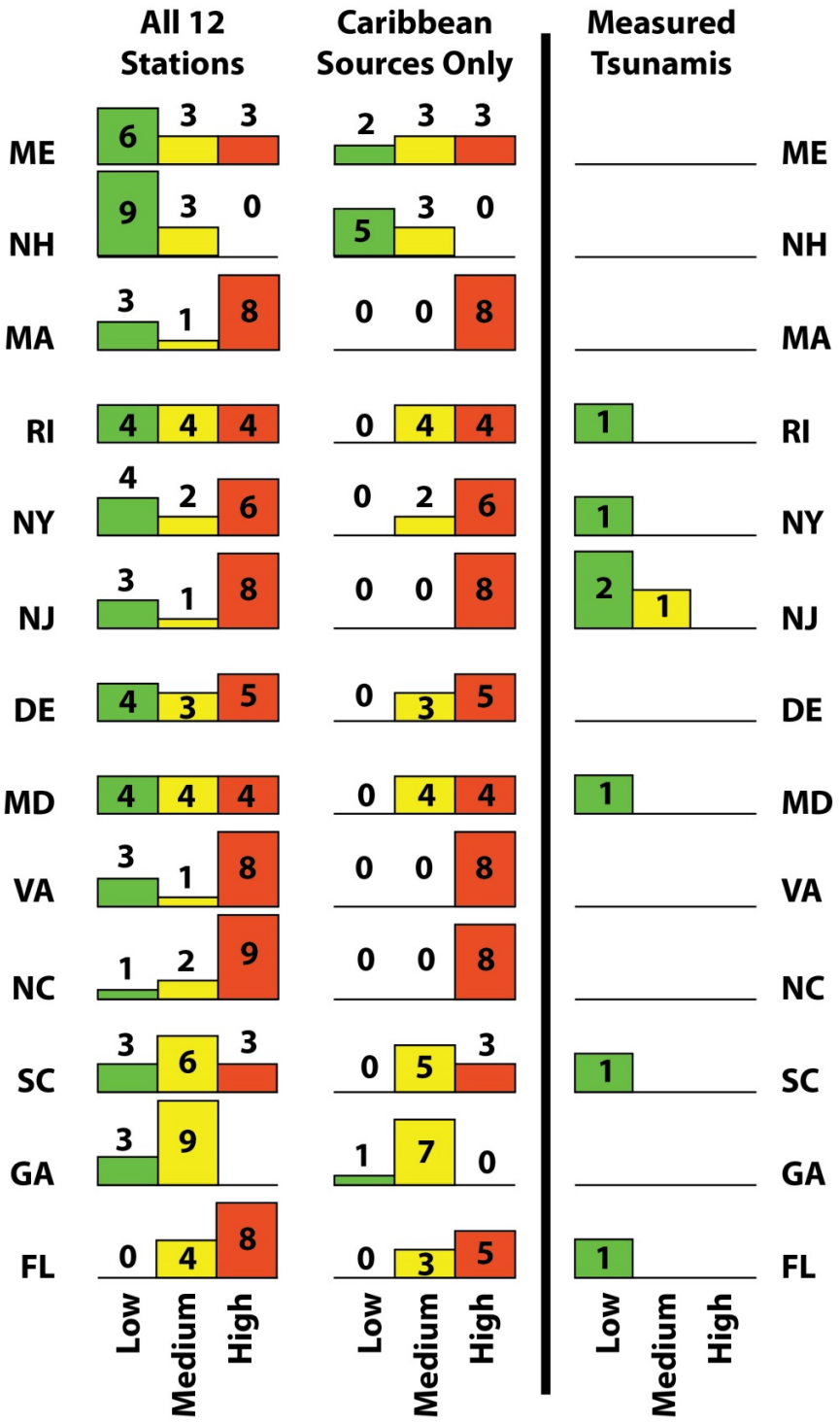

Figure 2.11: Distribution by state of inshore impact of synthetic west and east Atlantic source scenarios contrasted with the historical record reported by Dunbar and Weaver (2008). Run-up is the measure of impact employed with categories Low (< 0.5 m), Medium (0.5 – 1.0 m), and High (1.0 – 3.0 m). The full set of model results (left column) and those for Caribbean (center column) suggest a more evenly distributed threat than might be inferred from the sparse observational record.

2.6 Bibliography

Bird, P. (2003). An updated digital model of plate boundaries, *Geochem. Geophys. Geosyst.*, *4(3)*(1027), doi:10.1029/2001GC000252.

Coffin, M.F., Gahagan, L.M., and Lawver, L.A. (1998), Present-day Plate Boundary Digital Data Compilation, University of Texas Institute for Geophysics *Technical Report* No. 174, pp. 5

Dunbar, P. K., and C. Weaver (2008). U.S. states and territories national tsunami hazard assessment: Historical records and sources for waves, *Technical Report,* National Tsunami Hazard Mitigation Program, Seattle, WA.

Gica, E., M. Spillane, V. Titov, C. Chamberlin, and J. Newman (2008). Development of the forecast propagation database for NOAA's short-term inundation forecast for tsunamis (SIFT). NOAA Technical Memorandum OAR PMEL-139, *Technical Report*, NOAA Pacific Marine Environmental Laboratory, Seattle, WA.

Jay, D.A. (1991). Green's law revisited: Tidal long-wave propagation in channels with strong topography, *JGR*, Oceans, 96, p. 20585–20598, DOI: 10.1029/91JC01633.

Liu, P.L.F., Woo, S.B., and Cho, Y.S. (1998). Computer Program for Tsunami Propagation and Inundation, sponsored by National Science Foundation, http://ceeserver.cee.cornell.edu/pll-group/comcot_down.htm

Okada, Y. (1985). Surface deformation due to shear and tensile faults in a half-space, *Bull Seism. Soc. Am.*, *75*, 1135–1154.

Synolakis, C.E. (1991). Green's law and the evolution of solitary waves, *Phys. Fluids A*, vol. 3, no. 3, p490.

ten Brink, U. S., D. Twichell, E. Geist, J. Chaytor, J. Locat, H. Lee, B. Buczkowski, R. Barkan, A. Solow, B. Andrews, T. Parsons, P. Lynett, J. Lin, and M. Sansoucy (2008). Evaluation of tsunami sources with the potential to impact the U.S. Atlantic and Gulf coasts – an updated report to the Nuclear Regulatory Commission, *Tech. rep.*, U.S. Geological Survey (ML082960196).

3. HAZARD ASSESSMENT USING NOAA INUNDATION MODELS

3.1 Background and Objectives

Since the 2004 Indian Ocean tsunami, the most destructive tsunami in recorded history, worldwide awareness of tsunami hazard has peaked and global expansion of tsunami forecasting tools has made dramatic progress in both instruments and technology. Two of the most seminal advances in tsunami forecast since the Indian Ocean tsunami are: 1) the deployment of an extensive network of sensors to acquire deep ocean tsunami measurements, and 2) the introduction of real time numerical simulation as a vital tool in tsunami forecasting (Bernard and Robinson, 2009). To date, the number of deep-ocean tsunameters has grown from 9 in 2004 to 56 in 2016 (Figure 3.1), forming a global tsunami monitoring network in the Pacific, the Indian Ocean and the Atlantic that is currently co-managed by Australia, Chile, China, Indonesia, Russia, Thailand and the United States.

Since 2005, these tsunameters have detected more than 20 tsunamis generated by major earthquakes in the Pacific, Atlantic and Indian Ocean, building growing confidence of accuracy and reliability in far-field tsunami forecasting (Titov, 2009). As shown in the devastating 11 March 2011 Japan tsunami, the rapid and accurate determination of tsunami source from real-time tsunameter measurements has the great potential to improve tsunami forecast in the near field when facilitated with tsunami inundation models (Tang et al., 2012; Wei et al., 2012). The global implementation of these deep-ocean tsunami detectors has significantly accelerated the development and implementation of more accurate tsunami forecasting systems. Previous systems, relying on seismometers or coastal tide gauges, had resulted in 15 of the 20 tsunami false alarms since 1949 (Bernard and Robinson, 2009). Currently, three tsunami forecast systems, developed by Japan (Kuwayama, 2007; Tatehata, 1997), Australia (Greenslade and Titov, 2008), and the United States (Titov et al., 2005; Wei et al., 2008; Tang et al., 2009; Titov, 2009; Whitmore, 2009) respectively, are monitoring worldwide tsunami activity for rapid forecast to minimize tsunami impact for at-risk coastal communities. While the Japan and Australia systems are based on seismic data and propagation modeling, the United States is in the process of testing the next-generation forecast methodology that combines the real-time deep-ocean measurements with validated forecast inundation models (Synolakis et al., 2009) to produce real-time tsunami forecast for coastal communities.

NOAA's tsunami forecast system utilizes a best fit between pre-computed tsunami simulations stored in a forecast database and real-time deep-ocean tsunami measurements provided by an array of tsunameters to constrain the tsunami source. This produces estimates of tsunami characteristics in deep water that can be used as initial and boundary conditions for high-resolution forecast models with nonlinear inundation computation, which are designed to simulate 4 hours of coastal tsunami dynamics in less than 10 minutes. The results are made available in real time to the Tsunami Warning Centers (TWCs) and to local emergency management to aid in hazard assessment and decision-making before the tsunami reaches at-risk communities. Since 2005, NOAA has developed 75 high-resolution forecast models along the U.S. coasts, and all of them are now available for real-time forecasting. Since the 2004 Indian Ocean tsunami, the tsunami forecast system has been exercised for all 20 tsunamis that were detected and measured by the tsunameters, 17 in the Pacific and 3 in the Indian Ocean, demonstrating promising forecast accuracy, lead time, and coverage for far-field coastal communities.

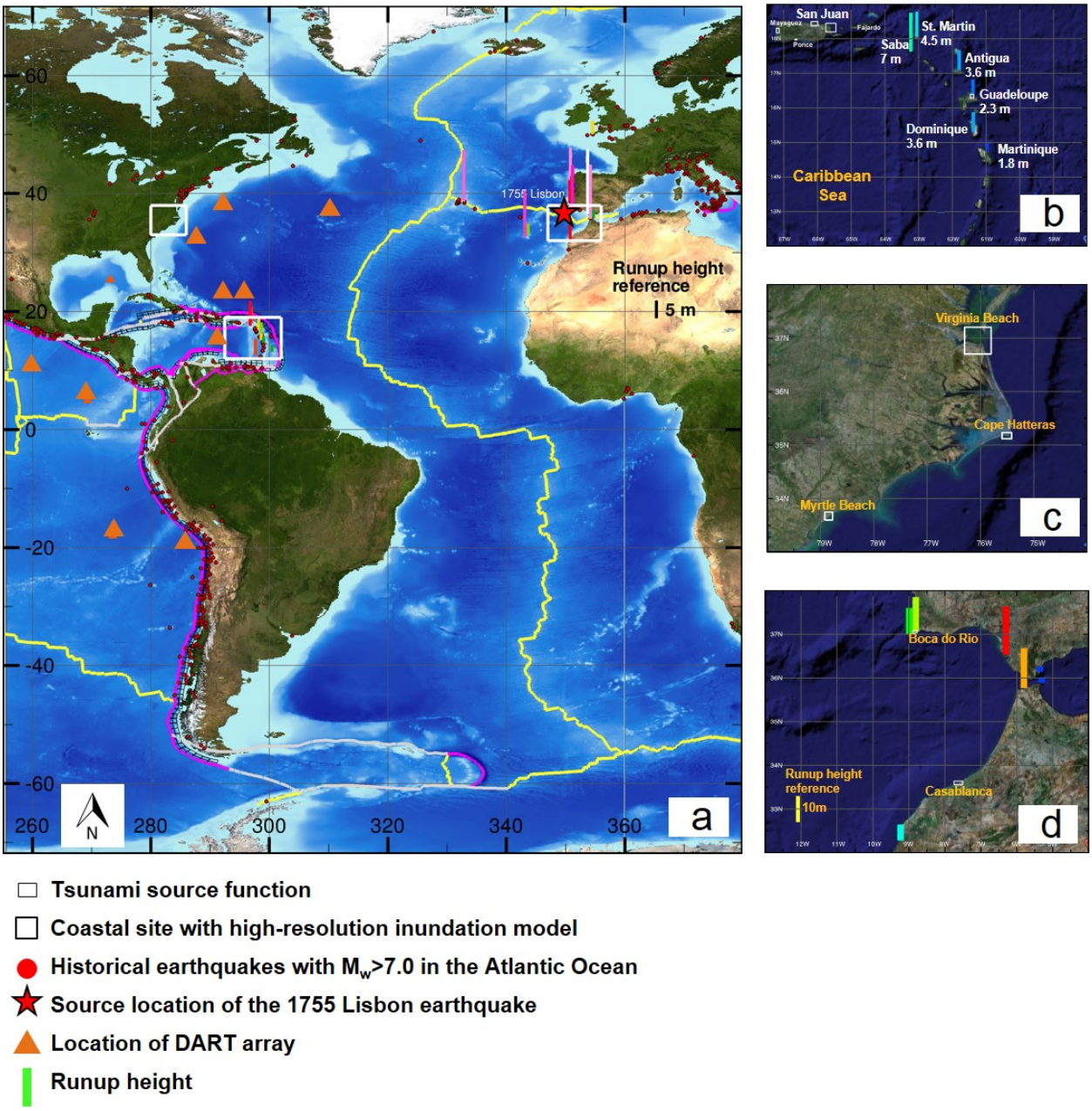

Figure 3.1: Historical records of runup height in the Atlantic Ocean due to the 1755 Lisbon tsunami, (a) in the Atlantic; (b) in the Caribbean; (c) in the US East Coast; (d) in the near field.

A total of 100 nuclear power reactors operate in the U.S., providing 20 percent of the nation's power. Eighty-nine of these reactors reside in the Eastern U.S., with 17 along the Atlantic coast (http://www.nrc.gov/reactors/operating/map-power-reactors.html). Impact on any of these nuclear reactors due to tsunami flooding may severely affect residents living within miles of the plant. It highlights the need of assessing potential tsunami hazard, in senses of both short-term and long-term, for tsunami susceptible plants. A short-term tsunami hazard assessment involves a real-time tsunami inundation forecast to determine, within a certain lead time, the height of tsunami waves at the facility site. A long-term tsunami hazard assessment involves

the use of the operational tsunami forecast models to identify the long-term impact of tsunamis at the facility site. The return period under consideration for a long-term tsunami hazard assessment varies with respect to different design requirements (annual exceedance rate of tsunami wave height).

The tsunami forecast system, under development by Pacific Marine Environmental Laboratory (PMEL), provides a set of tools for various tsunami hazard assessment studies. Tang et al. (2009) described the methodology of developing tsunami forecast models for real-time tsunami forecast. Each of these forecast models was validated for accuracy, efficiency, and robustness using historical tsunami records, higher-resolution reference models, and artificial mega- and micro-tsunami scenarios. A model database of tsunami propagation scenarios is being developed as part of the SIFT system. A study using the database can provide detailed analysis of the tsunami potential for a coastal region or a coastal community and pinpoint high-impact sources for a given coastal location. Comprehensive analyses are feasible because more than a thousand propagation scenarios for all major seismic tsunami source areas are readily available from the database.

3.2 Modeling the 1755 Lisbon Tsunami

The Indian Ocean tsunami of December 26, 2004, has changed the perception of a tsunami as a low-risk hazard for coastal infrastructures. In order to evaluate the tsunami risk along the U.S. East Coast and the Gulf of Mexico from seismic sources in the Atlantic and the Caribbean, a key action is the modeling assessment of the trans-Atlantic tsunami impact caused by the 1755 Lisbon earthquake, one of the most hazardous, yet understudied, historical earthquake-generated tsunami events in the Atlantic. Using high-resolution inundation models, the present study focuses on assessing the distant impact of the 1755 tsunami at multiple sites along the U.S. Atlantic coast and the Caribbean, specifically its near-shore dynamics in the harbors, inlets, and waterways. While helping to identify the tsunami source due to the Lisbon earthquake (Baptista et al., 2003; Roger et al., 2010a; Roger et al., 2010b), this study emphasizes the significance of the tsunami magnitude, source location, bathymetry, and topography in understanding the progression of tsunami waves offshore and near-shore. This study sets an example of extending NOAA's existing tsunami forecast system to identify tsunami vulnerability for global coastal communities at risk.

Figure 3.1 shows the historical records of runup height for the 1755 Lisbon tsunami in the Atlantic coastlines. Also shown in the figure are the coastal locations where the high-resolution inundation models have been developed in the near field, Portugal and Morocco, and in the far field, the U.S. East Coast and the Caribbean.

3.2.1 Earthquake Sources of the 1755 Lisbon Tsunami

The earthquake source of the 1755 tsunami is not fully understood. Previous studies have proposed a few source mechanisms that may have potentially produced this basin-wide tsunami as shown on Figure 3.2 (Baptista et al., 2003; Roger et al., 2010a; Roger et al., 2010b). The magnitude of the proposed earthquake ranges from M_w 8.0 to 8.6, while the rupture area varies between 6000 km^2 and 28000 km^2. Some of these sources have been tested against local historical records. Roger et al. (2010a, 2010b) examined the historical records in Martinique and Guadeloupe using inundation models with a M_w 8.3 source. ten Brink et al. (2008) suggested a M_w 8.7 source with a fault strike of 345º gave best match of all the tsunami records in Lesser Antilles, while produced low runup in the East Coast of the U.S. Muir-Wood and Mignan (2009) proposed a magnitude of 9.0 for the 1755 Lisbon source based on their

examination of the historical records in near- and far-field. As far as a basin-wide tsunami is concerned, the modeling results need to be validated in both close and distant locations to avoid misleading and bias definition of the source. This study aims to identify a best-available tsunami source for the 1755 Lisbon earthquake by virtue of high-resolution modeling studies, both near and far field, in the Atlantic.

Table 3.1: Source parameters of the possible scenarios for the 1755 Lisbon earthquake that generated the destructive tsunami. The scenario numbers correspond to those shown in Figure 2.2, where scenario 3 includes an earthquake source contributed by two faults, namely Horseshore Fault and Marques de Pombal fault.

Scenario or Source Number	Longitude	Latitude	Strike (º)	Dip (º)	Length (km)	Width (km)	Slip (m)	M_w	Source Name
1	10.1561°W	37.8864°N	340	45	210	75	13.6	8.5	Baptista's source
2	11.2164°W	36.519°N	51.2	35	120	60	7.8	8.1	Gorringe Bank north
3	9.6956°W	35.6422°N	41.3	35	106	70	11.2	8.2	Horseshoe Fault
	9.5332°W	36.5259°N	12.6	35	88	70	9.6	8.1	Marques de Pombal
4	8.5257°W	36.3999°N	274	40	102	50	10.2	8.0	Portimao Bank
5	7.4560°W	35.6124°N	334.4	2	139	200	11.8	8.6	Cadiz Wedge Fault

3.2.2 Tsunami Energy Projection in the Atlantic

The computed maximum tsunami wave amplitude illustrates the energy distribution and the directionality of the tsunami in the ocean. The comparison of the maximum tsunami wave amplitude in the deep ocean for all five scenarios indicates that scenario number 1, shown on Figure 3.3a, produces the most severe tsunami impact in the Caribbean and U.S. East Coast. Computational results obtained from all five scenarios show that Florida may be the most affected coastline in the far field during the 1755 Lisbon tsunami. The comparison of the maximum wave amplitude between scenario 1 (Figure 3.3a) and scenario 5 (Figure 3.3d), highlights the difference between near and far field inundation and runup. The tsunami impact caused by these two scenarios are similar in the near field, while in the far-field they are significantly different. This phenomenon emphasizes the necessity of tsunami impact study at different coasts both in the far and near field to resolve the complexity of the tsunami source.

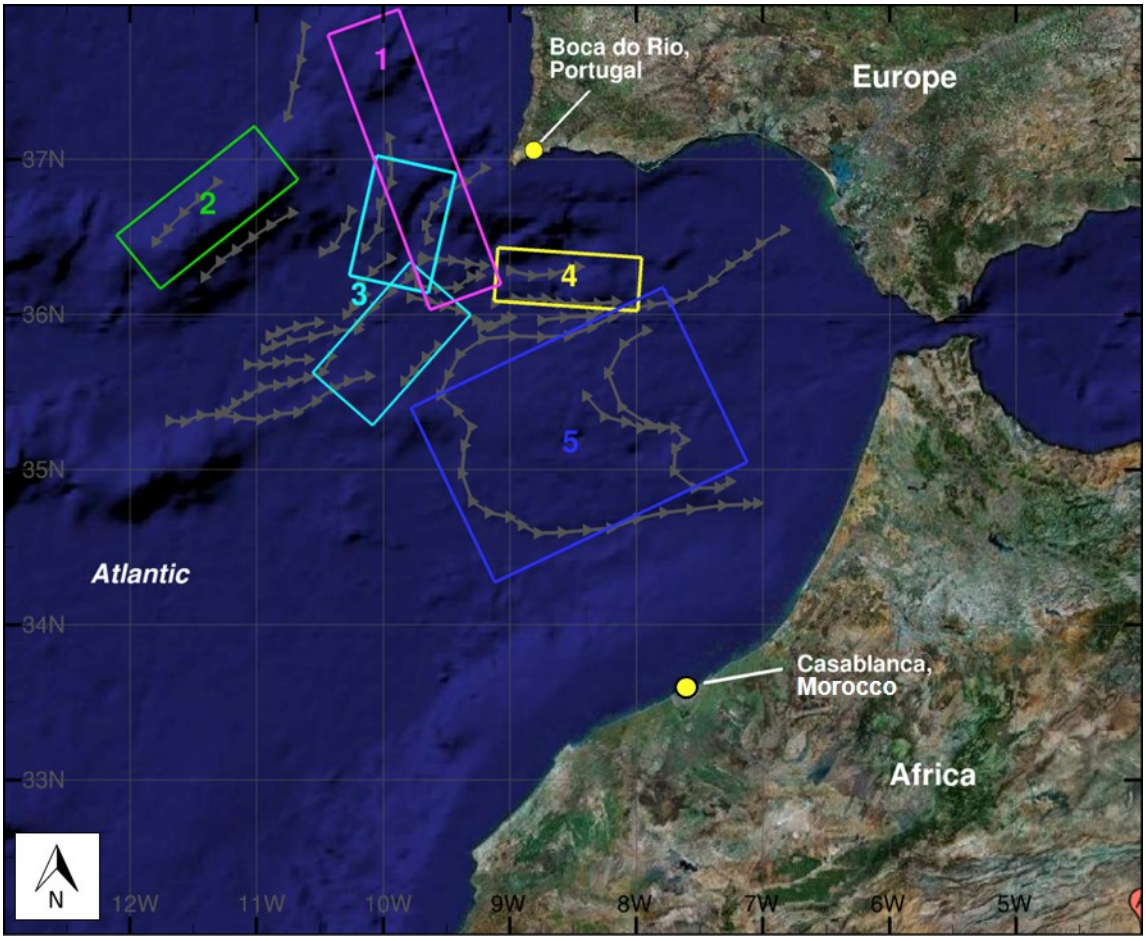

Figure 3.2: Possible earthquake rupture sources of the 1755 Lisbon tsunami used in the present study. The corresponding source parameters are listed in Table 3.1.

3.2.3 Tsunami Impact in the Near Field

In addition to the severe damage caused by the earthquake, the tsunami impact in the near field was also catastrophic following the 1755 Lisbon tsunami which devastated the Iberian and northern Moroccan coasts, causing great damage and casualties. It was observed all over North Atlantic coasts and in Central and South America. Tsunami waves of 10 to 15 m were reported at Cape St. Vincent and along the Gulf of Cadiz (Baptista and Miranda, 2009). Using the near-shore bathymetry and topography data (Omira et al., 2012), models are developed to compute the tsunami runup and inundation for two near-field coasts - Boca do Rio in Portugal and Casablanca in Morocco, where the historical records of runup and inundation are available at a grid resolution of 3 arc-second (~ 70 m).

Figure 3.4 shows the comparison of computed runup heights and inundation limits due to all five possible sources against historical records. The historical record of flow depth at Boca do Rio is greater than 13 m (Baptista et al., 2003). The maximum computed flow depth produced by scenario 1 is about 15 m near the coastline, and about 10 m inland, which agrees well with the observations. The Portimao source gives the second largest flow depth, nearly 10 m, while other sources produce 5 m flow depth. Figure 3.5 shows comparison of computed runup

heights and inundation limits for the five proposed sources in Casablanca, the largest city in Morocco. Nearly every source produces significant flooding in the harbor of Casablanca.

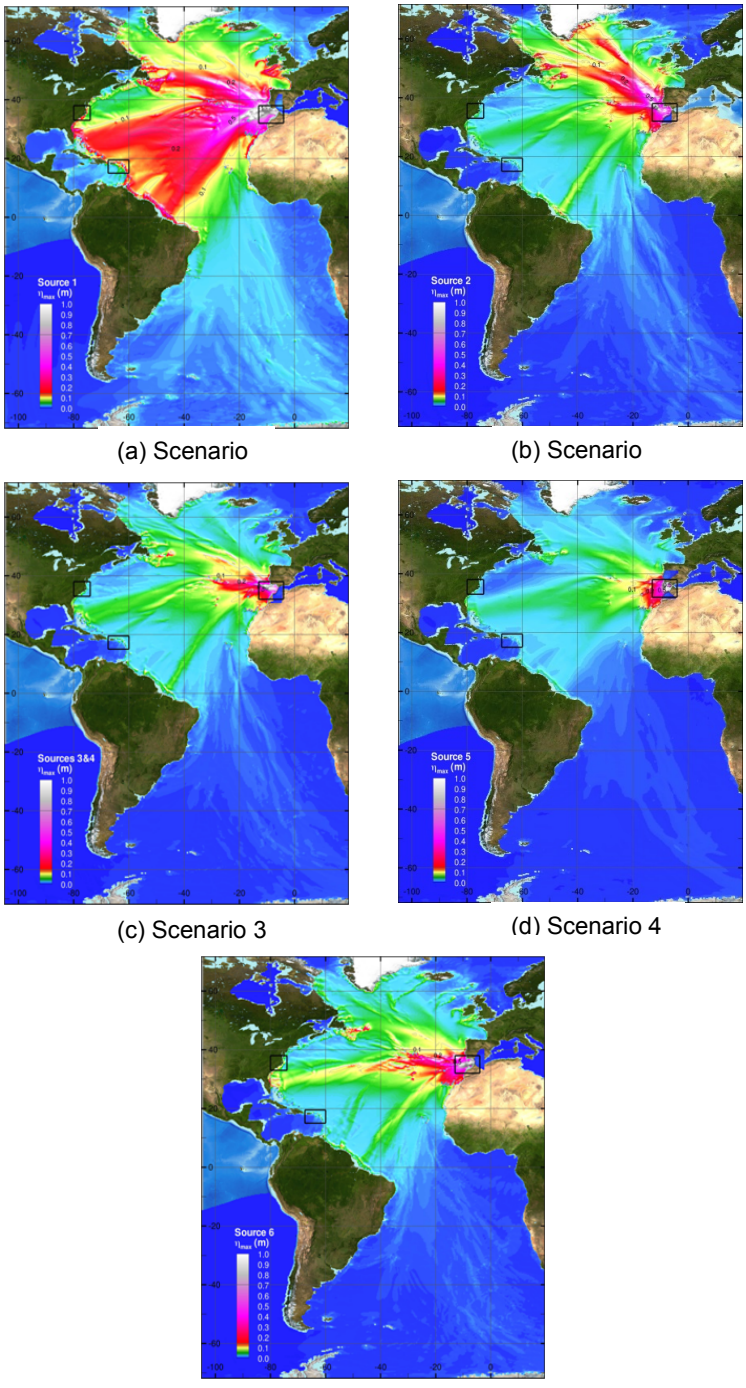

(a) Scenario (b) Scenario

(c) Scenario 3 (d) Scenario 4

(e) Scenario

Figure 3.3: Comparison of the maximum tsunami offshore wave amplitude in the Atlantic ocean due to the five scenarios presented in Figure 3.2 and Table 3.1, (a) scenario 1; (b) scenario 2; (c) scenario 3; (d) scenario 4; (e) scenario 5.

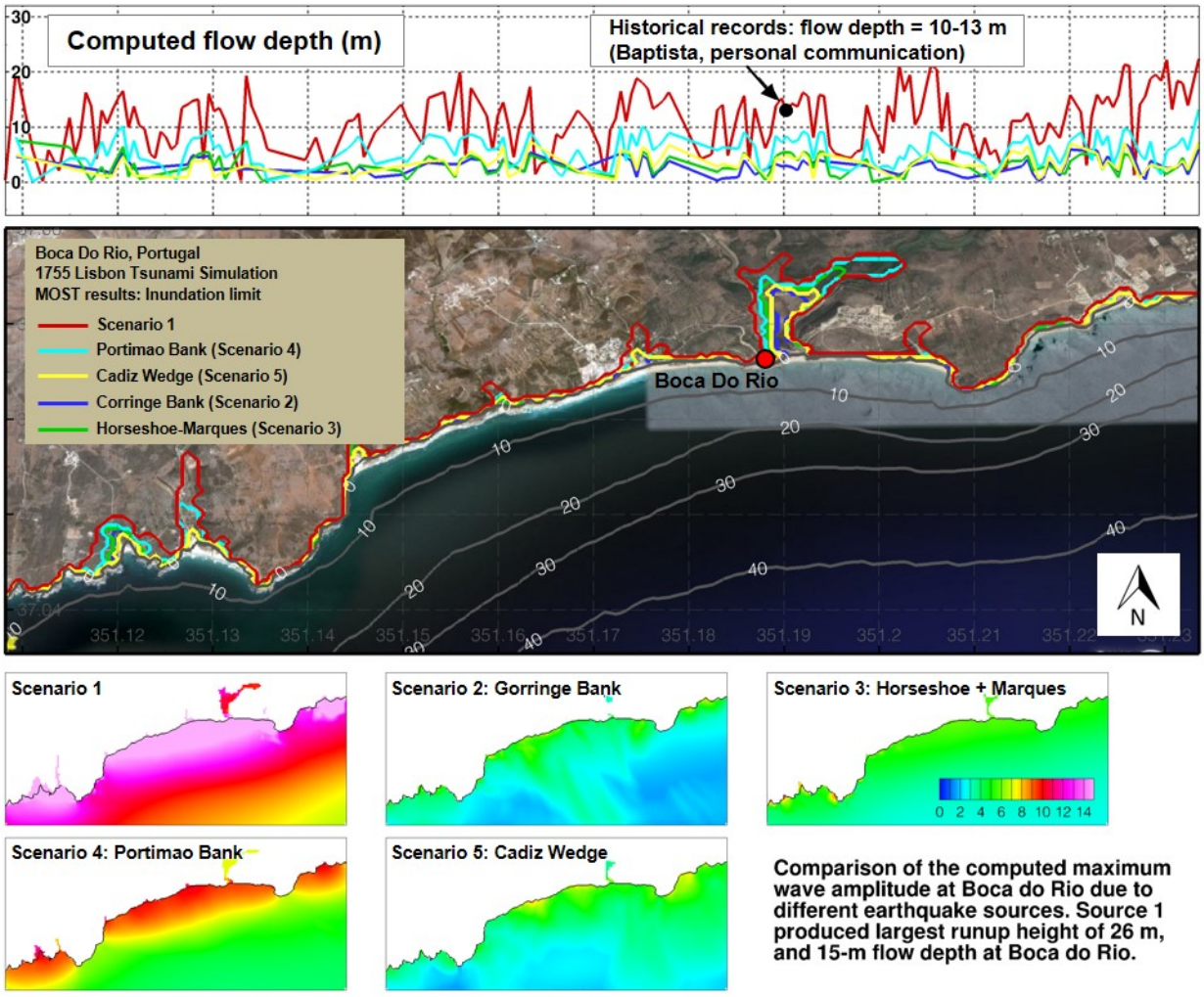

Figure 3.4: Comparison of the computed tsunami flow depth, inundation extent, and maximum wave amplitude in Boca Do Rio, Portugal caused by five earthquake scenarios shown in Figure 3.2.

Despite the fact that the Portimao source is only a M_w8.0 earthquake, the modeling results indicate it may cause more flooding than the Cadiz source, an M_w 8.6 scenario earthquake located closer to the coasts of North Africa. This is a typical example showing the importance of the directionality of tsunamis–the south-north orientation of Portimao fault directed most of the tsunami energy to the northwest coasts of Africa and southwest coasts of Europe, whereas the northeast-southwest orientation of Cadiz fault caused most of the tsunami energy to propagate into the Atlantic and have minimal impact in Casablanca.

3.2.4 Tsunami Impact on the Caribbean Coasts

NCTR has developed tsunami inundation forecast models for many harbors in the U.S. and Puerto Rico. These models have been developed at 1 to 3 arc-second (30 to 90 m) grid resolution to forecast coastal runup and inundation in real time. In addition to the existing forecast models, this study has also specifically developed a model for the south shore of Guadeloupe, where a recent survey (Roger et al., 2009) estimated a tsunami height of 3.2 m and a 200 m inundation at Sainte Anne (Figure 3.6). The modeling results show tsunami waves with amplitudes up to 1.8 m (lower than surveyed data) along the coastline of Sainte Anne. This

underestimation probably can be attributed to either the tsunami source estimation, or that the modern topography used in the model may not fully represent the coastline topography of Sainte Anne in 1755. There have been very few historical records of the 1755 Lisbon tsunami in Puerto Rico. The computed maximum tsunami runup at the Atlantic coasts of Fajardo due to source 1 is 2 m, with tsunami flooding at its headlands and harbors. This implies that the computed runup and inundation on the Atlantic coasts of the Caribbean islands may be more significant, as is indicated by the energy pattern in Figure 3.3a. Lesser Antilles, the island chain southwest of Puerto Rico, has historical runup records up to 7 m (Figure 3.1). Figure 3.6 to Figure 3.10 show the computed runup and inundation using inundation models in Guadeloupe, Fajardo, Ponce, Mayaguez, and San Juan. Source 1 produced some significant inundation in the low-lying area of Fajardo. No significant inundations were observed at other locations when all seismic sources were considered.

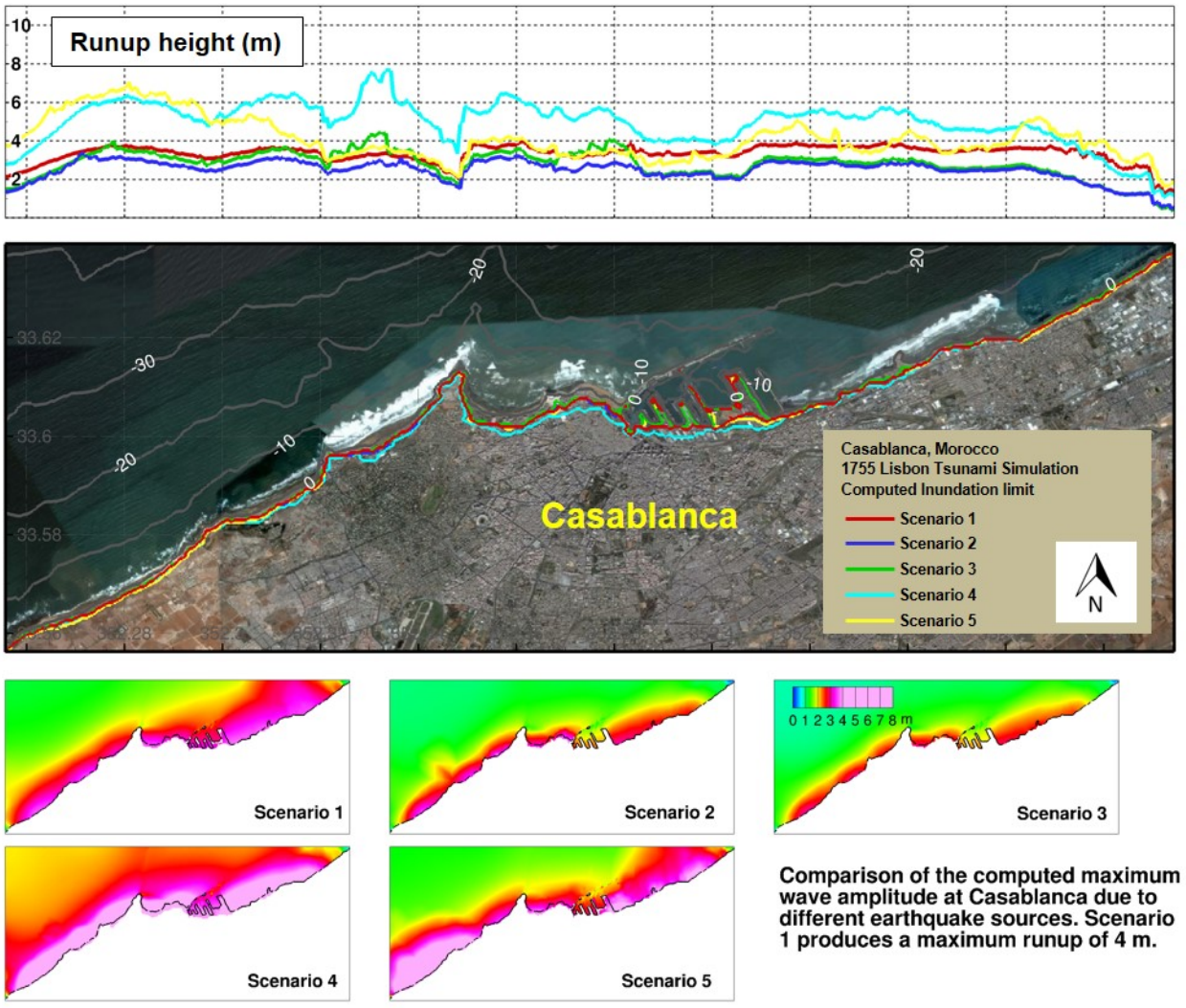

Comparison of the computed maximum wave amplitude at Casablanca due to different earthquake sources. Scenario 1 produces a maximum runup of 4 m.

Figure 3.5: Comparison of the computed tsunami flow depth, inundation extent, and maximum wave amplitude in Casablanca, Morocco caused by five earthquake scenarios shown in Figure 3.2.

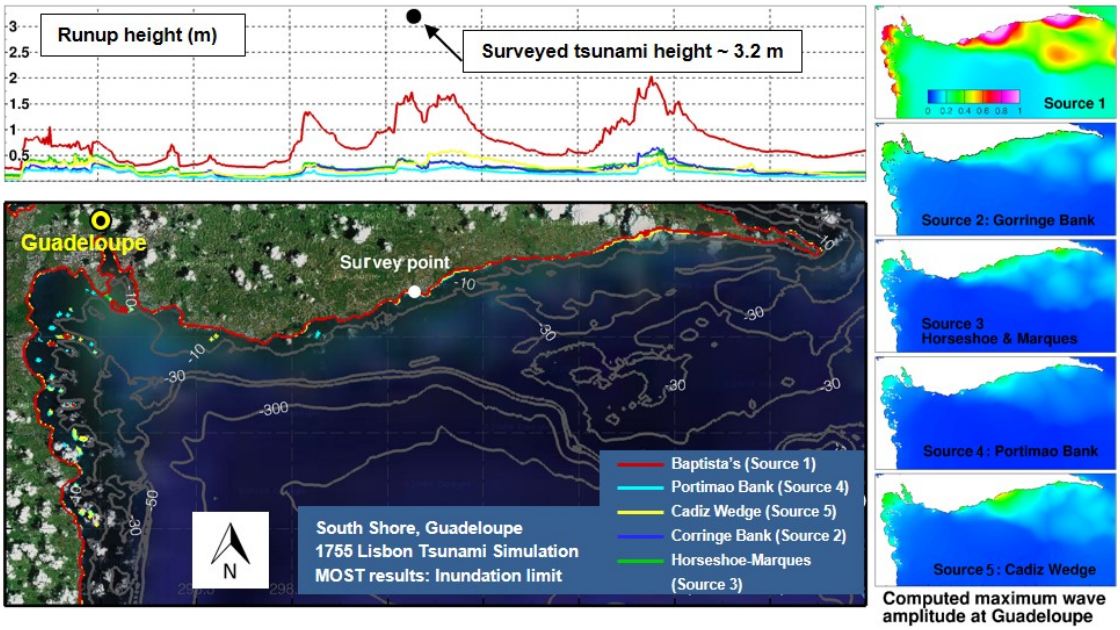

Figure 3.6: **Comparison of the computed tsunami flow depth, inundation extent, and maximum wave amplitude in Guadeloupe caused by five earthquake scenarios shown in Figure 3.2.**

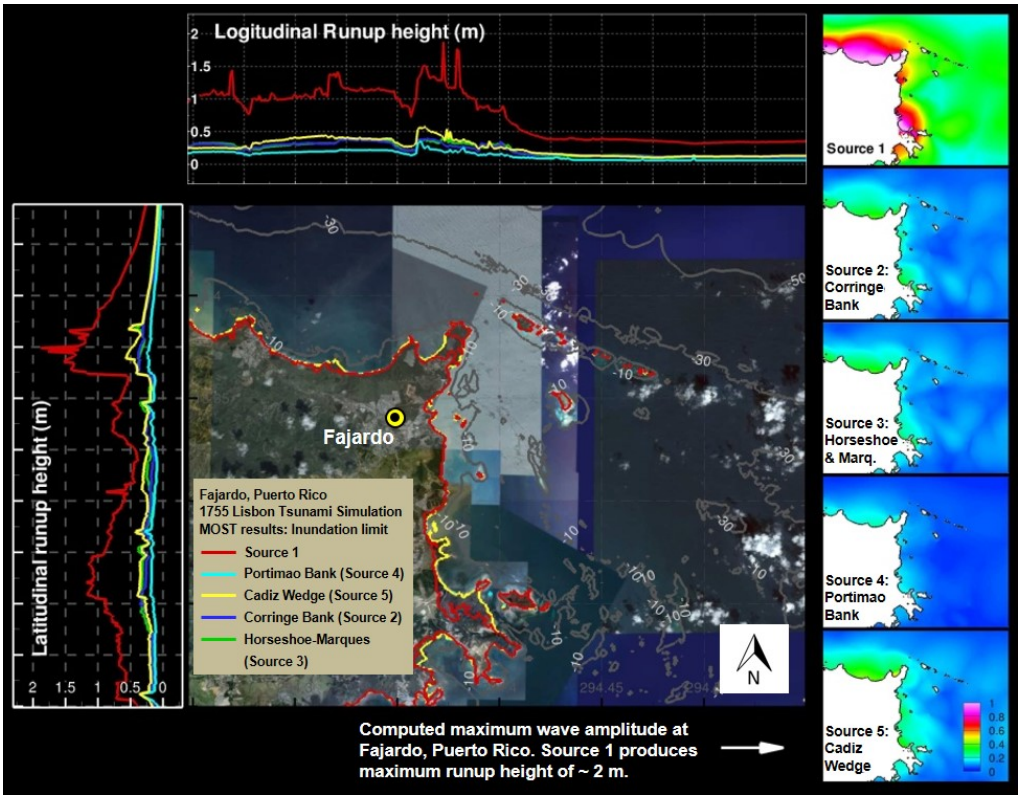

Figure 3.7: **Comparison of the computed tsunami flow depth, inundation extent, and maximum wave amplitude in Fajardo, Puerto Rico caused by five earthquake scenarios shown in Figure 3.2**

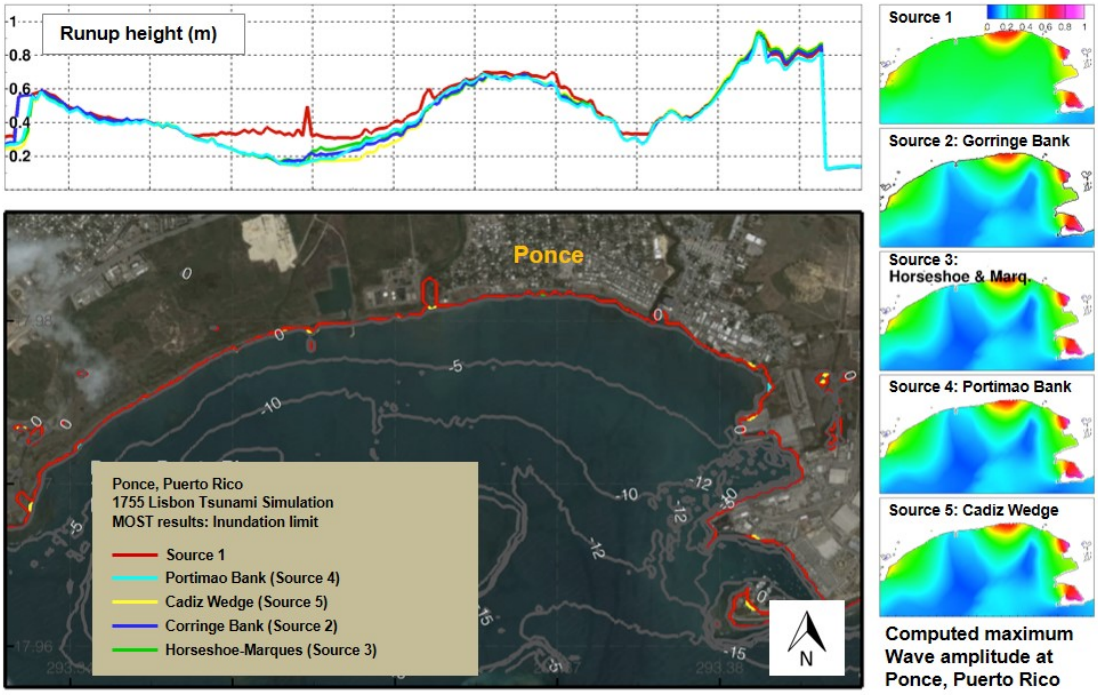

Figure 3.8: Comparison of the computed tsunami flow depth, inundation extent, and maximum wave amplitude in Ponce, Puerto Rico caused by five earthquake scenarios shown in Figure 3.2.

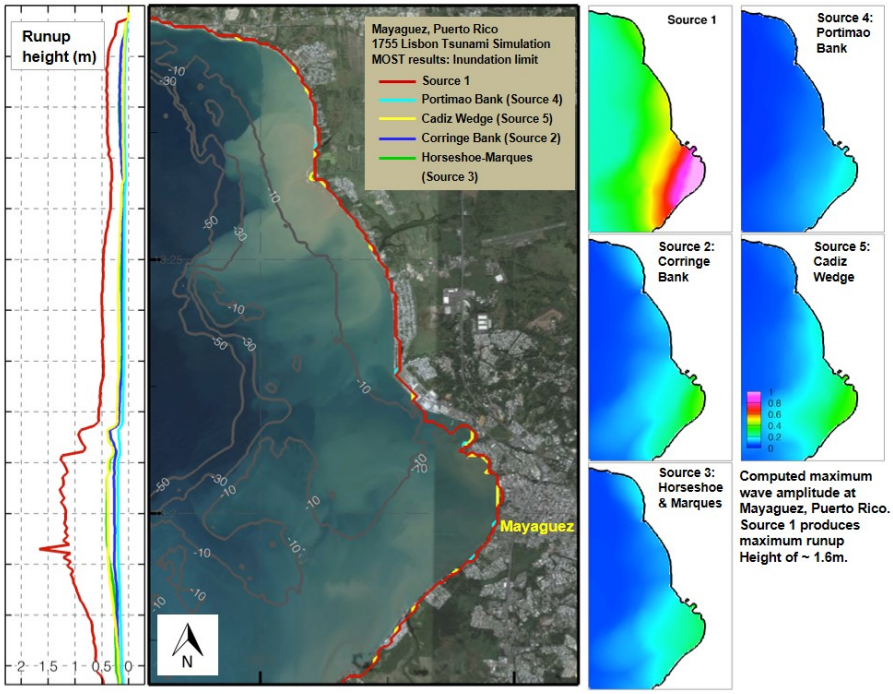

Figure 3.9: Comparison of the computed tsunami flow depth, inundation extent, and maximum wave amplitude in Mayaguez, Puerto rico caused by five earthquake scenarios shown in Figure 3.2.

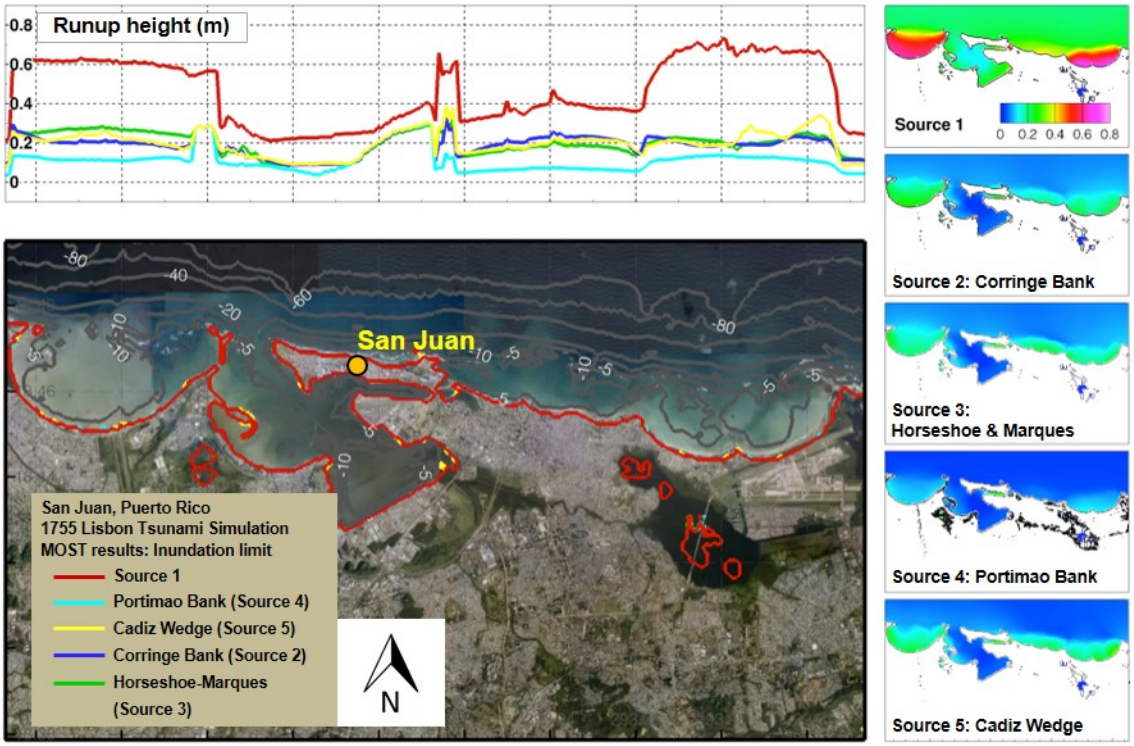

Figure 3.10: Comparison of the computed tsunami flow depth, inundation extent, and maximum wave amplitude in San Juan, Puerto Rico caused by five earthquake scenarios shown in Figure 3.2.

3.2.5 Tsunami Impact in the U.S. East Coast

The U.S. East Coast has been identified as a low-runup area for the 1755 Lisbon tsunami. The computed maximum tsunami height is 1.5 m at Virginia Beach (Figure 3.11), 1 m at Cape Hatteras (Figure 3.12), and 0.4 m at Myrtle Beach (Figure 3.13). Although the continental shelf is believed to have dissipated the tsunami energy, this study shows that the width of the continental shelf may also affect the harbor oscillation, and thus influence the local tsunami runup in the harbor.

3.3 Tsunami Hazards from Potential Earthquake Sources in the Caribbean Sea

3.3.1 Historical Tsunamis in the Caribbean

Aside from the Pacific plate margin of North America, the North American-Caribbean plate boundary is the closest active plate boundary to coastal areas in the Gulf of Mexico and the U.S. Atlantic seaboard at a distance of about 2,000 km. The North America-Caribbean plate boundary extends over 3200 km from northern Central America through the Greater Antilles (Jamaica, southern Cuba, Hispaniola, Puerto Rico, and the Virgin Islands) to the northern end of the Lesser Antilles subduction zone. Global positioning system (GPS) studies have shown that the Caribbean plate is moving in the east-northeast direction at a rate of 18.0 to 20.0±0.4mm/yr relative to North America (DeMets et al., 2000).

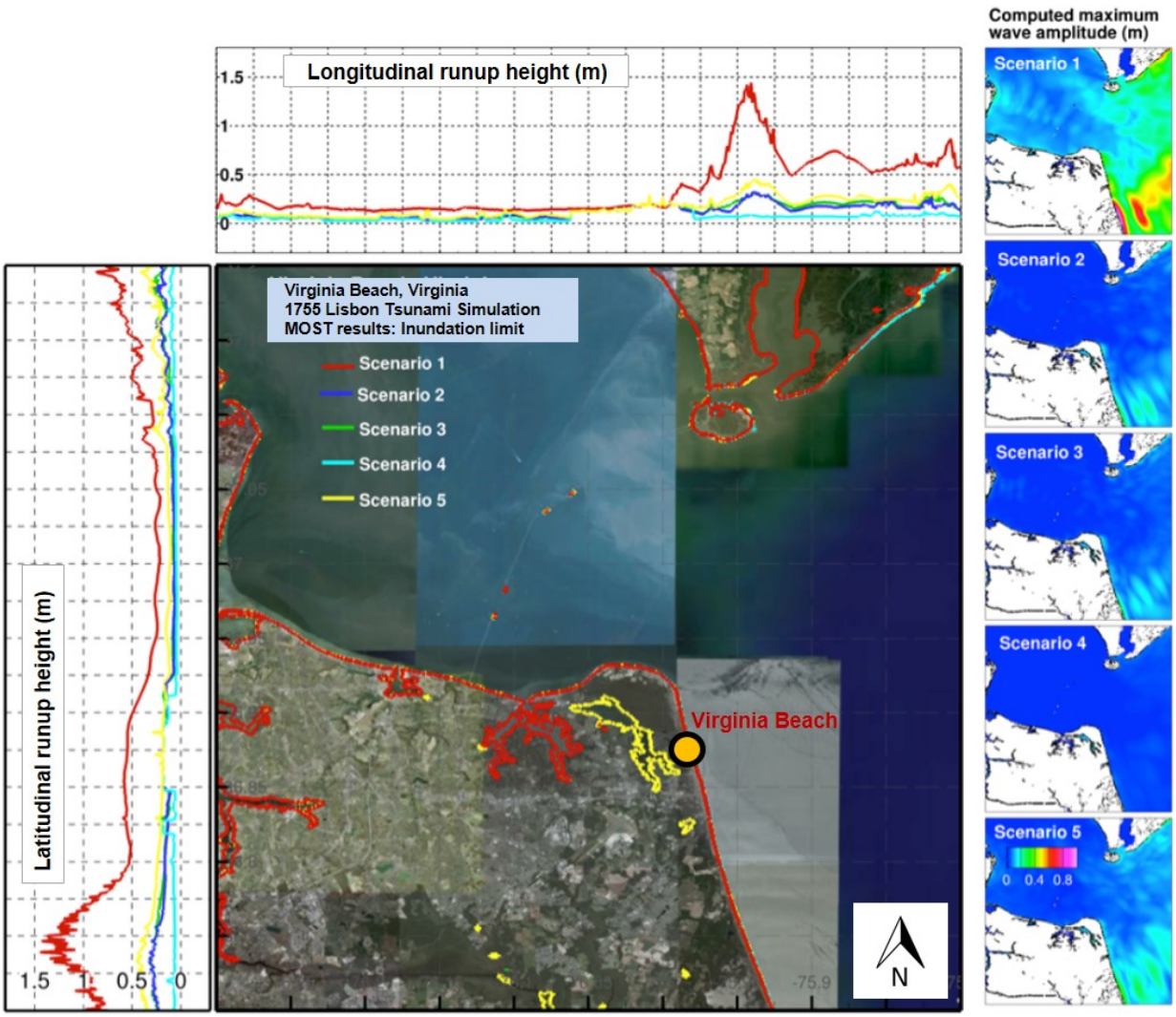

Figure 3.11: Comparison of the computed tsunami runup height, inundation extent, and maximum wave amplitude in Virginia Beach caused by five earthquake scenarios shown in Figure 3.2.

The geologic and tectonic setting of the northern Caribbean is capable of generating tsunami waves of up to 12 m high and extended to distances of up to 2,200 km (Grindlay and Hearne, 2005). There have been 124 reported tsunami events in the Caribbean Sea since the 16th century (O'Loughlin and Lander, 2003) that caused extensive damage and casualties; 53 were reported as reliable occurrences, 8 probably occurred, 19 may or may not have occurred, and 44 are doubtful or improbable occurrences. The most famous of these events include the 1530 Venezuela, the 1690 U.S. Virgin Islands and northern Lesser Antilles, the 1692 Port Royal, Jamaica, the 1755 Martinique, the 1867 St. Thomas, the 1918 Puerto Rico, and the 1946 Dominican Republic tsunamis. Although there have been deadly tsunamis in the northwestern Caribbean during the last century, including a 1918 event resulting in 42 deaths and 100 missing and a 1946 event resulting in 1790 deaths, it is a recurrence of the 1867 tsunami in the US Virgin Islands that may pose the greatest hazard.

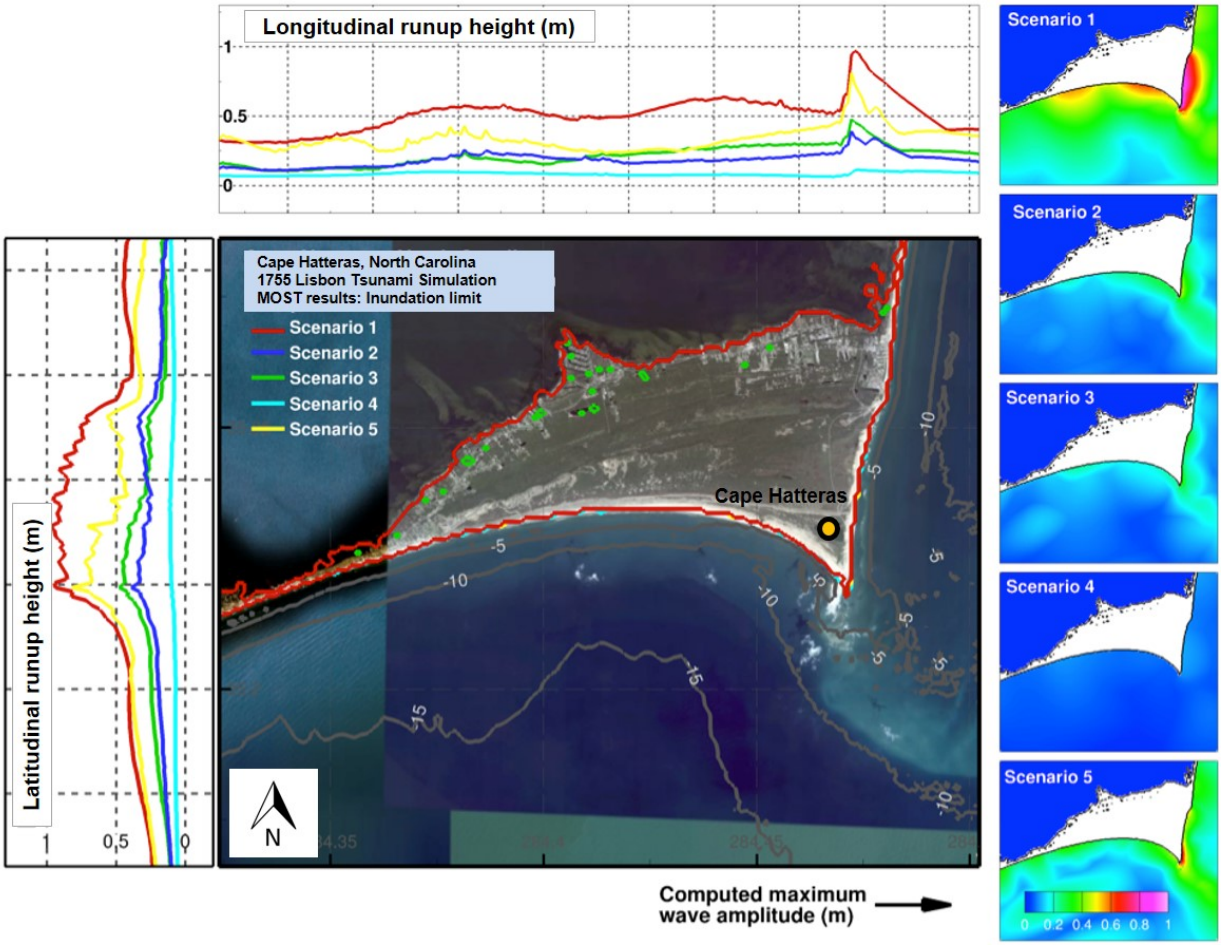

Figure 3.12: Comparison of the computed tsunami runup height, inundation extent, and maximum wave amplitude at Cape Hatteras caused by five earthquake scenarios shown in Figure 3.2.

The Caribbean region is prone to tsunamis because it has all of the possible tsunami-generating sources within a small geographical area including:

1) Subduction zone earthquakes along the Lesser Antilles and the Hispaniola (1946 tsunami) trench and the Puerto Rico trench of the type that generated the 2004 Indian Ocean tsunami.
2) Other moderately large earthquakes due to more local tectonic activity take place probably once a century, such as in Moa Passage (1918 tsunami),
3) In the Virgin Islands, landslides occur even more frequently. Submarine landslides contributed an unknown amount of energy to the tsunami sources mentioned above.
4) An active underwater volcano has been found near Grenada, where sea floor maps show previous episodes of flank collapse.
5) Above-water volcanic activities along much of the Lesser Antilles periodically generate landslides that enter the sea.

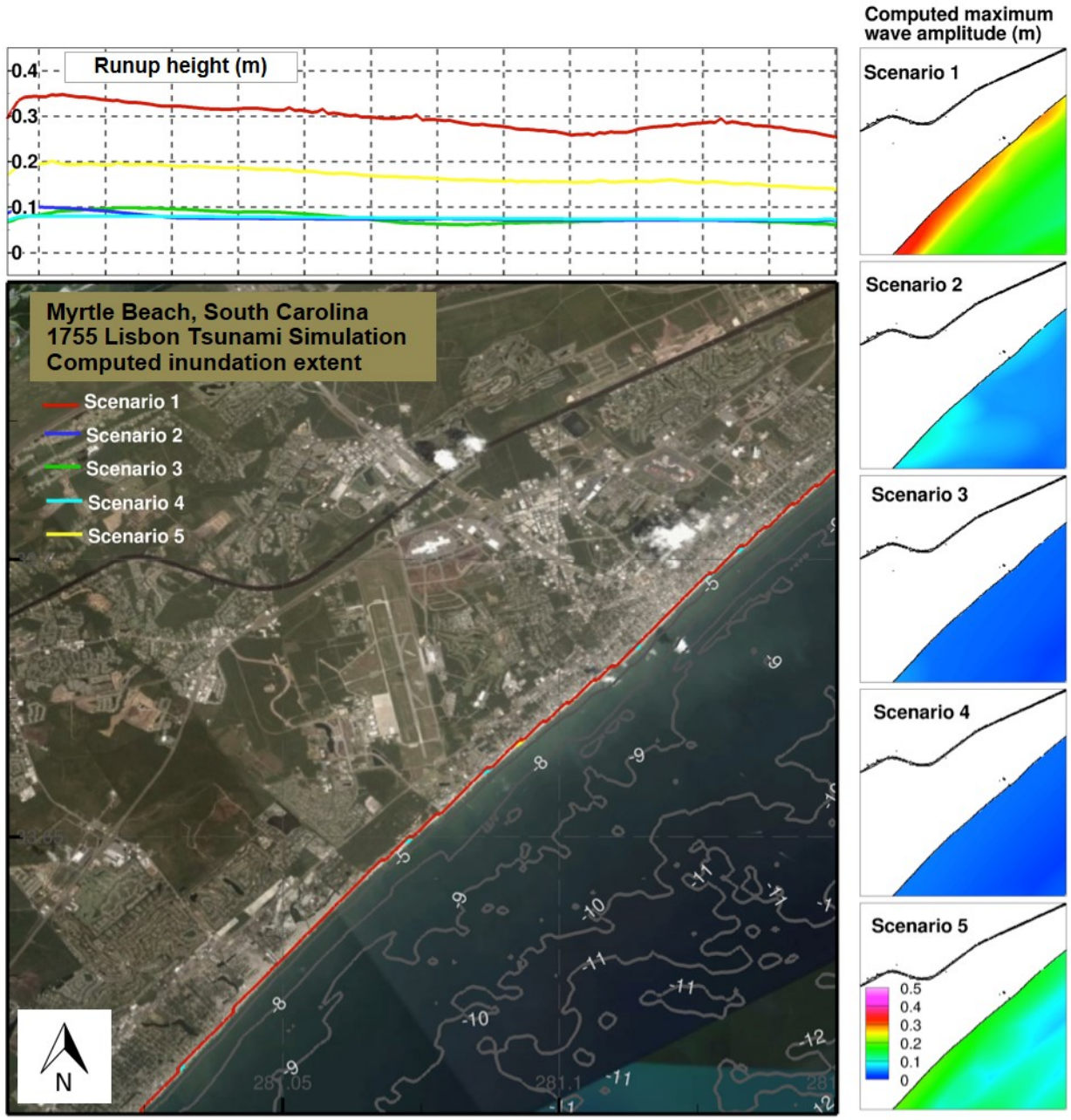

Figure 3.13: Comparison of the computed tsunami runup height, inundation extent, and maximum wave amplitude in Myrtle Beach caused by five earthquake scenarios shown in Figure 3.2.

3.3.2 Caribbean Tsunami Propagation Database for Hazard Assessment

The tsunami propagation database is set up by pre-computed earthquake events. Developing the offshore forecast database is possible because of the linearity of the generation and propagation dynamics of tsunamis. That is, base scenarios can be combined linearly to relate the earthquake parameters to the generated tsunami's height, period, and directionality offshore. The results of the propagation scenario also serve as input for the forecast model that

numerically predicts the tsunami wave height, current speeds, and inundation extent at a specific coastal area of interest.

The main objective of the pre-computed tsunami database is to provide offshore forecast of tsunami amplitudes and other wave parameters without having to run simulations immediately after a tsunamigenic event. The goal is to define an earthquake source region such that a linear combination of a finite number of tsunami sources in the database could closely reproduce the tsunami time series of the actual event. Each pre-defined earthquake source is referred to as a unit source. Gica et al. (2008) provided detailed procedures for developing the forecast propagation database for NOAA's tsunami forecast system. Each unit source has a default length of 100 km, a width of 50 km, and a fault-slip value of 1 m, corresponding to an M_w 7.5 earthquake. The strike angle for each unit source is set to align with the orientation of the subduction zone locally. The rake angle is set at 90°, since this is the most effective orientation for tsunami generation. The dip angle and depth values are based on a USGS study in progress that later led to the establishment of Slab Model 1.0 (Hayes et al., 2012). In the absence of a depth value, the B unit source uses a value of 5 km (depth of the top edge of the unit source), since it is believed that shallow faulting of large subduction zones are most effective in the generation of tsunamis. The depth value of the A unit source is easily calculated using simple trigonometry. Two rows of unit sources are set up, one for the shallower region and one for the deeper region. Additional rows may be possible depending on the characteristics of the region. These unit sources are located along the known fault zone for the entire Pacific, the Caribbean, and the Indian Ocean.

Figure 3.14 shows the layout of unit sources in the Caribbean source region. A total of 92 pairs of unit sources were developed to account for the tsunami sources based on the geological tectonic settings in the Caribbean.

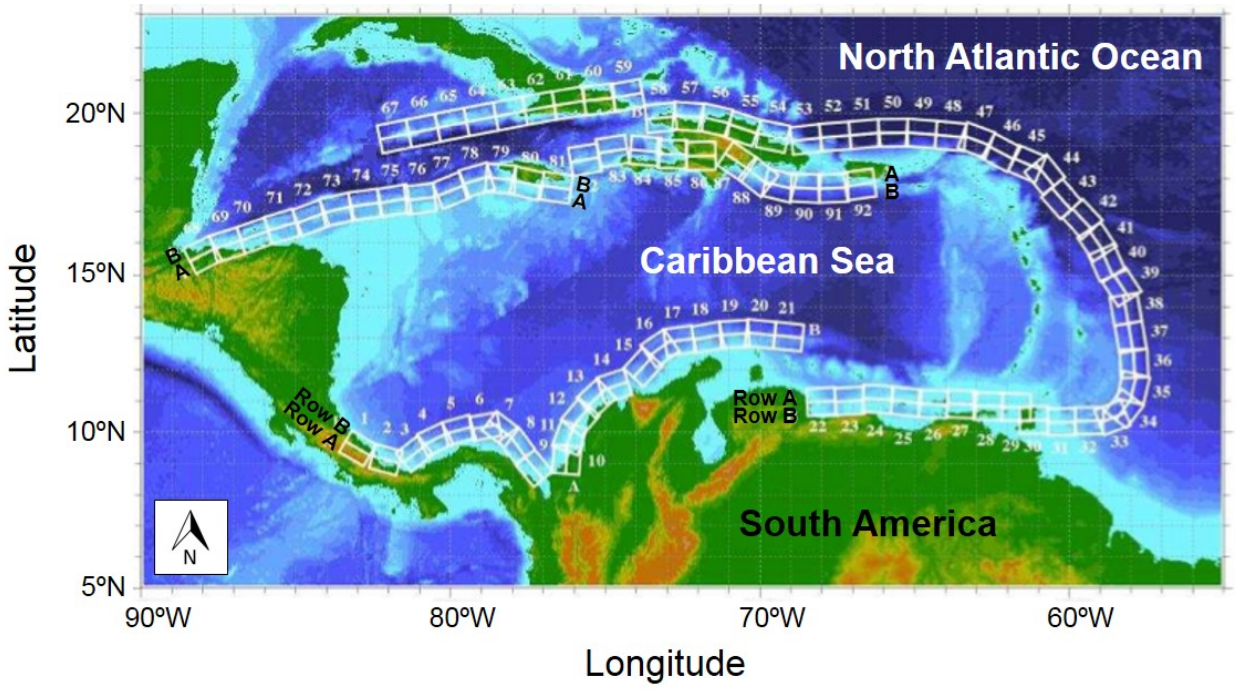

Figure 3.14: Tsunami unit sources in Caribbean source zone.

3.3.3 Scenario Tsunami Hazard Assessment along the U.S. East Coast

A tsunami hazard assessment for a model site can provide forecast guidance by determining in advance which subduction zone regions and tsunami magnitudes pose the greatest threats to the location. The validated forecast models, in combination with the forecast tsunami database, provide powerful tools to address this long-term forecast.

To date NOAA has completed the development of high-resolution tsunami forecast models for 75 coastal communities in the United States. All models have been thoroughly validated and tested. Among these forecast sites, the City of Virginia Beach happens to be within the second emergency planning zone (up to 80 km radius) of the Surry Nuclear Power Plant (Figure 3.15), and is thus chosen as an example to demonstrate the methodology of deterministic tsunami hazard assessment.

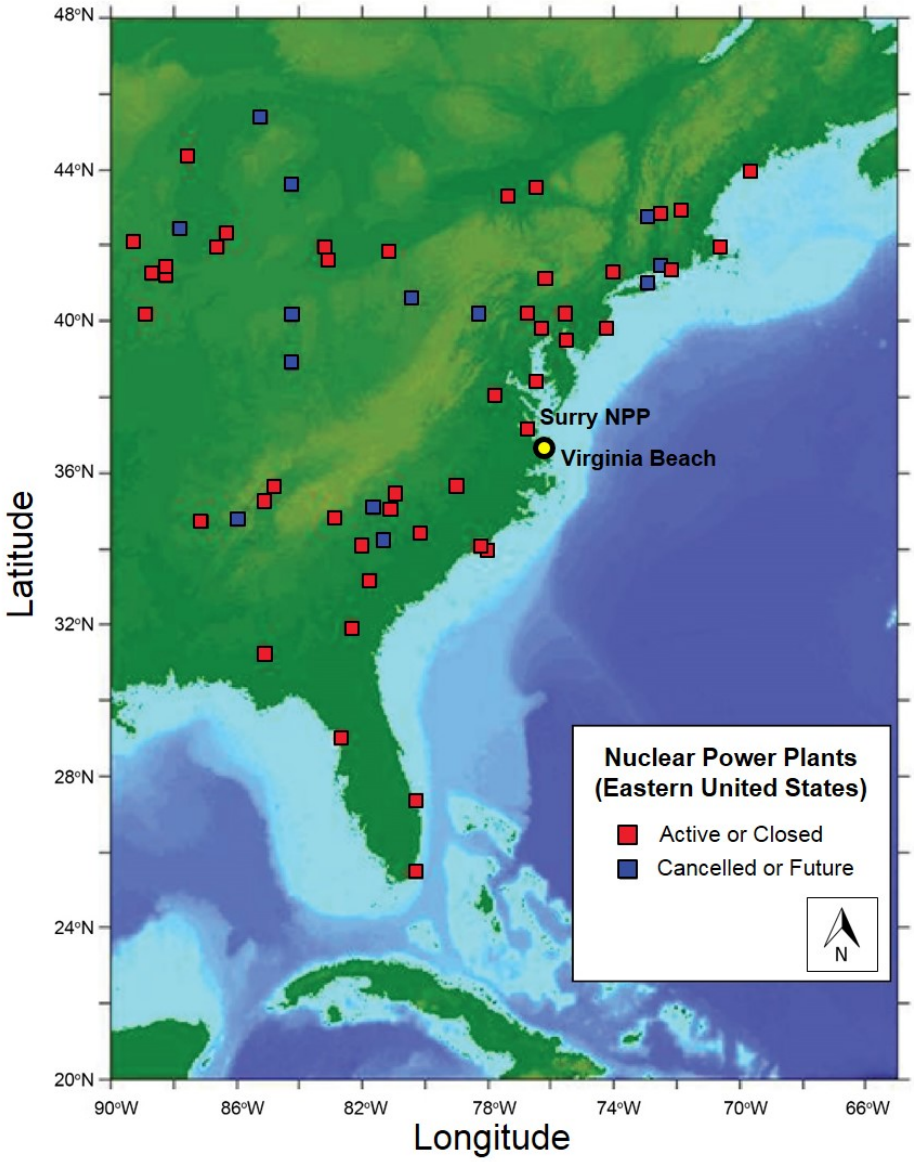

Figure 3.15: Locations of nuclear power plants in the Eastern United States.

Figure 3.16 shows the telescoped Digital Elevation Model (DEM) grids of Virginia Beach forecast model at increasing spatial resolution of 24 arc-second (≈600 m), 8 arc-second (≈200 m), and 3 arc second (≈75 to 90 m). The regional model studies in Section 3.1 have shown that a coarse resolution of 4 arc minutes (~7200 m) cannot fully resolve tsunami waves propagating on the continental shelf, and a grid resolution finer than 30 arc second (≈750 m) is needed to accurately model the tsunami dynamics in the shelf area. The eastern boundary of the outermost grid is placed further offshore, where water depth is greater than 2500 m, to smoothly adapt the boundary and initial conditions from the tsunami propagation database. The width of the continental shelf at Virginia Beach is approximately 120 km, and the average water depth is about 20 to 30 m. The water depth at the edge of the shelf break is about 50 m. The shallow shelf largely reduces the propagation speed of the tsunami waves to 14 to 17 m/s, about one order of magnitude smaller than in the deep ocean. However this increases the chances of a tsunami bore formation at the targeting coastline in the case of a major tsunami event. Mercado (2007) described in detail the development, modeling validation, and testing of the Virginia Beach forecast model.

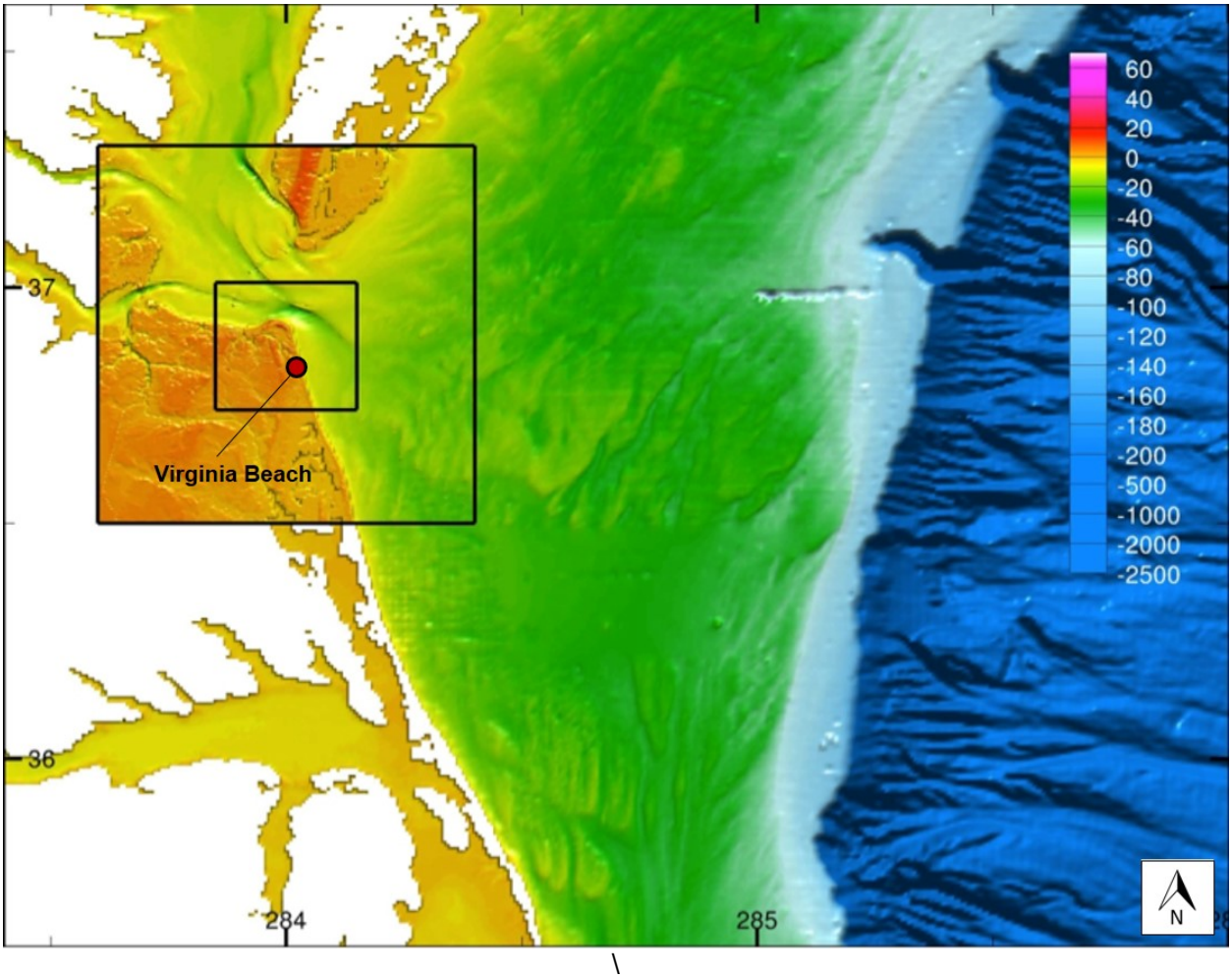

Figure 3.16: The telescoped Digital Elevation Model (DEM) grids of Virginia Beach forecast model at increasing spatial resolution of 24 arc-second (≈600 m), 8 arc-second (≈200 m), and 3 arc-second (≈75 m).

The developed forecast model is applied to provide long-term forecast assessment for Virginia Beach in the present study. There are no historical records of large earthquakes along the Puerto Rico Trench. The largest instrumentally recorded earthquake in the area is the 1943 M_w 7.3 event northwest of Puerto Rico (Dolan and Wald, 1998). ten Brink et al. (2008) proposed that a large, rare earthquake scenario for a fault rupture along the Puerto Rico Trench is a single rupture of a 675 km segment with a 10 m slip (a rupture area of 68,850 km^2), resulting in a M_w 8.8 event. The proposed slip direction is N60°E along an inclined interface with dip of 20°. In contrast to the Puerto Rico trench, slip on the Hispaniola segment of the trench further west is sub-perpendicular to the trench, hence a larger vertical motion is expected for a given magnitude of slip. ten Brink et al. (2008) proposed a M_w 8.1 earthquake with 10 m slip on a rupture area of 61,425 km^2.

In the present study, a total of 810 tsunami scenarios for five different moment magnitudes of 7.5, 7.9, 8.1, 8.6, and 8.9, in the Caribbean are computed to assess the tsunami impact along the coastline of Virginia Beach. Results from the modeled tsunami sources, detailed in Table 3.2, are summarized in Figure 3.17 to Figure 3.25 The modeling results show the most dangerous tsunami source areas in the Caribbean for Virginia Beach, and provide an overview of potential runups. Table 3.2 also summarizes the range of the maximum tsunami runups at Virginia Beach with respect to tsunamis generated from different magnitude sources in the Caribbean. One can see that the most critical tsunami source region in the Caribbean for Virginia Beach is the northern Caribbean plate, where the Hispaniola Trench, Puerto Rico Trench, and Lesser Antilles Trench are located. By inference, it was suggested that the Puerto Rico Trench is probably capable of generating a mega-tsunami that will affect the Atlantic coast of the U.S. ten Brink et al. (2008) pointed out that there are some fundamental differences between the Sumatra-Andaman trench and the Puerto Rico Trench. During the 2004 Indian Ocean tsunami, the slip in Sumatra was sub-perpendicular to the trench, despite the highly oblique convergence angle. ten Brink and Lin (2004) showed that slip during earthquakes in the Puerto Rico Trench is highly oblique and almost parallel to the convergence direction. Therefore, only a small component of thrust motion is expected during large earthquakes. The proposed N60°E slip direction (ten Brink et al., 2008) may generate only half the tsunami energy as compared with a pure thrust event, but the resulting M_w 8.8 event would be still large enough to produce damage to much of the U.S. East Coast.

Table 3.2: Source parameters and computational results of the tsunami scenarios in the Caribbean used for the hazard assessment study at Virginia Beach, Virginia. The unit sources in row b have a focal depth of 5 km, and the unit sources in row A are associated with a greater focal depth along the dip-slip direction of row B.

M_w	No. of unit sources	Source Length (km)	Source Width (km)	Fault Slip (m)	Row of sources	Number of scenarios	Range of max computed water level (m)
7.5[2]	1	100	50	1.0	A or B	184	0.0001 – 0.16
7.9	2	200	50	2.1	A or B	182	0.001 – 0.70
8.1	2	200	50	4.2	A or B	182	0.003 – 1.71
8.6	5	500	50	9.5	A or B	176	0.01 – 3.66
8.9	14	700	100	9.6	A or B	86	0.04 – 4.59

[2] A unit sub-fault in the PMEL pre-computed database has a moment magnitude of 7.5, assuming a crustal rigidity of 4×10^{11} dyne/cm^2.

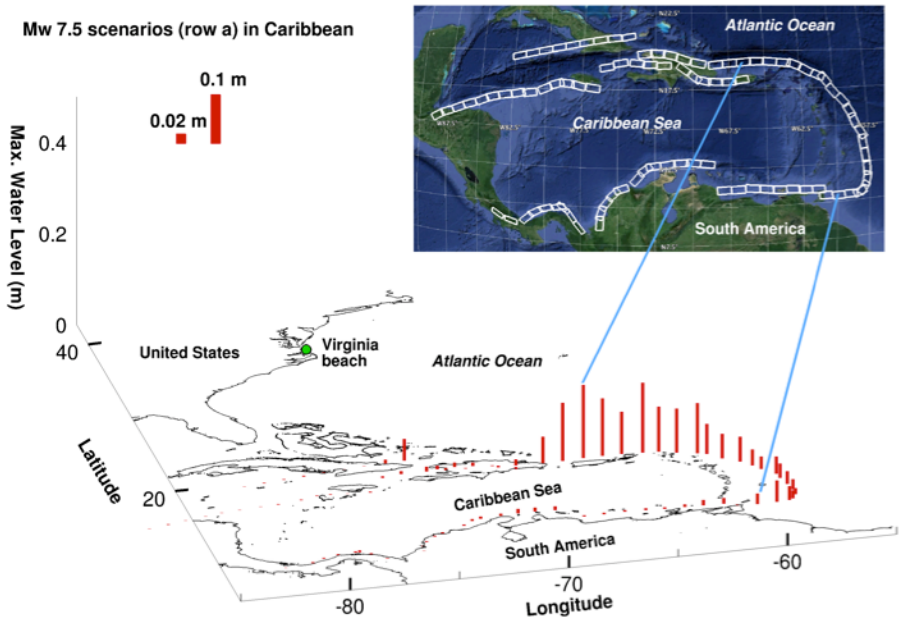

Figure 3.17: Computed maximum tsunami runup in Virginia Beach using high-resolution tsunami inundation forecast model due to a suite of M_w 7.5 (row A) tsunami scenarios in the Caribbean.

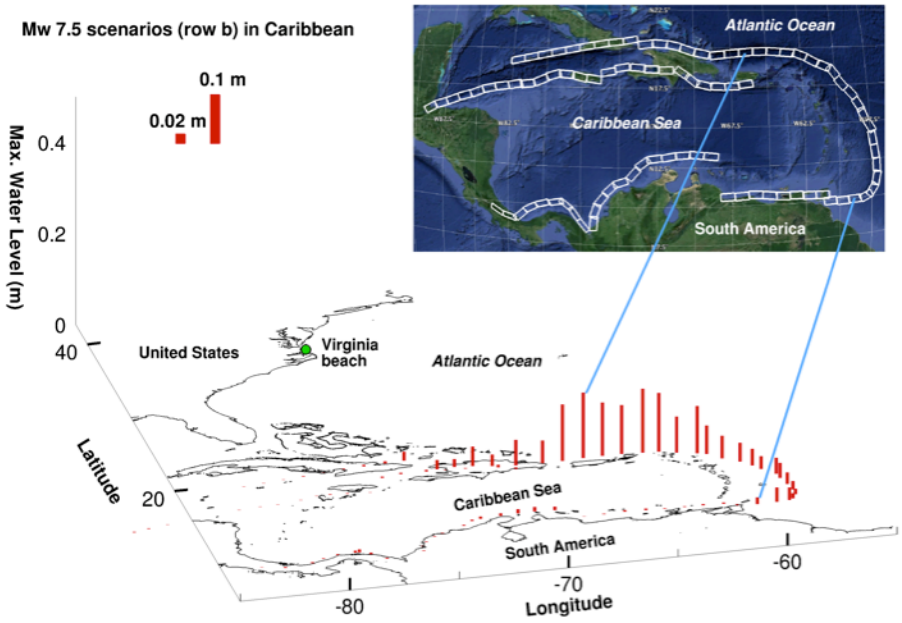

Figure 3.18: Computed maximum tsunami runup in Virginia Beach using high-resolution tsunami inundation forecast model due to a suite of M_w 7.5 (row B) tsunami scenarios in the Caribbean.

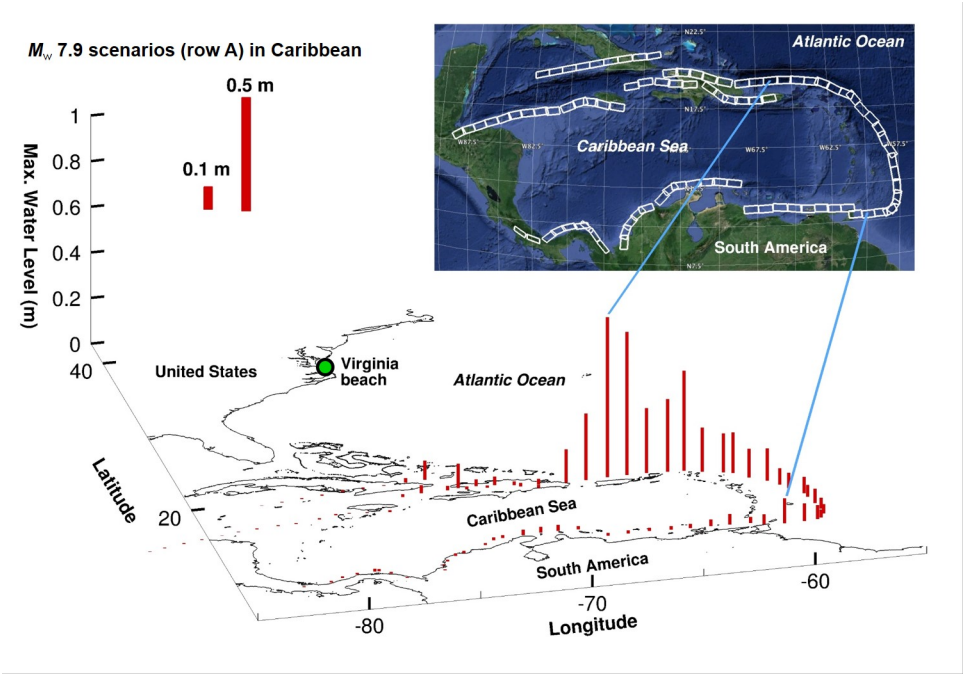

Figure 3.19: Computed maximum tsunami runup in Virginia Beach using high-resolution tsunami inundation forecast model due to a suite of M_w 7.9 (row A) tsunami scenarios in the Caribbean.

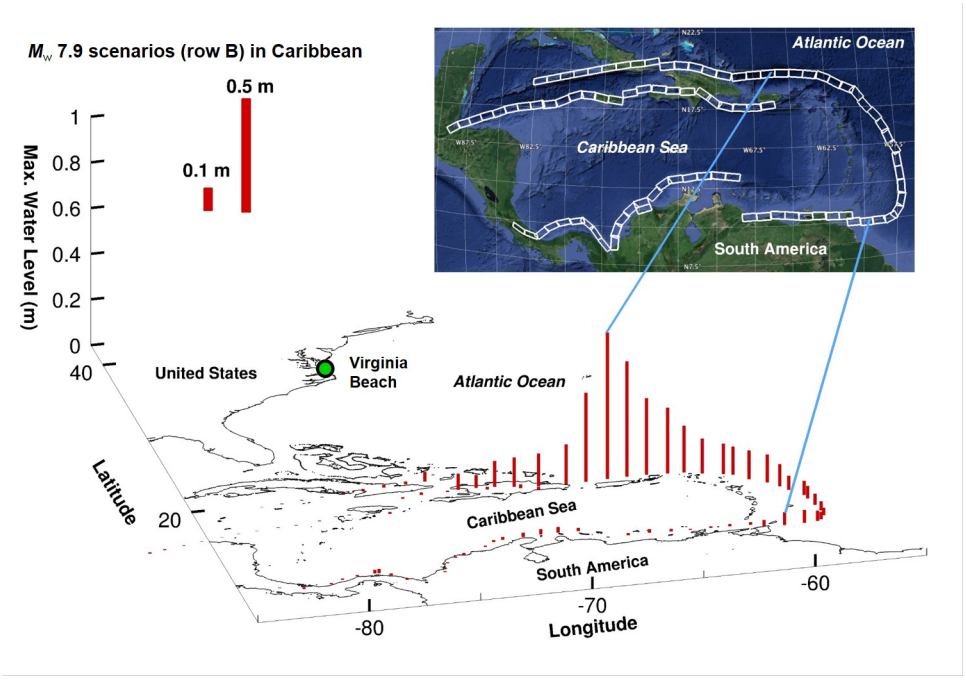

Figure 3.20: Computed maximum tsunami runup in Virginia Beach using high-resolution tsunami inundation forecast model due to a suite of M_w 7.9 (row B) tsunami scenarios in the Caribbean.

Figure 3.25 shows the computed maximum tsunami water level generated by a M_w 8.9 earthquake may reach about 4.6 m above the Mean High Water (MHW) along the coastline of Virginia Beach. Figure 3.26 and Figure 3.27 show the maximum wave amplitudes and current

speeds, respectively, due to a M_w 8.9 tsunami scenario in the Puerto Rico Trench. This scenario consists of 14 unit sources with a 9.6 m slip over a fault area of 70,000 km^2 (numbering from 49 to 55 in Figure 3.14). Figure 3.26 (a) shows that the main energy of the generated tsunami is directed to the U.S. East Coast. The wave amplitudes in the deep ocean exceeds 0.5 m, which is comparable to the offshore wave amplitudes observed during the 2004 Sumatra tsunami. Figure 3.26 (b), (c), and (d) show tsunami focusing due to local bathymetric and topographic features, which results severe impact along the coastline of the City of Virginia Beach and its vicinity. The computed current speed along this segment of coastline is generally greater than 2 m/s (Figure 3.28).

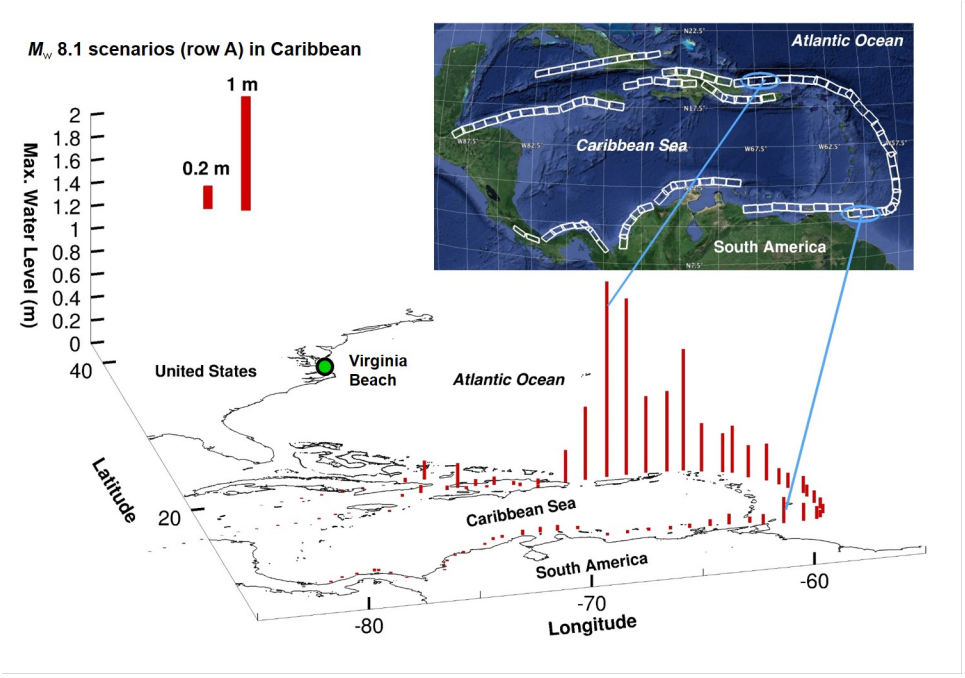

Figure 3.21: Computed maximum tsunami runup in Virginia Beach using high-resolution tsunami inundation forecast model due to a suite of M_w 8.1 (row A) tsunami scenarios in the Caribbean.

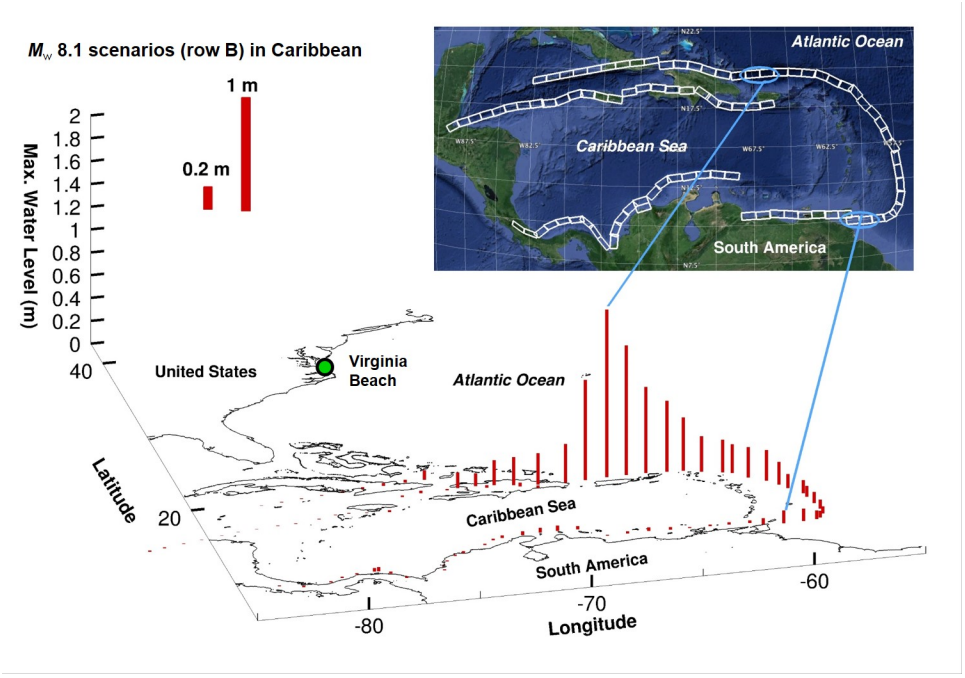

Figure 3.22: Computed maximum tsunami runup in Virginia Beach using high-resolution tsunami inundation forecast model due to a suite of M_w 8.1 (row B) tsunami scenarios in the Caribbean.

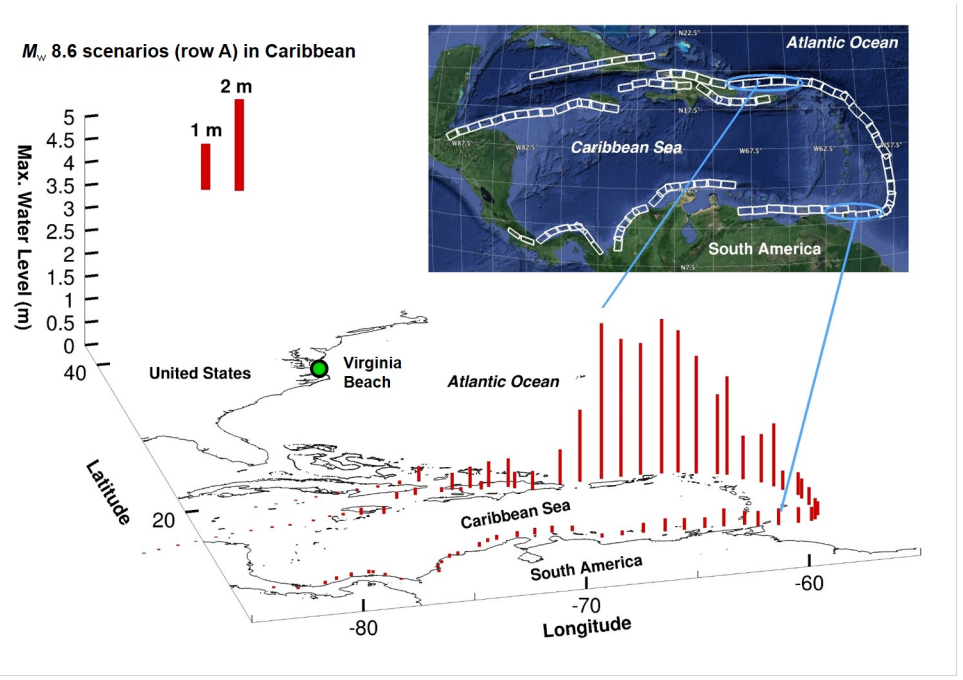

Figure 3.23: Computed maximum tsunami runup in Virginia Beach using high-resolution tsunami inundation forecast model due to a suite of M_w 8.6 (row A) tsunami scenarios in the Caribbean.

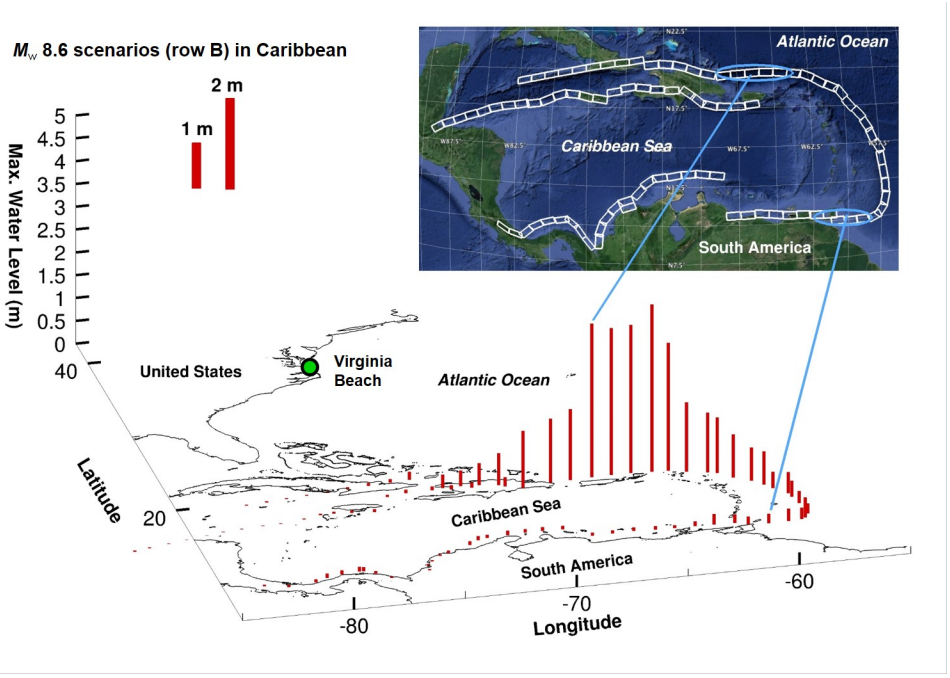

Figure 3.24: Computed maximum tsunami runup in Virginia Beach using high-resolution tsunami inundation forecast model due to a suite of M_w 8.6 (row B) tsunami scenarios in the Caribbean.

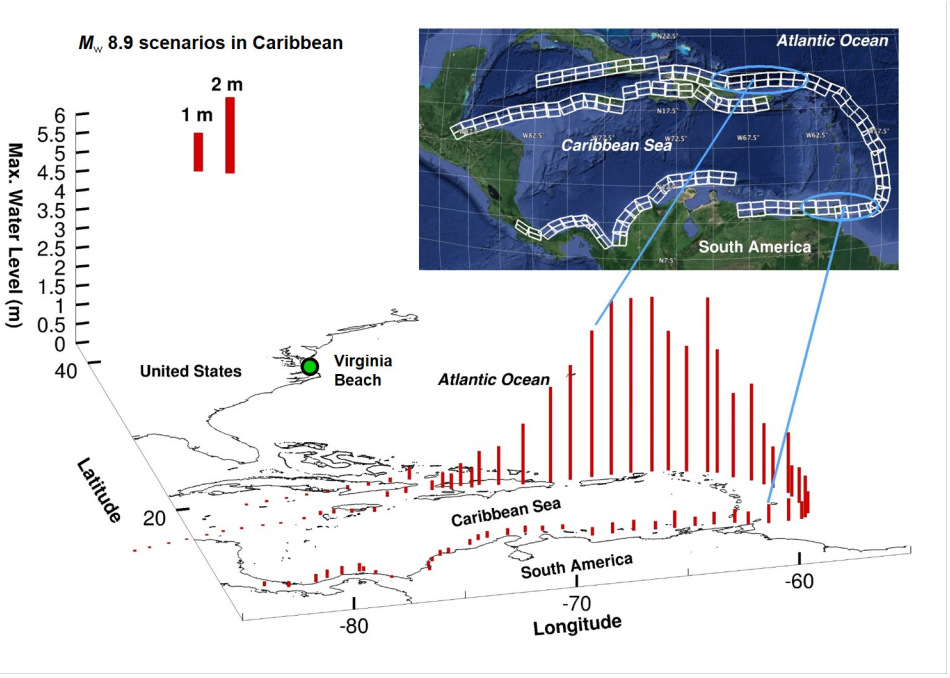

Figure 3.25: Computed maximum tsunami runup in Virginia Beach using high-resolution tsunami inundation forecast model due to M_w 8.8 tsunami scenarios in the Caribbean.

As commented in the regional study in Section 3.1, the directionality and local bathymetry are the fundamental factors that influence the energy distribution of tsunami waves. A model that is

not fine enough to resolve local bathymetric, is not capable of producing accurate (or correct) modeling results for a specific coastline. An ocean-scale tsunami propagation modeling with a coarse grid resolution may provide an overview of the affected segments of the coastline, but overlook tsunami energy focusing as shown in Figure 3.26 and Figure 3.27 due to lack of detailed modeling of tsunami dynamics over local features, particularly with the existence of continental shelf. Tang et al. (2009) also showed that larger amplitudes offshore do not necessarily produce larger amplitudes at the coastline, and that larger tsunami magnitudes may not produce larger waves. The trend of offshore - coastline wave amplitudes are site specific. High-resolution inundation models are developed to provide more accurate tsunami hazards assessment for coastal communities at risk, and therefore it is suggested in the present study that they are needed when tsunami risk is taken into account in siting studies of NRC.

3.3.4 Tsunami Wave Dynamics over the Continental Shelf

Tsunami wave dynamics at the coastline and in the harbors is affected by the depth ratio and the width of the continental shelf (Liu, 1983). The width of continental shelf at Virginia Beach is about 120 km, and the water depth ratio $h_1/h_2 \leq 1/60$, where h_1 is the water depth on the continental shelf and h_2 is the water depth in the ocean basin.

Figure 3.28 shows the computed maximum wave amplitude and maximum current speed along a profile running from a depth of 2,500 m outside the continental shelf, to a depth of 5 m along the coastline, across the whole width of the continental shelf. One can clearly see three-stage amplification in wave amplitudes and current speed: before the continental shelf, over the continental shelf, and at the coastline. Outside the continental shelf, the maximum wave amplitude increases smoothly as the water depth decreases. However, the current speed remains nearly constant until the tsunami wave encounters the edge of the continental shelf, where the water depth drops abruptly from 2,000 m to 50 m.

Figure 3.28b shows an increase in the maximum wave amplitude from 0.5 m to 1 m, as the tsunami waves propagate from deep ocean to the top of the continental shelf. At the same time, the current speed changes rapidly from 0.03 m/s to 0.5 m/s, a 17 fold increase. The amplification of tsunami waves over the continental shelf is gradual, less than 50 percent increase in both the wave amplitude and current speed, until the waves reach the coast and start to intensify over a short distance. The wave height at virtual gauge 11 is about 2.1 m, lower than the maximum wave height of 4.6 m in the grid in the vicinity of Virginia Beach (Section 3.3.3 and Table 3.2). A tsunami bore is likely to form upon reaching the shoreline, where wave amplitude decreases while the current speed increases (between gauge 10 and 11).

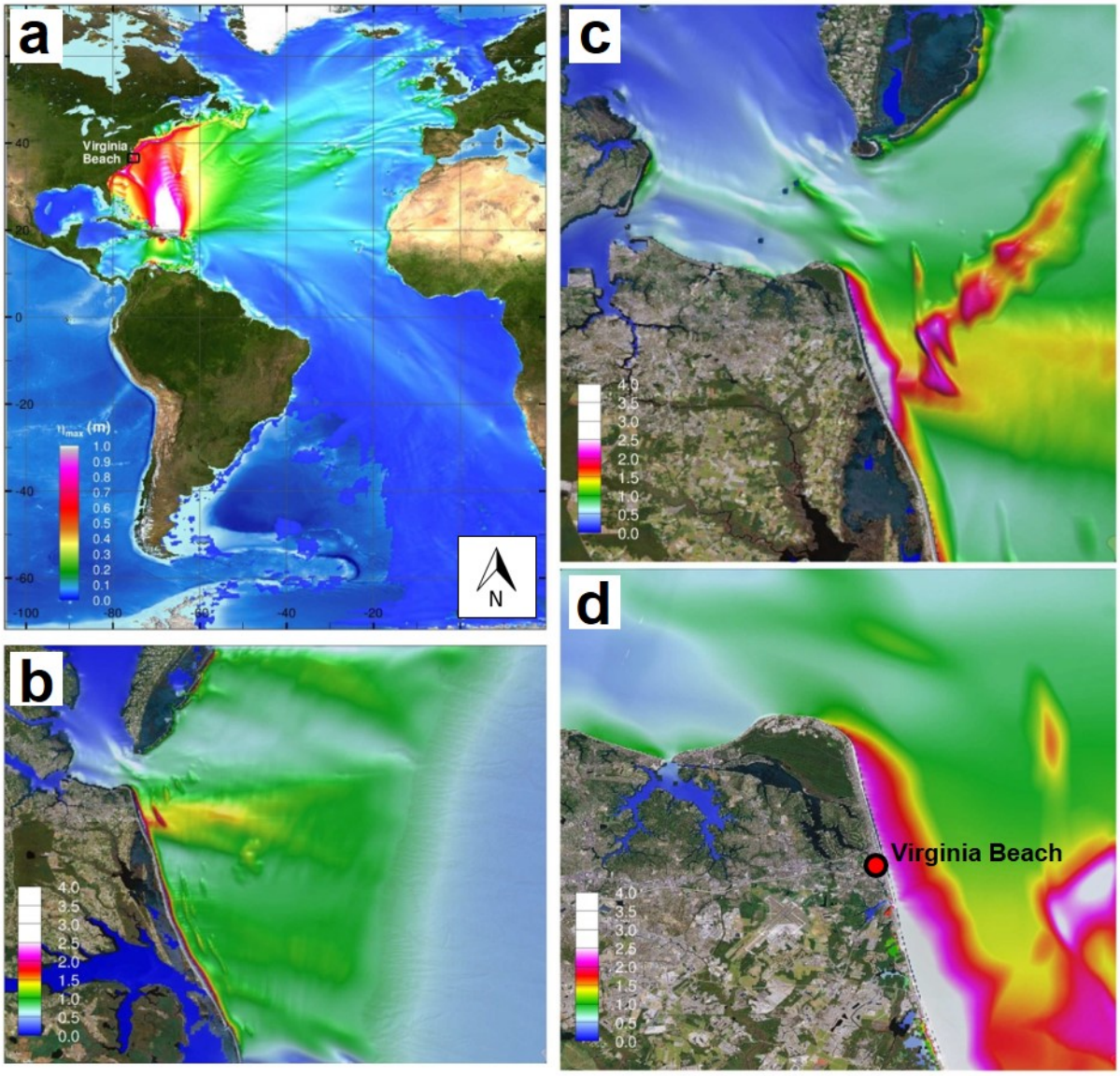

Figure 3.26: Computed maximum tsunami wave amplitude from an M_w 8.8 tsunami scenario using two rows of unit sources 49 to 55: (a) Atlantic Basin; (b) over continental shelf of Virginia Beach; (c) coastal area of Virginia Beach; and (d) coasts of Virginia Beach.

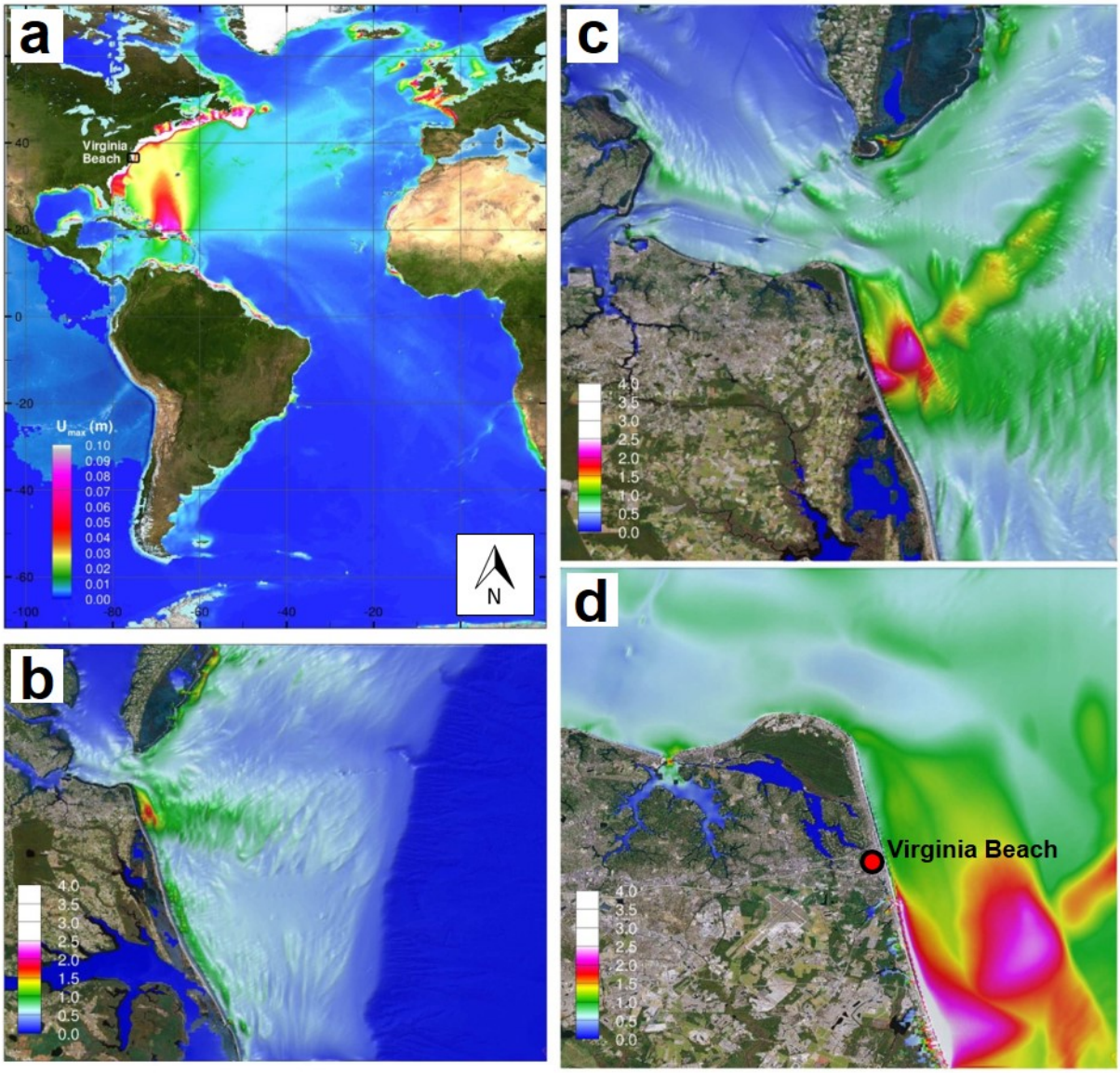

Figure 3.27: Computed maximum tsunami current speed from an M_w 8.8 tsunami scenario using two rows of unit sources 49 to 55: (a) Atlantic Basin; (b) over continental shelf of Virginia Beach; (c) coastal area of Virginia Beach; and (d) coasts of Virginia Beach.

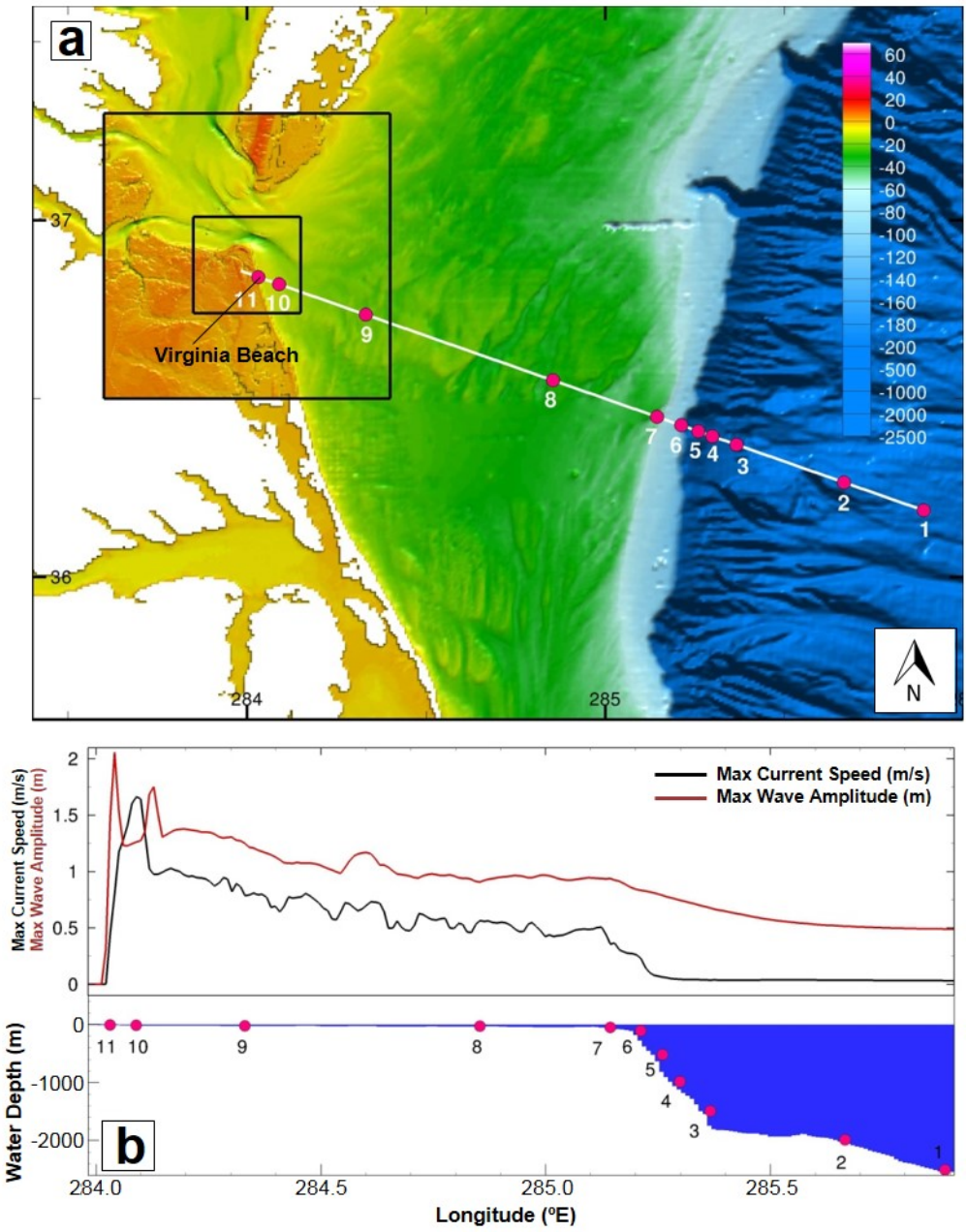

Figure 3.28: Computed maximum tsunami wave amplitude and current speed along a profile from deep ocean to coastline across the continental shelf of Virginia Beach. (a) Modeling profile and location of virtual gauges; (b) Maximum wave amplitude and current speed along the profile.

Figure 3.29 shows the time series of tsunami waves at the 11 virtual gauges shown in Figure 3.28a. Figure 3.29 demonstrates the evolution of the tsunami waves from deep ocean to coastline, over the continental shelf. The red line is the modeling time series computed by the high-resolution forecast model, and the black line is the modeling time series extracted from the propagation database run at a 4 arc-minute grid resolution. Figure 3.29 clearly demonstrates the importance and necessity of a high-resolution model in order to accurately and correctly compute the tsunami dynamics in the coasts. The time series at gauge 1 to 3, located in deep

water (≥1,500 m), shows nearly identical computation results between high-resolution inundation model and propagation model, indicating the linearity of the tsunami waves in the

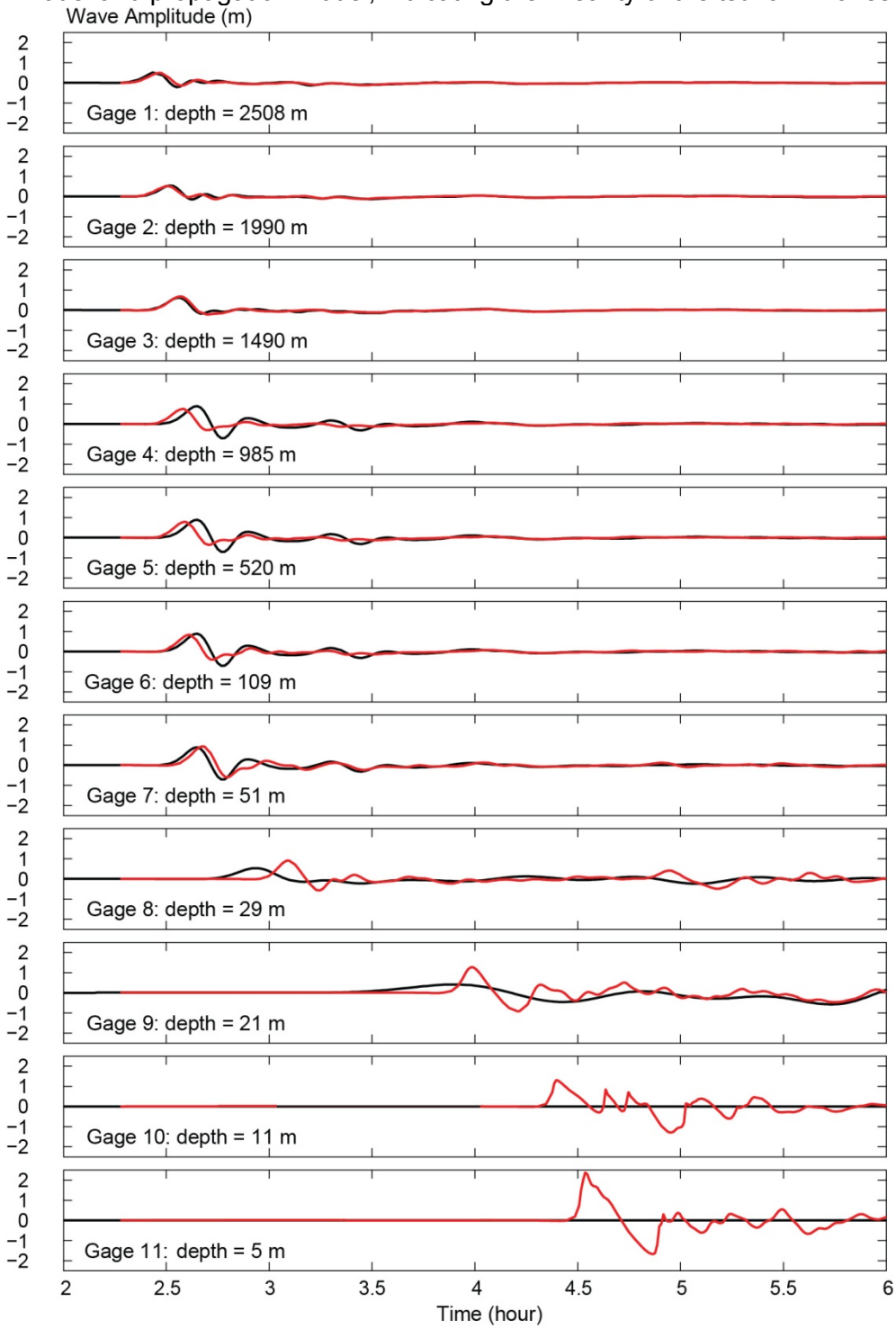

Figure 3.29: Modeled time series at virtual gauges along the profile depicted in Figure 3.11, where the black line indicates time series extracted from propagation database (Gica et al., 2008), and the red line indicates time series computed from high-resolution inundation forecast model.

deep ocean. The modeled waves start to show differences, mainly when the waves are in the transition from deep ocean to continental shelf. Larger discrepancies, in both arrival time and wave amplitude, are seen at gauges 8 and 9, where the tsunami waves propagate over the continental shelf. The propagation model significantly underestimates the tsunami wave amplitude, which may be caused by both the bathymetric inaccuracy and coarse grid resolution.

Although the tsunami wave dynamics over the continental shelf needs to be carefully investigated in a systematic manner, the example given in Figure 3.28 and Figure 3.29 has re-emphasized the importance of using a high-resolution inundation forecast model to compute the tsunami dynamics in coastal areas rather than directly obtaining them from a propagation model. The nonlinearity of tsunami wave dynamics due to local bathymetric feature and shoaling effect can only be fully modeled with a high-resolution inundation model. A short-term or long-term tsunami hazard forecast based on purely linear propagation model may result in false decisions, and endanger the community.

3.4 Conclusions

The high-resolution tsunami inundation model and pre-computed tsunami propagation database developed within NOAA's tsunami forecast system have largely improved the capability of short-term and long-term tsunami forecast and hazard assessment.

The great Lisbon earthquake of November 1, 1755, with an estimated moment magnitude of 8.0 to 9.0, was the most destructive earthquake in European history. The associated tsunami runup was reported to have reached 5 to 15 m along the Portuguese and Moroccan coasts. The present study employs high-resolution tsunami inundation forecast models to simulate the 1755 Lisbon tsunami dynamics in the coasts where historical accounts are available. The present study investigated the tsunami impact due to the 1755 Lisbon earthquake at two near-field coasts (Boca do Rio in Portugal and Casablanca in Morocco), five coasts in the Caribbean (Guadeloupe, Fajardo, Ponce, Mayaguez, and San Juan), and three coasts in eastern U.S. (Virginia Beach, Cape Hatteras, and Myrtle Beach). Among all 5 proposed earthquake sources, the inundation study results are in favor of a tsunami due source number 1 (M_w 8.5 with an east-northeast fault orientation). The inundation modeling of this source resulted in up to a 15 m flow-depth at Boca Do Rio. This is comparable to the historical records of a 10 m flow depth. Modeling in the Caribbean shows this source has produced significant tsunami flooding at Fajardo, Puerto Rico, but shows no inundation at other Caribbean coasts investigated in the present study. This source resulted in minor tsunami impact at the three U.S coasts with a maximum wave amplitude of 1.5 m at Virginia Beach. A recent publication by Muir-Wood and Mignan (2009) has proposed a M_w 9.0 scenario for the 1755 Lisbon tsunami, which was not considered in the present study but will be evaluated in the near future.

The north Caribbean plate is capable of generating tsunamis comparable to the destructive 2004 Indian Ocean tsunami. Tsunami arising from the Caribbean earthquakes may be hazardous for many parts of the U.S. East Coast. The present study describes a methodology of utilizing the previously developed tsunami propagation database and the high-resolution tsunami inundation model to conduct a deterministic tsunami hazard assessment. Linear combinations of the unit tsunami propagation sources are used to construct tsunami scenario earthquakes of different magnitudes (M_w 7.5, 7.9, 8.1, 8.6, and 8.9). To demonstrate the application of this methodology, a total of 810 tsunami scenarios at these magnitudes were used to study the tsunami inundation impact for Virginia Beach, where the Surry Nuclear Power Plant is located 50 miles inland from the City of Virginia Beach. The high-resolution Virginia

Beach tsunami inundation forecast model indicates that the maximum tsunami runup heights are 0.2 m, 0.7 m, 1.7 m, 3.7 m, 4.6 m, for earthquake magnitudes of M_w 7.5, 7.9, 8.1, 8.6, and 8.9, respectively. The modeling results also indicate that among all of the Caribbean tsunami sources, the subducting segment (C51) in the Puerto Rico Trench produces the most serious tsunami impact at the coastline of Virginia Beach. The numerical study using the worst-case M_w 8.9 tsunami scenario showed the importance of implementing a high-resolution tsunami inundation model rather than estimation from a linear tsunami propagation model.

The inundation study illustrated in the present study highlights the necessity of high-resolution tsunami forecast models in short-term and long-term tsunami forecast and hazard assessment. A tsunami forecast or hazard assessment without such models may lead to false decisions and endanger the coastal communities or facilities.

3.5 Bibliography

Baptista, M.A., J.M. Miranda, F. Chiericci, N. Zitellini (2003). New study of the 1755 earthquake source based on multi-channel seismic survey data and tsunami modeling, *Nat. Hazards and Earth Syst. Sci.*, 3, 222-340.

Bernard, E., and A. Robinson (Eds.) (2009). *The Sea, Volume 15: Tsunamis*, 450 pp., Harvard University Press, Cambridge, MA and London, England.

DeMets, C., P. Jansma, G. Mattioli, T. Dixon, F. Farina, R. Bilham, E. Calais, and P. Mann (2000). GPS geodetic constraints on Caribbean-North American plate motion, *Geophys. Res. Lett.*, pp. 437–440.

Dolan, J., and D. Wald (1998). The 1943-1953 north-central Caribbean earthquakes: Active tectonic setting, seismic hazards, and implications for Caribbean-North America plate motions, *Geological Society of American Special publications*, *326*, 143–170.

Gica, E., M. Spillane, V. Titov, C. Chamberlin, and J. Newman (2008). Development of the forecast propagation database for NOAA's short-term inundation forecast for tsunamis (SIFT). NOAA Technical Memorandum OAR PMEL-139, Tech. rep., NOAA Pacific Marine Environmental Laboratory, Seattle, WA.

Greenslade, D., and V. Titov (2008). A comparison study of two numerical tsunami forecasting systems, *Pure Appl. Geophys.*, *165*, 1991–2001, doi:10.1007/s00024-008-0413-x.

Grindlay, N., and M. Hearne (2005). High risk of tsunami in the northern Caribbean, *EOS, Transactions, American Geophysical Union*, *86(12)*, 121–126.

Hayes, G. P., D. J. Wald, and R. L. Johnson (2012), Slab1.0: A three-dimensional model of global subduction zone geometries, J. Geophys. Res., 117, B01302, doi:10.1029/2011JB008524.

Kuwayama, T. (2007). Quantitative tsunami forecast system, ICG/PTW Tsunami Warning Center Coordination Meeting, Honolulu, HI, 17-19 January 2007.

O'loughlin, K.F. and J.F. Lander (2003). Caribbean Tsunamis–A 500-year History from 1498-1998, Kluwer Academic Publishers, 263pp.

Omira, R. M.A. Baptista, S. Mellas, F. Leone, N. Meschinet de Richemond, B. Zourarah and J-P. Cherel (2012). The November, 1st, 1755 Tsunami in Morocco: Can Numerical Modeling Clarify the Uncertainties of Historical Reports?. InTech Book Chapter 4, doi: 10.5772/51864.

Roger, J., M.A. Baptista, A. Sahai, F. Accary, S. Allgeyer, and H. Hebert (2010a). The transoceanic 1755 Lisbon tsunami in Martinique, Pure and Appl. Geophys.,168(6-7), 1015-1031.

Roger, J., S. Allgeyer, H. Herbert, M.A. Baptista, A. Loevenbruck, and F. Schindele (2010b). The 1755 Lisbon tsunami in Guadeloup Archipelage: source sensitivity and investigation of resonance effects, *The Open Oceangra. Journal*, 4, 58-70.

Synolakis, C., E. Bernard, V. Titov, U. Kaˆnogˇ lu, and F. Gonza´lez (2009). Validation and verification of tsunami numerical models, *Pure Appl. Geophys*, *165*((11-12)), 2197– 2228.

Tang, L., V. V. Titov, and C. D. Chamberlin (2009). Development, testing, and applications of site-specific tsunami inundation models for real-time forecasting, *J. Geophys. Res.*, 114, C12025 doi: 10.1029/2009JC005476.

Tatehata, H. (1997). The new tsunami warning system of the Meterological Agency, 175-188 pp., Kluwer.

ten Brink, U., and J. Lin (2004). Stress interaction between subduction earthquakes and forearc strike-slip faults: modeling and application to the northern Caribbean plate boundary, *J. of Geophys. Res., B12310*, 109, doi: 12310.11029/12004JB003031.

ten Brink, U.S., D. Twichell, E. Geist, J. Chaytor, J. Locat, H. Lee, B. Buczkowski, R. Barkan, A. Solow, B. Andrews, T. Parsons, P. Lynett, J. Lin, and M. Sansoucy (2008). Evaluation of tsunami sources with the potential to impact the U.S. Atlantic and Gulf coasts – an updated report to the nuclear regulatory commission, Tech. rep., U.S. Geological Survey (ML082960196).

Tang, L., V.V. Titov, E.N. Bernar, Y. Wei, C.C. Chamberlin, M. Eble, C. Moore, B. Uslu, J. C. Newman, C. Pells, M. Spillane, H.O. Mofjeld, and L. Wright (2013). Direct energy estimation of the 2011 Japan tsunam using deep-ocean pressure measurements, *J. Geophys. Res.*, in press.

Tang, L., V. V. Titov, and C. D. Chamberlin (2009). Development, testing, and applications of site-specific tsunami inundation models for real-time forecasting, *J. Geophys. Res.*, 114, C12025, doi:10.1029/2009JC005476.

Titov, V. (2009). *The Sea, Volume 15, Chapter 12: Tsunami forecasting*, 371-400 pp., Harvard University Press, Cambridge, MA and London, England.

Titov, V., F. Gonza´lez, E. Bernard, M. Eble, H. Mofjeld, J. Newman, and A. Venturato (2005). Real-time tsunami forecasting: Challenges and solutions, *Nat. Hazards*, *35(1), Special Issue, U.S. National Tsunami Hazard Mitigation Program*, 41.

Wei, Y., E. Bernard, L. Tang, R. Weiss, V. Titov, C. Moore, M. Spillane, M. Hopkins, , and U. Kaˆnogˇ lu (2008). Real-time experimental forecast of the Peruvian tsunami of August 2007 for U.S. coastlines, *Geophys. Res. Lett.*, *35* (L04609), doi:10.1029/2007GL032250.

Wei, Y. C.D. Chamberlin, V.V. Titov, L. Tang, and E.N. Bernard (2012). Modeling of the 2011 Japan tsunami – lessons for near-field forecast. *Pure and Applied Geophysics*, in review.

Whitmore, P. (2009). *The Sea, Volume 15, Chapter 13: Tsunami warning systems*, 401-442pp., Harvard University Press, Cambridge, MA and London, England.

4. LANDSLIDE HAZARDS FROM LA PALMA ISLAND

4.1 Introduction

This study investigates the possible effect on the U.S. Atlantic coast of a tsunami generated by the hypothetical collapse of the Cumbre Vieja volcano located on the Isla La Palma in the Canary Islands. Well-publicized studies of this scenario conducted by Ward and Day (2001) and Løvholt et al. (2008) suggest that the impact may be severe. Subsequent to the initial publication, more credible worst-case scenarios have been modeled to study wave evolution in the impact zone, open ocean, and continental shelf. However, these more recent studies lack an inundation model, and use a crude Green's law scaling assumption to estimate wave heights at the beach. In this study, an Eulerian-Lagrangian hydrocode is used to simulate the landslide impact, a numerically dispersive linear shallow-water model (MOST) for open-ocean propagation, and a nonlinear inundation model to quantify impact at the coast. These more robust approaches provide a better estimate of the potential hazard on the U.S. coastline posed by the Cumbra Vieja volcano.

This research aims to characterize landslide tsunami sources that can have significant impact to the Gulf Mexico and the Atlantic Coasts of the USA. The development and testing of the new landslide hydrocode within the NOAA modeling approach will allow us to apply this well-benchmarked numerical technique to both evaluate the Canary Islands' possible impact on the coastal United States, and to use field data to investigate landslide locations at the continental slope. This report gives an overview of progress to date.

4.2 Modeling Setup

The geometry of the various models used is shown in Figure 4.1. Using the Impact Simplified Arbitrary Lagrangian-Eulerian (iSALE) multi-material hydrocode, a landslide at La Palma is simulated in one horizontal dimension (1HD) assuming an instantaneous flank release at Cumbre Vieja. A total slide volume of 430 km^3 is used in the model. The iSALE code is discussed in more detail in Section 4.3. The volume and geometry, which were taken from Ward and Day (2001), are thought by many, including Masson et al. (2006), to be highly unrealistic. However, these parameters were used to represent the extreme upper limit. For the landslide simulation, a grid with a 125 km horizontal extent and 25 m resolution was used. The resulting waveform from this landslide model was passed to the MOST numerical model for the propagation phase, assuming a plane-wave solution at the end of the iSALE grid extent ($T = 320\ s$). The MOST model for propagation is a linear shallow-water model, the output of which is used to drive a non-linear version of MOST for modeling wave evolution across the continental shelf at several locations along the U.S. Atlantic coast. The MOST model is the core numerical code used for tsunami hazard modeling for the U.S. tsunami warning system, and is discussed further in Section 1.2.

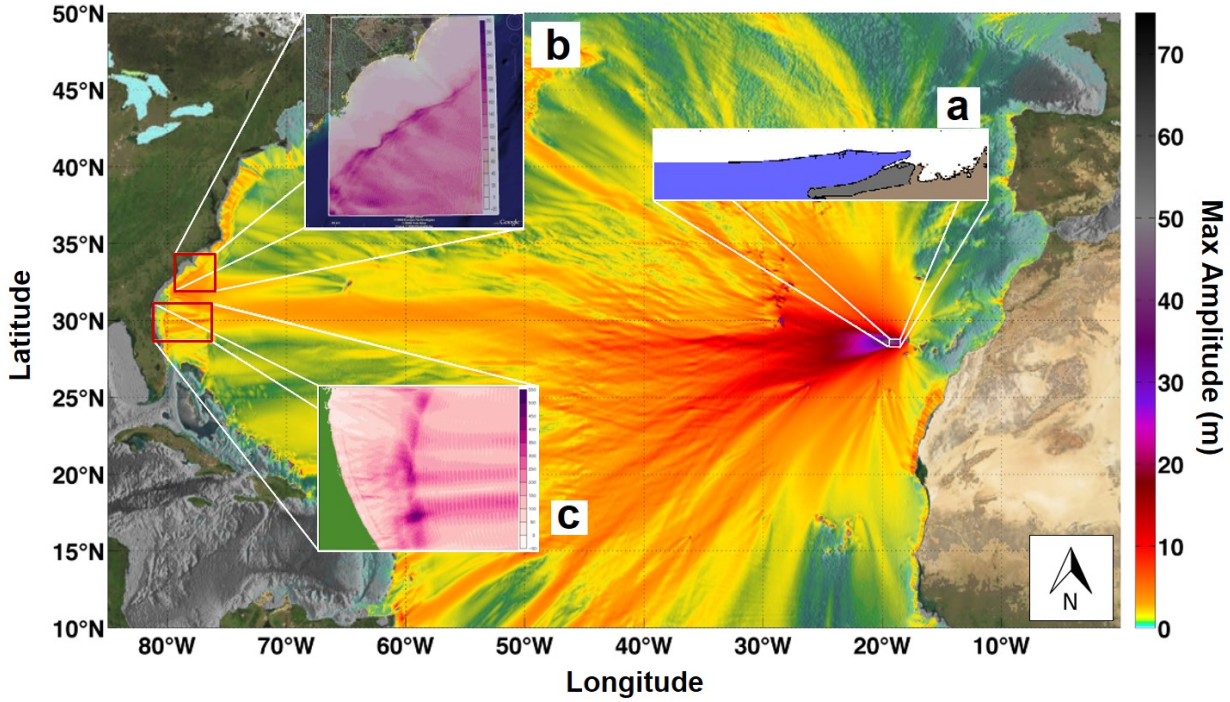

Figure 4.1: Model run maximum amplitude results (in meters) of landslide source at La Palma, coupled to propagation model. (a) Vertical section of iSALE lanslide model shows impact of flank slide body (grey), basement (tan) and wave generation (blue). See Figure 3.8 for detail. Maximum amplitude and inundation plot are shown at (b) Myrtle Beach, and (c) Daytona Beach to estimate runup and inundation.

4.3 Landslide Impact: iSALE

The iSALE model is a multi-material, finite-difference hydrocode for simulating fluid flows and deformations of solid bodies at subsonic and supersonic speeds. The iSALE code was directly developed from the simplified ALE code developed by Amsden et al. (1980) for the purpose of modeling asteroid impact. To develop iSALE, ALE was modified to allow landslide generation through the introduction of a third material layer (water), and through the adjustment of the asteroid projectile to include a porosity compaction model that is able to more accurately model slide-body deformation and advection during the run. While the model is available in both one- and two-horizontal dimension versions, the one-horizontal dimension (1HD) version is the only version that has been extensively benchmarked for tsunami generating landslide simulations.

4.3.1 iSALE Benchmarking for Landslide Simulations

The iSALE tsunami model was benchmarked against the 10 July 1958 Lituya Bay landslide event as described in Weiss et al. (2009) and illustrated on Figure 4.2. This event, which occurred in a U-shaped bay, resulted in the largest tsunami runup in recorded history (524 m). Fritz et al. (2003) performed a laboratory experiment in which a slide mass was accelerated by a pneumatic actuator into a 2D physical model of the Gilbert inlet as shown on Figure 4.3. A capacitive wave gauge and laser velocimeter were installed to measure the resulting wave amplitudes and velocities.

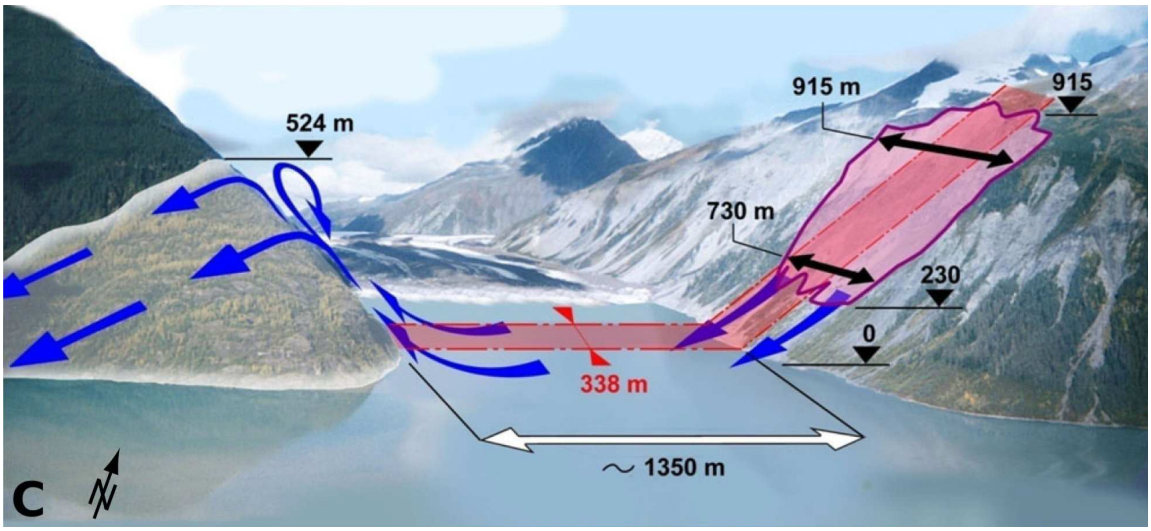

Figure 4.2: Gilbert Inlet, Lituya Bay slide geometry

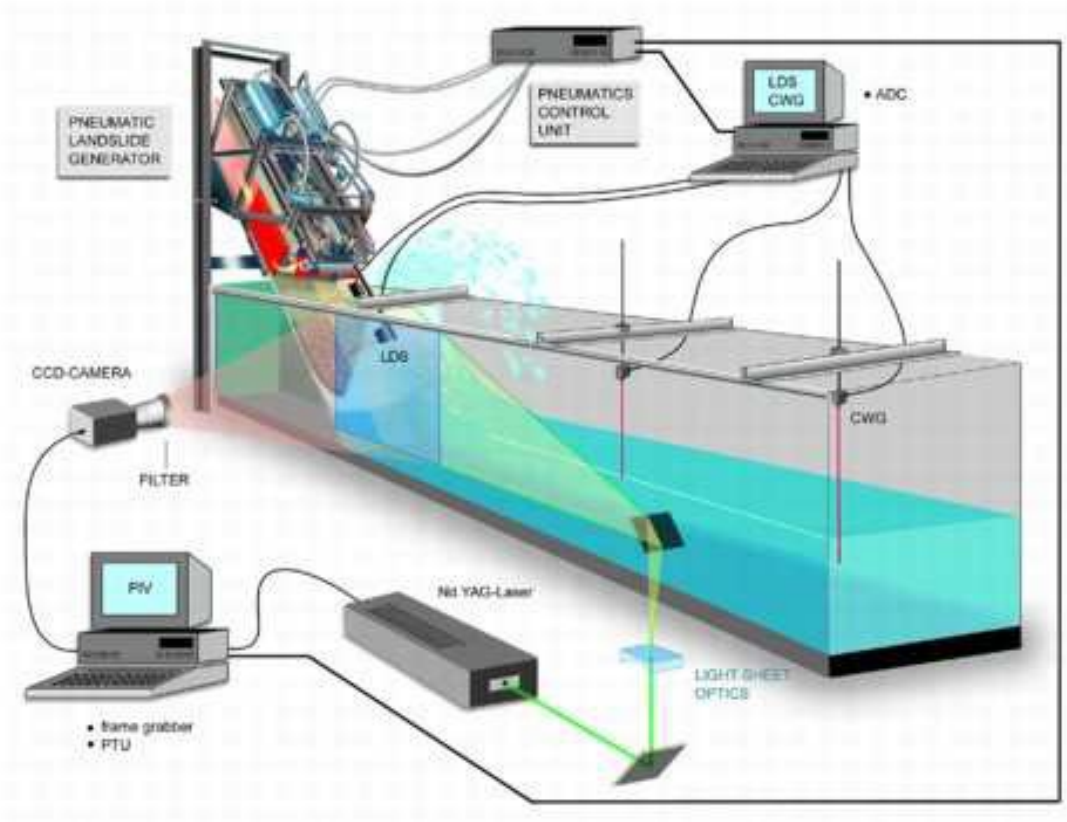

Figure 4.3: Lituya Bay laboratory experiment setup

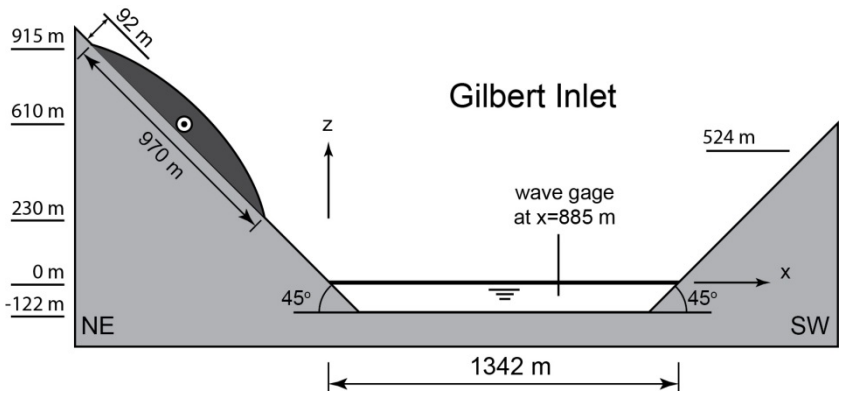

Figure 4.4: Lituya Bay laboratory experiment geometry

As part of the benchmarking of the enhanced code used in this study, the physical model was replicated numerically. For this purpose, the geometry was duplicated in an iSALE grid shown on Figure 4.4. A slide body with the same mass and physical characteristics, as well as initial conditions mimicking the laboratory experiment were also used in the numerical model.

The simulation results are shown in Figure 4.5. This figure shows the slide body forcing a wave across the basin, and up the headland slope. The simulated maximum runup of 518 m was close to the real-event maximum of 524 m. Figure 4.5 also shows a comparison of the recorded laboratory experiment wave gauge data maxima (shown as a dashed black line), with the iSALE model results (shown as a solid red line). This favorable comparison between and iSALE simulation results, a physical model study, and the historic field data that resulted from an actual mega-tsunami event gives confidence in the iSALE code's ability to capture the physics of large-volume, high-energy landslide generated impact tsunamis.

4.3.2 iSALE Geometry: Cumbre Veija

Because the Cumbre Vieja rift zone is oriented along a north-south axis, geometry for the landslide run was created based on the profile of La Palma in the east-west direction along a latitude of 28.65°N as shown on Figure 4.6. Submarine field surveys have identified evidence of 14 large slides within the Canary Islands. The debris fields from the identified events range from 50 to 500 km^3 in volume, and at times extend more than 130 km from their source (Whelan and Kelletat, 2003).

For this study, the credible worst-case scenario was modeled using a slide body volume of 430 km^3, an estimate that falls between that of Ward and Day (2001) (500 km^3) and Gisler et al. (2006) (375 km^3). A slightly slower slide velocity than Gisler et al. (2006) was used. The geometry was defined with a submarine emergent boundary and a total peak height of 2,500 m as shown on Figure 4.7, which matches the physical characteristics of La Palma. The computational domain is 125 km in extent, with 25 m initial grid resolution in both the x- and y-directions.

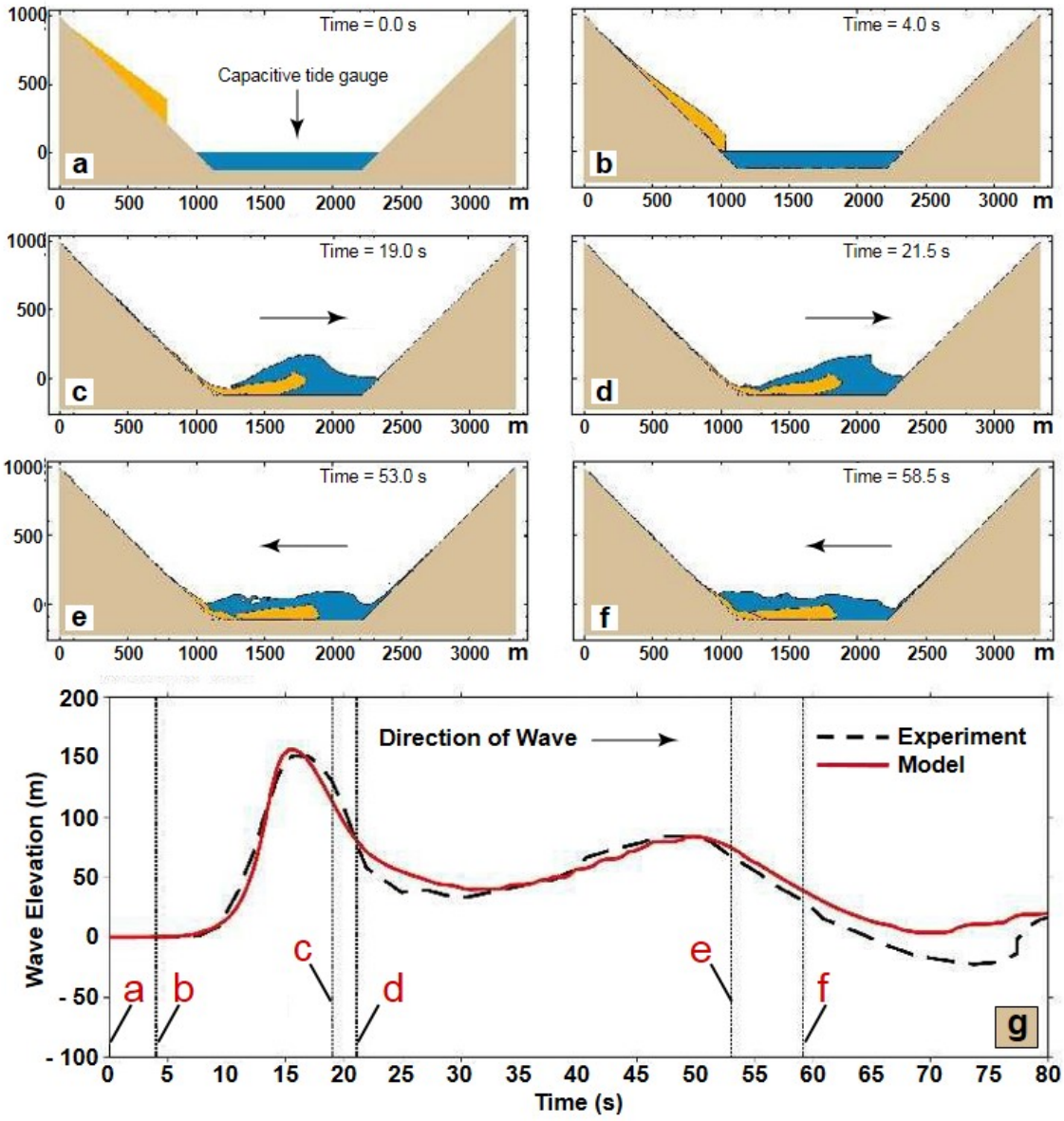

Figure 4.5: **(a) to (f) Snapshots of iSALE output illustrating the direction of water movement associated with the maxima in the time series. (g) Tsunami wave gauge record at location x = 885 m Dashed red lines indicate the timing of the results shown in figures (a to f).**

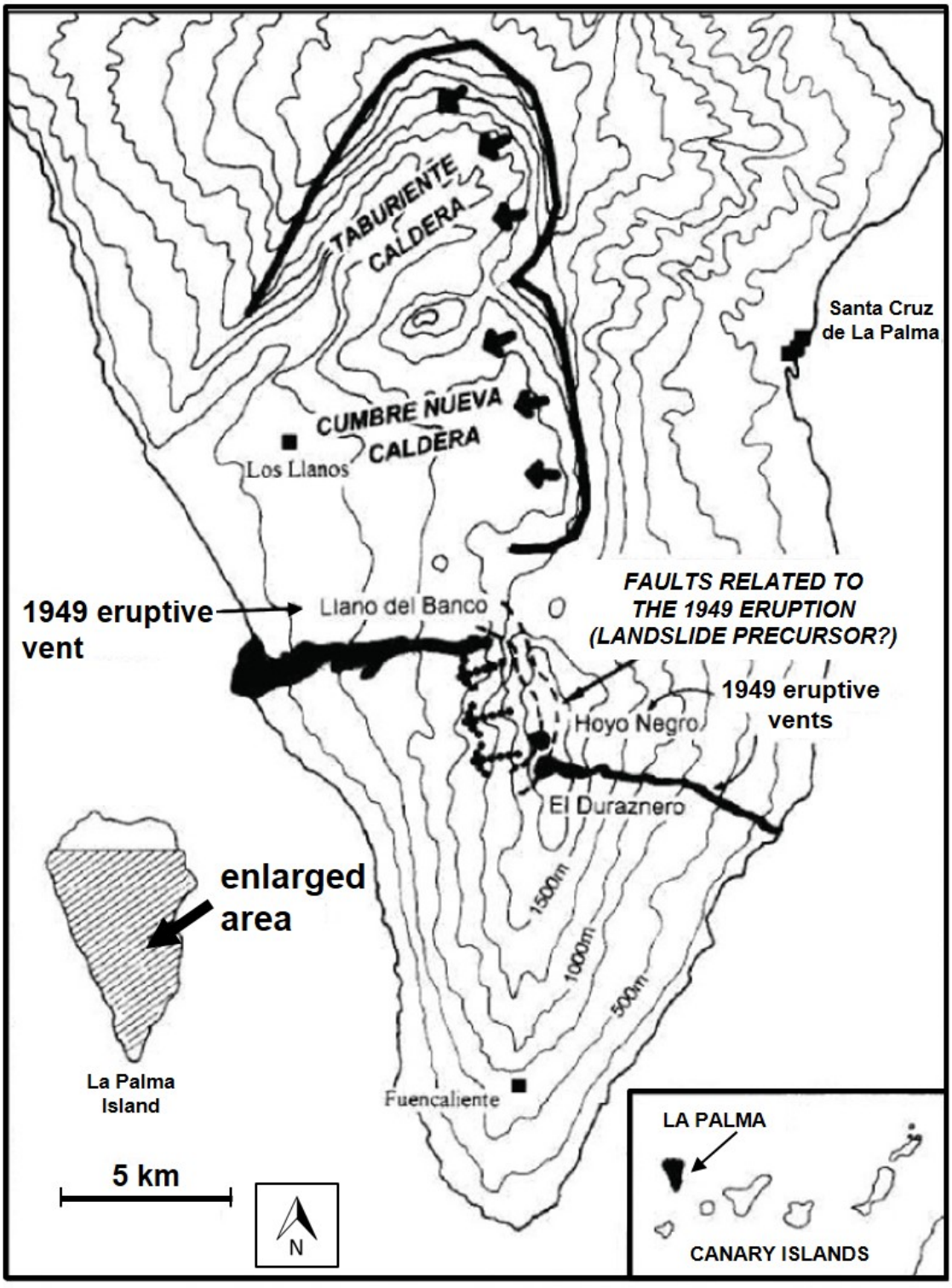

Figure 4.6: The Canary Islands and La Palma rift systems (from Carracedo, 1994) showing flank size and orientation.

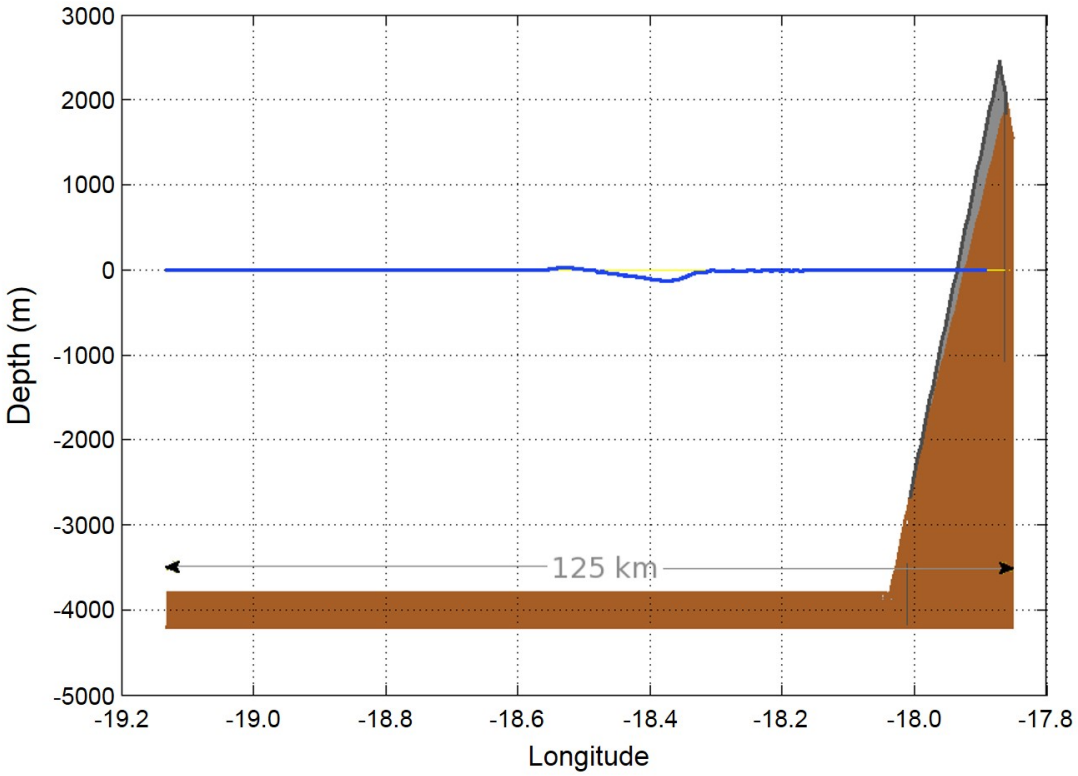

Figure 4.7: iSALE2D landslide geometry, used to simulate the worst case scenario of a La Palma flank collapse. The landslide mass has total volume of 430 km^3 and the horizontal domain extends 125 km. Blue line represents the initial waveform from the iSALE model used to force the coupled MOST model.

4.3.3 iSALE Results

During the run, the slide body velocities approach 100 m/s, and the initial impact produces a displacement wave with an amplitude of over 1,000 m. A snapshot of the iSALE output showing the material boundaries and the impact wave amplitude at time $T = 17$ s is shown in Figure 4.8.

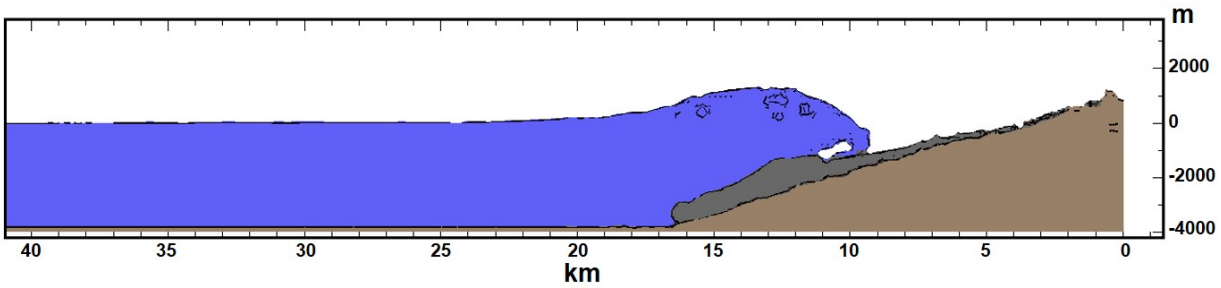

Figure 4.8 iSALE2D results: waveform at time T=17 s

The initial wave inundates the caldera, producing an outgoing waveform with an initial positive displacement and a larger negative depression following. This waveform continues to evolve through the computational domain; propagating to the edge of the grid with a resulting positive

amplitude of 20 m and negative amplitude of 140 m as shown on Figure 4.9. This profile is used as the input force in the propagation phase of this coupled model system.

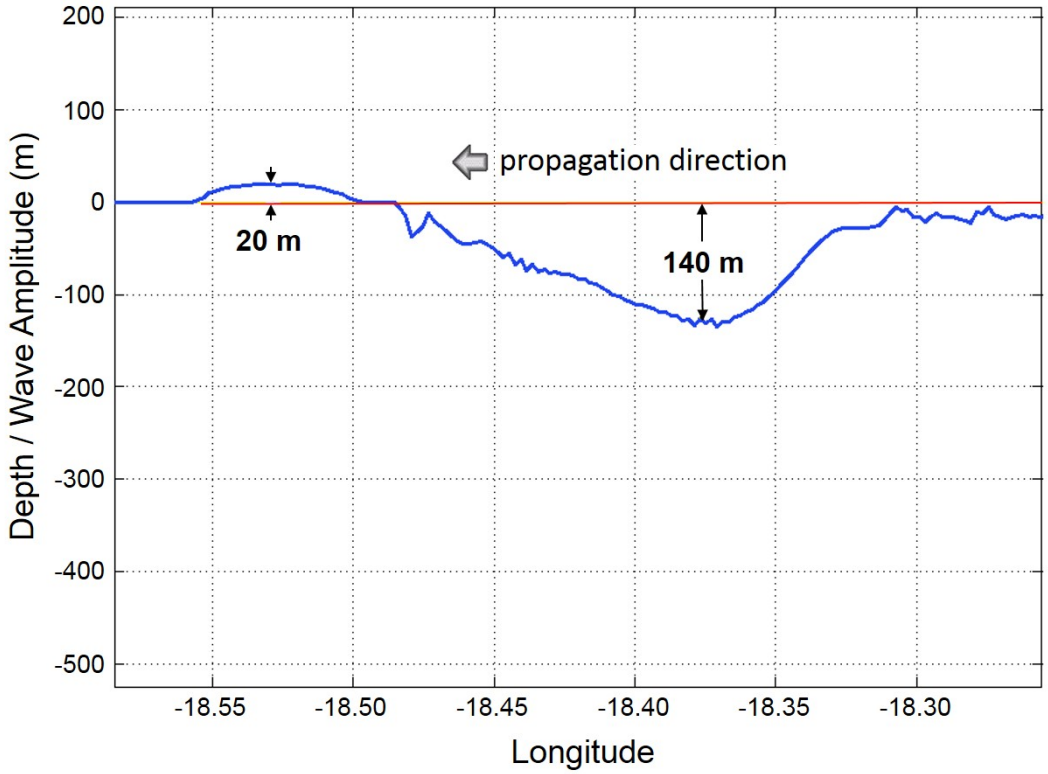

Figure 4.9: iSALE2D results: waveform at time T=320 s, crest amplitude 20 m, trough 140 m.

4.4 Propagation Phase: MOST

4.4.1 Grid Generation and Coupling

The waveform exiting the grid of the 1HD landslide model (iSALE2D) is used to force the MOST numerical model by applying the waveform as a sea-surface displacement, assuming a finite planar wave source near La Palma, and subsequently matching the velocity boundary conditions for the propagating wave as shown on Figure 4.10. The width of the Cumbre Vieja rift is taken to be 31 km (Carracedo, 1994). The width of the forcing region 60 km from the impact zone, based on geometric spreading, is 178 km (1.6 degrees of latitude), or nearly the full north-south extent of La Palma island. The bathymetric grid is modified from the Earth Topography (ETOPO1) global relief model with 1 arc-minute resolution. The use of a fairly high-resolution grid represents a necessary compromise that allows us to resolve waves from the 1HD landslide model, to couple to higher resolution inundation grids at Myrtle Beach and Daytona Beach, and to still have a model that was computationally feasible. Wave reflections outside this grid are not taken into account.

4.4.2 Propagation Results: MOST

The waveform from the iSALE 1HD landslide model is input into the MOST model and initially propagates as a sickle shaped wave with a leading crest and larger following trough (Figure 4.11a) with a wavelength almost twice as long (approximately 20 km). Within 15 minutes, this leading crest is overtaken by the trough, which dominates throughout the propagation phase (Figure 4.11b-d), and which has an amplitude of over 10 m in open ocean.

As the wave front reaches the mid-Atlantic ridge, it diffracts though the ridge, creating a complex pattern of constructive and destructive interference (Figure 4.12). The gaps through the disturbing topographic features are on the order of the wavelength of the wave train. This causes a classical diffraction pattern that in turn causes the waves to become highly disorganized. The wave front is also seen to refract around Bermuda in this narrow computational grid.

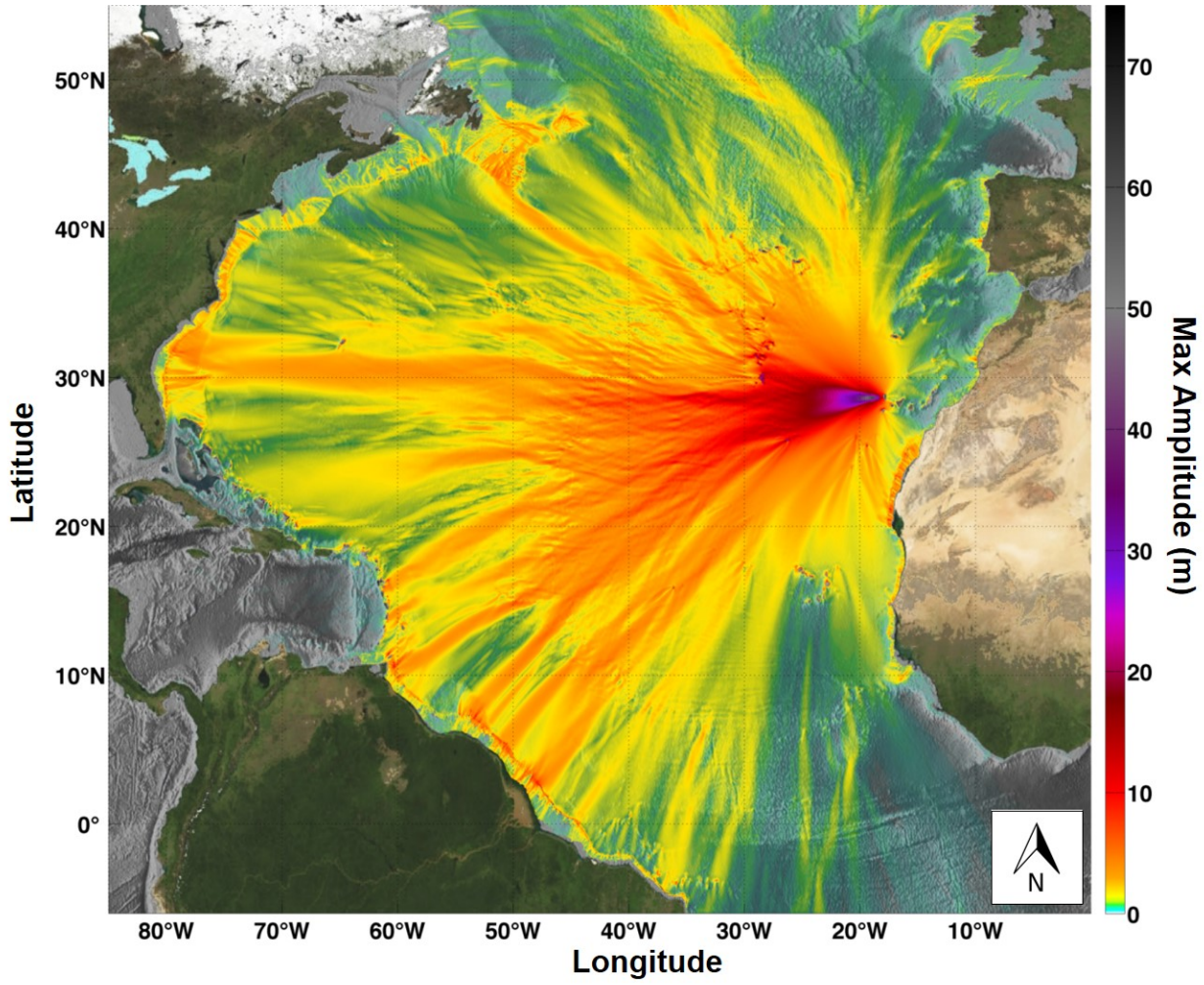

Figure 4.10: Maximum wave amplitude, in meters, from MOST model using iSALE waveform at T=320 s

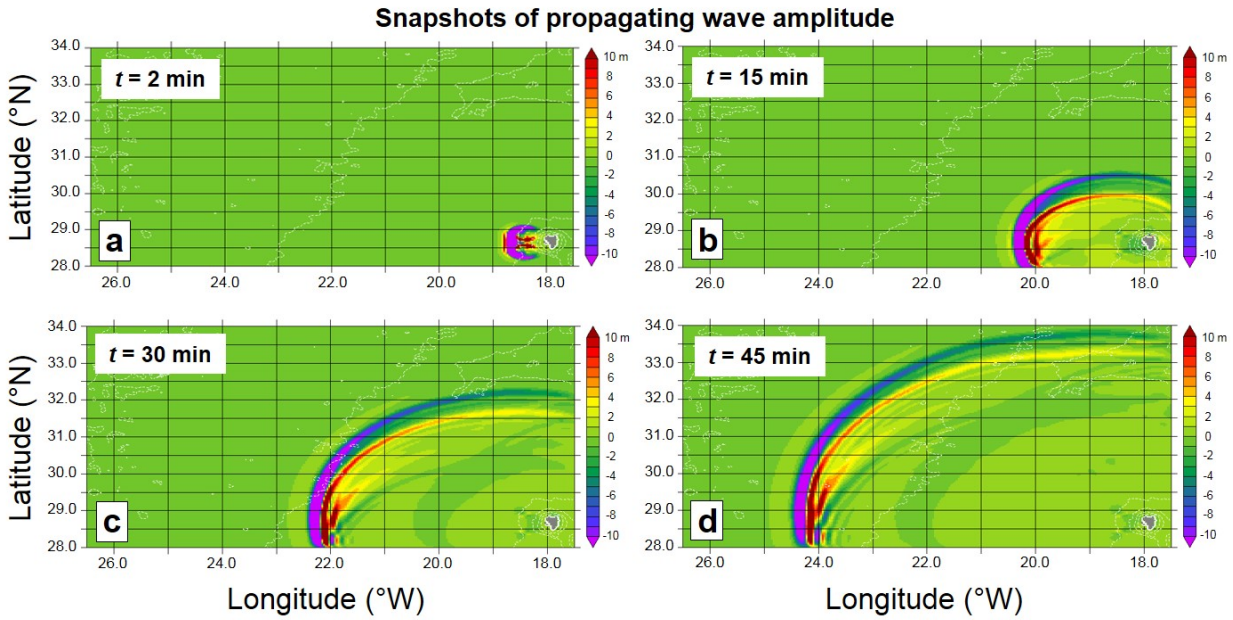

Figure 4.11: MOST Propagation results: initial coupling and wave formation

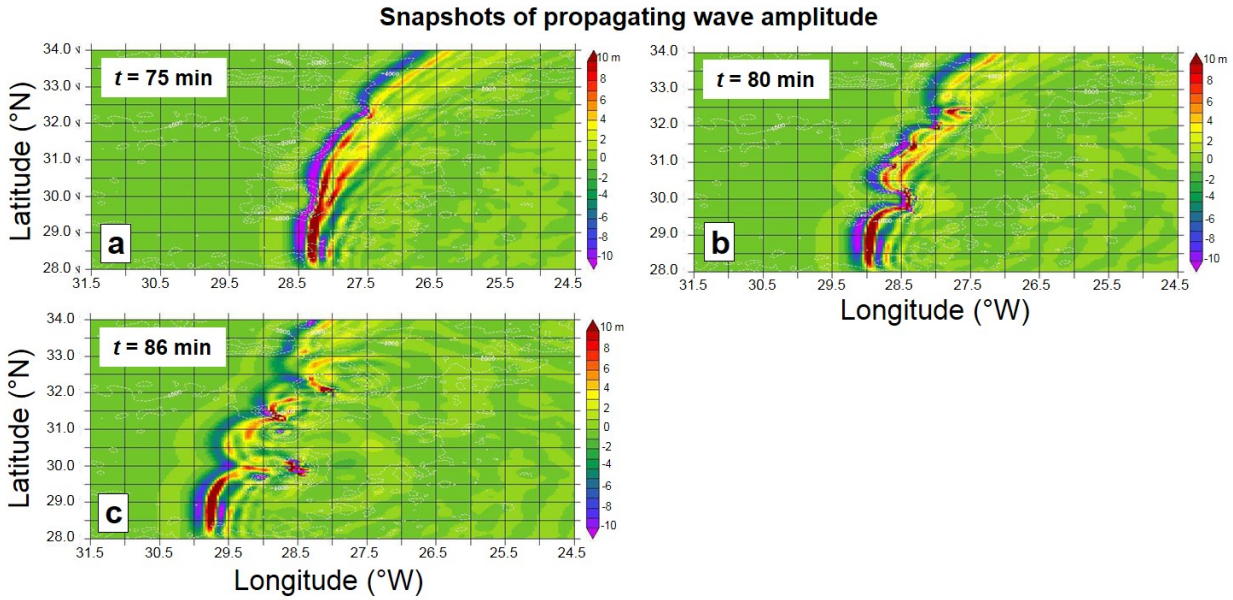

Figure 4.12: MOST Propagation results: diffraction through Mid-Atlantic Ridge

The effect of the continental shelf on the wave is remarkable. The wavelength decreases from approximately 20 km in the deep ocean to about 5 km over the slope. Beyond the 100 m depth contour, the amplitude of the waves drops significantly (Figure 4.13). The shallow shelf appears to dissipate the wave energy as it propagates across. There is a risk of violating the shallow-water approximation at this point in the simulation. However, experience has shown that the nonlinear version of MOST used in this portion in the analysis simulates well the shorter wavelengths that are of interest (Wei et al., 2008). Ignoring the possible limits of the linear

shallow-water assumptions, ten Brink, et al.(2008) have shown that there are significant differences between the linear and weakly nonlinear solutions over the continental shelf and shelf break, consistent with the results of this analysis. Figure 4.14 shows the maximum wave amplitude over time along a cross-section of the continental shelf. This figure shows similar behavior to ten Brink's model in terms of representing peak amplitudes at the shelf break and subsequent dissipation as the wave approaches the beach. In ten Brink et al. (2008), the landslide source is at the nearby continental slope, so direct comparison might not be appropriate. Section 4.6 describes and shows the results using the nonlinear inundation code.

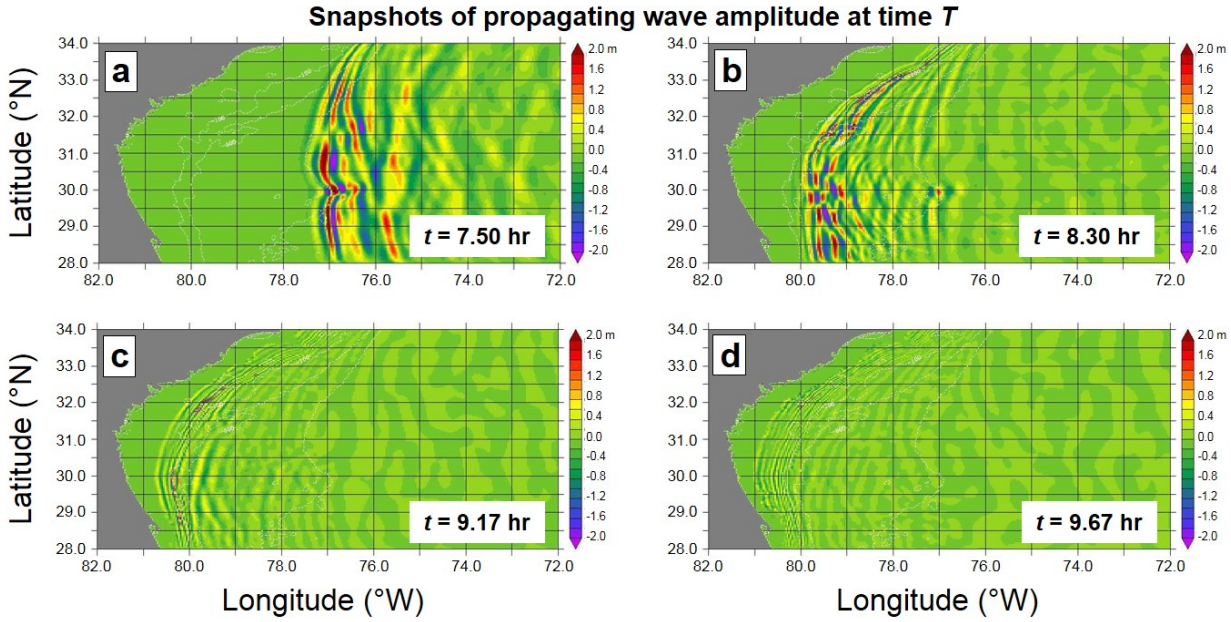

Figure 4.13: MOST Propagation results: wave dissipation over the continental shelf

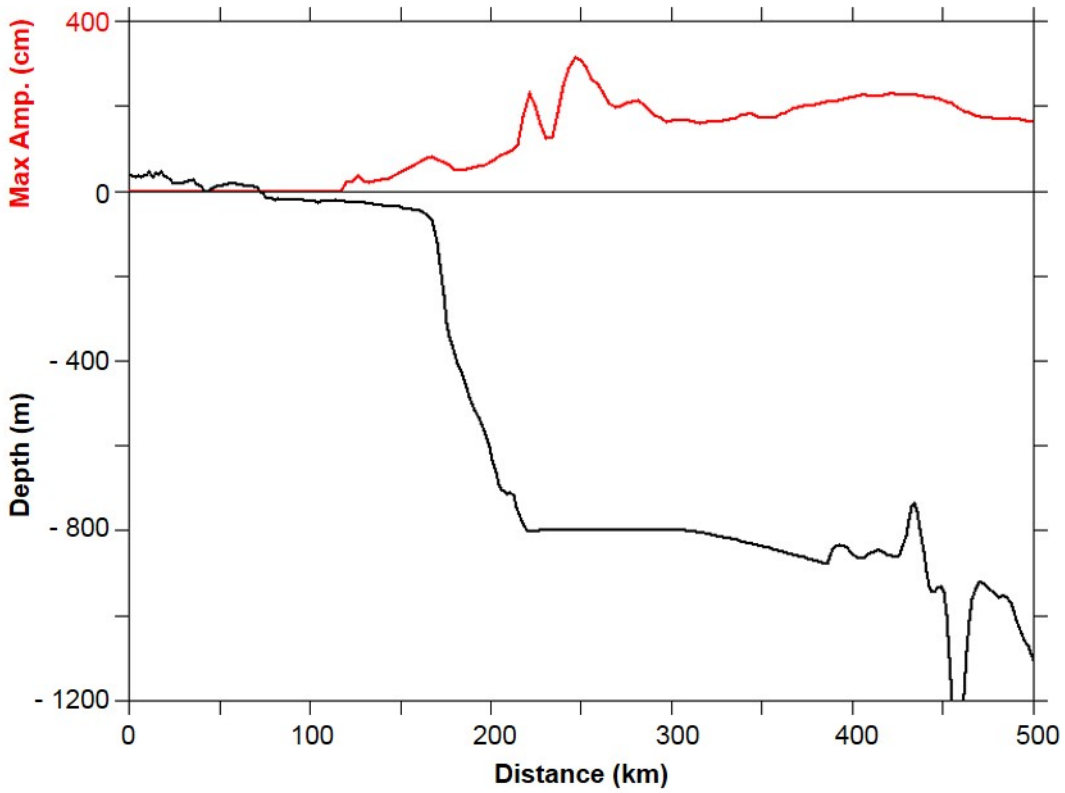

Figure 4.14: MOST Propagation results: maximum wave amplitude (red) over the slope and shelf (black) along a longitude section at 31.0° N latitude. Note the different scales for amplitude and depth.

4.4.3 Boussinesq Numerical Approach

The weakly nonlinear Boussinesq equations with extended dispersive effects were originally derived by Nwogu (1993) in Cartesian coordinates. In order to consider the earth surface curvature and the Corriolis effects, Zhou et al. (2011) rewrote the original equations in geospherical coordinates. The numerical model is referred to as "GB" (Geological Boussinesq) hereafter in this report. As the waves approach shorelines in the shallow water, wave height increases due to shoaling effect and therefore nonlinearity becomes stronger. The wave propagation over the continental shelf and coastal runup with the fully nonlinear Boussinesq-type model was simulated based on the theory developed by Wei et al. (1995). Incorporated in this model are the physical features associated with bottom friction and wave breaking. Energy dissipation due to wave breaking is modeled with an empirical formulation, which was originally developed by Kennedy et al. (2000) and later modified by Lynett and Liu (2002). The fully nonlinear Boussinesq-type model in this study is a recreation of the numerical code FUNWAVE, which hereafter is referred to as ”FB” (Fully nonlinear Boussinesq). In both GB and FB, the slot scheme developed by Chen et al. (2000) and Kennedy et al. (2000) is used to track the moving waterline. Numerical solutions are obtained through a 4th-order finite difference scheme (Wei et al., 1995). Validation of GB and FB has been conducted against a number of benchmark experiments, including solitary wave runup on a conical island, solitary wave runup along smooth slope, and the transformation of solitary waves over composite bathymetry (Synolakis et

al., 2007). The details of model validations can be found in the publication of Zhou et al. (2011), but are omitted in this report for conciseness.

4.4.4 Boussinesq Propagation in the North Atlantic Basin

As with the MOST propagation model, the GB model is forced with the iSALE waveform shown in Figure 4.10. The initial horizontal water velocities u_α are computed based on the distribution of water surface elevations, ζ, assuming this wave is propagating in a unique direction.

The map in Figure 4.15 shows the computational domains covered in the simulation of tsunami propagation. In areas near the wave source, wavelengths are short and therefore fine resolution grid is required. Four grids were employed in different stages and in each grid, the grid sizes are determined upon numerical convergence tests. Grid A covers an area in latitudes from 24°N to 33°N and longitudes from 26°W to 15° W, and is discretized with grid sizes of $\Delta\varphi = 0.5'$ and $\Delta\theta = 0.5'$, where φ and θ denote the longitude and latitude, respectively. Bathymetry data are interpolated from the ETOPO1 1-minute global relief model. Surrounding this domain, the simple, fully reflective boundaries were employed and the simulation was terminated before waves reach the boundaries. A snapshot of the computed values of ζ and u_α in this grid are then interpolated and input into Grid B as initial conditions. Grid B covers an enlarged domain, which extends from 12°W to 30°W in longitudes, and 20°N to 38°N in latitudes. Uniform grid sizes of $\Delta\varphi = 1'$ and $\Delta\theta = 1'$ are applied. Here, as with Grid A, fully reflective boundary conditions are employed. Grid C extends from 90°W to 0° in longitude and from 10°N to 55° N in latitude, covering most of the North Atlantic Ocean. The computational domain is discretized with grid sizes of $\Delta\varphi = 4'$ and $\Delta\theta = 4'$. Absorbing layers are placed along the north and south boundaries, within which Newtonian cooling terms are added to the horizontal momentum equations. Grid D covers an area neighboring the U.S. East Coast. The limits of the computational domain in this layer are 82°W to 62° W and 24°N to 46° N. Input boundary conditions derived from Grid C are applied along the grid boundaries. The spatial resolution is $\Delta\varphi = 1'$ and $\Delta\theta = 1'$ in Grid C.

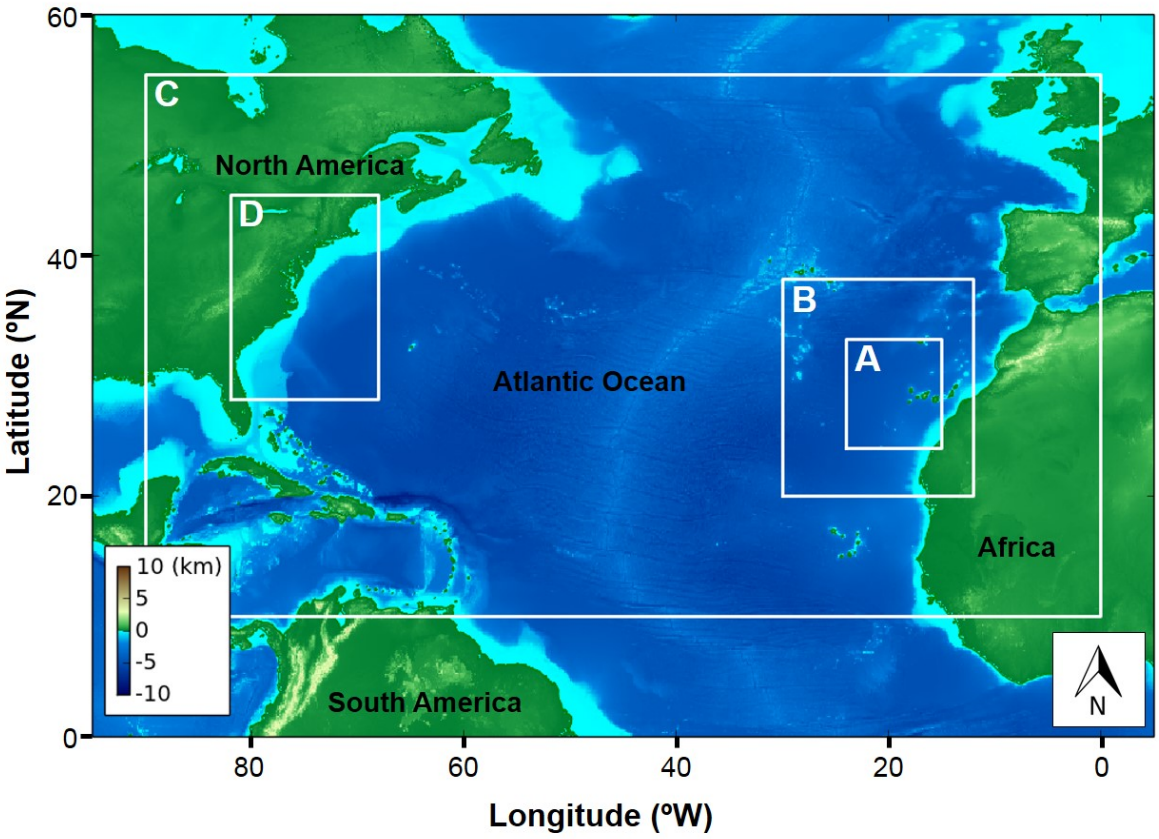

Figure 4.15: Boussinesq Propagation domain: four high-resolution grids surrounding the generation region (grids A and B), the computational region (grid C), and the U.S. coastal region (grid D) are outlined as white rectangles.

Figure 4.16 presents a number of snapshots of simulated water-surface disturbances near the source in Grids A and B (Figure 4.15). The depression overtakes the peak shortly after the waves are initiated, and a train of oscillatory waves develops behind the leading depression. In the early stage, the trailing waves have very short wave lengths for which the standard Boussinesq model described in depth-averaged velocities may be insufficient. As the waves with higher amplitudes move faster, the wavelengths become longer and dispersive effects weaken during the propagation.

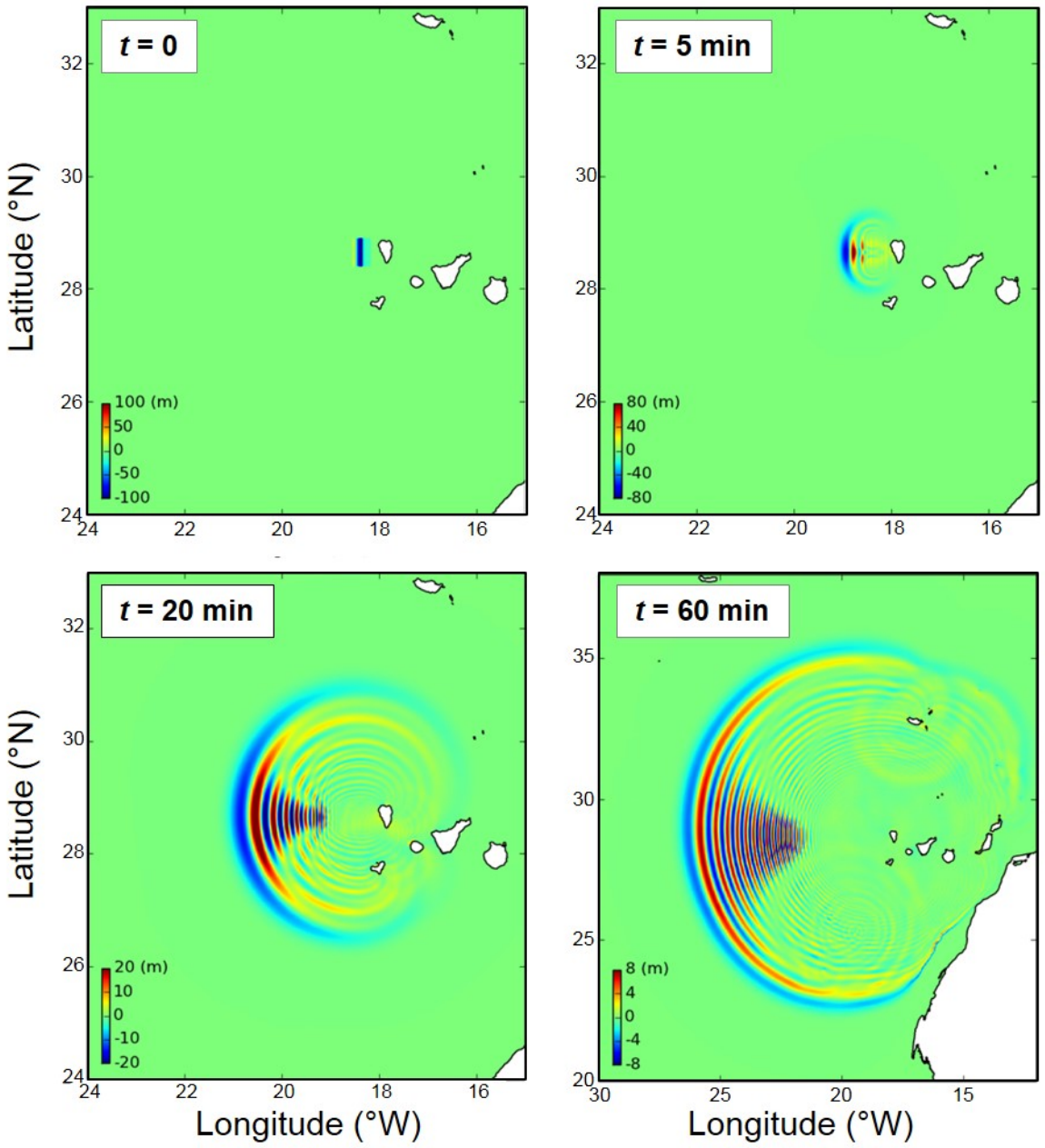

Figure 4.16: Boussinesq Propagation results: time evolution of waves near the La Palma forcing region.

Figure 4.17 plots the water surface near the North American coast at selected times. The leading depression approaches the base of the continental shelf 6.5 hours after the landslide occurs. At this moment, the wave heights are between 0.5 and 1.5 m, and the wavelengths between 50 km and 120 km. Considering the water depth is near 5000 m in open ocean, the waves have very weak dispersive effects. Over the continental shelf, the waves become shorter and higher due to shoaling effects. After 8.5 hours, the tsunami eventually approaches Florida.

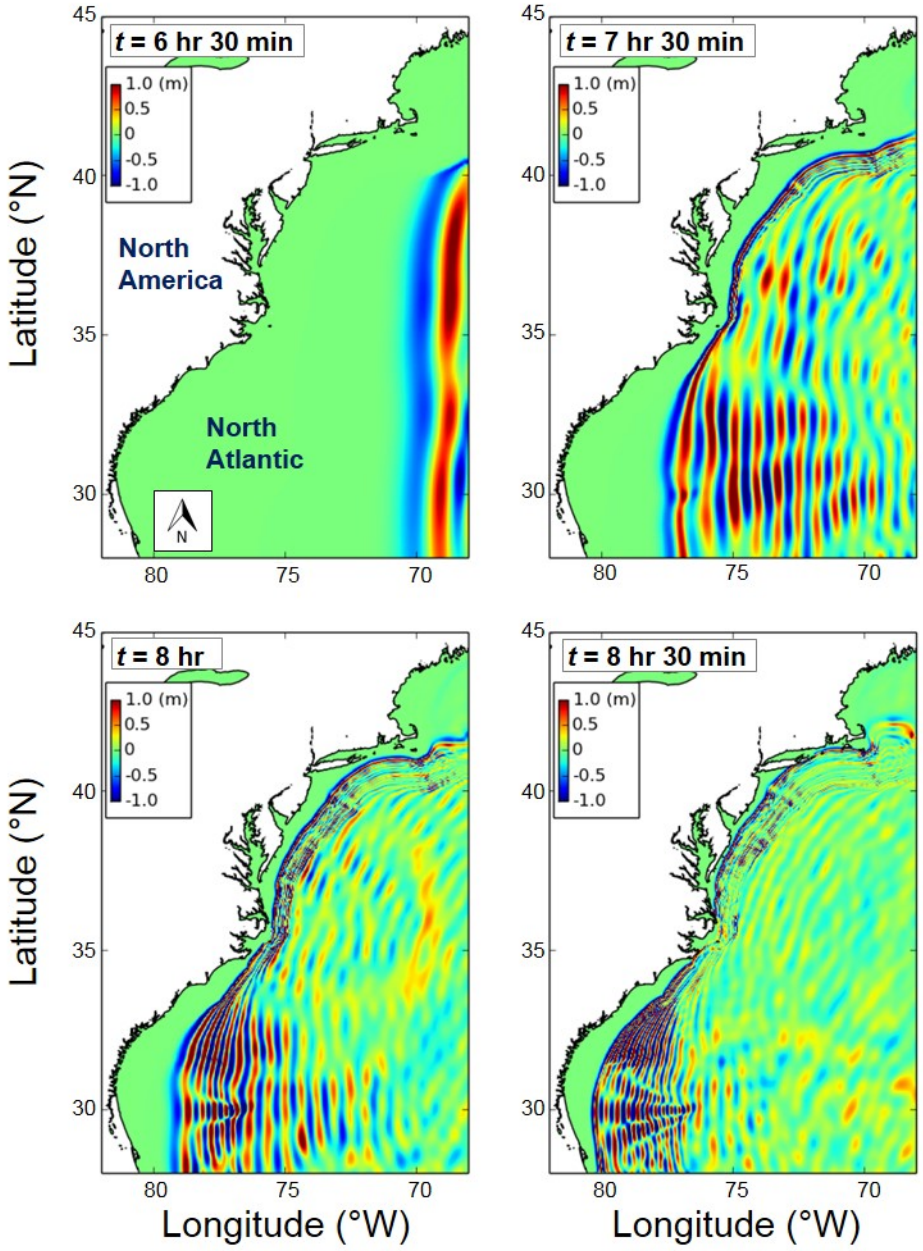

Figure 4.17: Boussinesq propagation results: time evolution of waves over the continental shelf.

4.4.5 Wave Fission and Runup

The continental shelf offshore the U.S. East Coast extends over a width of nearly 100 km and has water depth between 20 to 70 m in most areas. Due to dispersive effects, after propagating into the shallow water area over the continental shelf, the waves will disintegrate into trains of shorter components (Løvholt et al., 2008). This phenomenon is referred to as “wave fission”. In the present study, this process is investigated further through 1D high-resolution simulations

with FB. To apply the 2D numerical model in 1D cases, the computational domain has an assumed width of one grid cell. The bathymetry data are interpolated from the NOAA Coastal Relief Model of 3″ resolution.

Numerical studies are conducted between 81°18′ W and 80°12′ W longitude and along latitude 29°16′ N, which goes through the coastal city of Daytona Beach, Florida. Along this latitude, the waves are dominantly propagating in the East-West direction and therefore the 1D modeling is a reasonable approximation. A grid resolution of 1/6" is applied in this stage. Boundary conditions are derived from the simulations in Grid D (Figure 4.15).

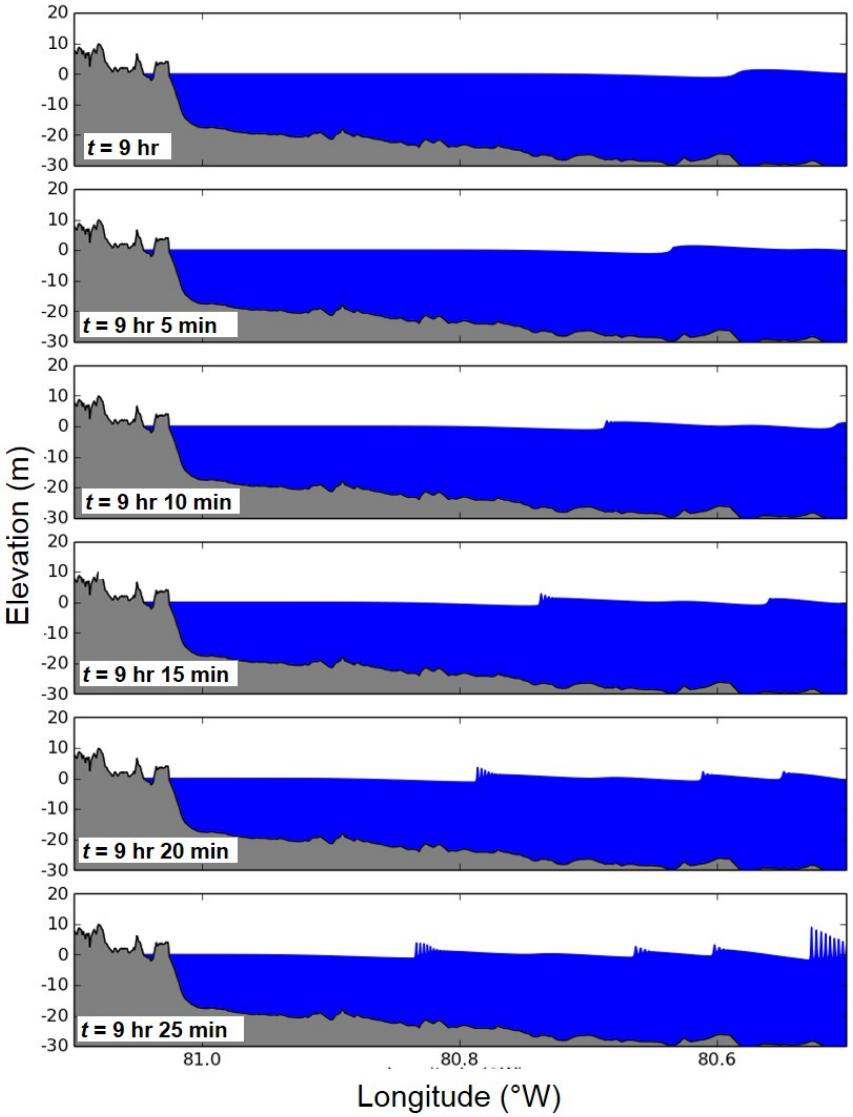

Figure 4.18: Boussinesq propagation results: water surface profiles illustrating the process of wave fission. Note that fission starts only after the waves pass the shelf break, and continue to develop as they progress over the entire width of the shelf.

Figure 4.18 shows a series of snapshots of the water surface profiles during the process of wave fission. Before disintegrating, the front face of a wave peak first becomes very steep, and then the peak breaks into a train of shorter waves. As the fission waves travel at slightly

different speeds, they eventually become fully separated. Most of the fully developed fission waves have wavelengths larger than 300 m. Some waves have very high wave heights, around 5 m, where the nonlinear effects become stronger.

The fission waves continue propagating towards the shoreline and eventually cause runup on the coast. During this process, wave energy is dissipated due to bottom friction and wave breaking. The numerical simulation predicts a maximum runup of 2.9 m, which may be considered a moderate impact on the coast. Figure 4.19 depicts the runup and drawdown of the fission waves. Considering the 1D simulations neglect the geometric spreading, the actual runup in 2D may be less. This suggests that the landslide on the La Palma Island is unlikely to cause severe tsunami impact on the U.S. East Coast, especially in areas facing a wide continental shelf.

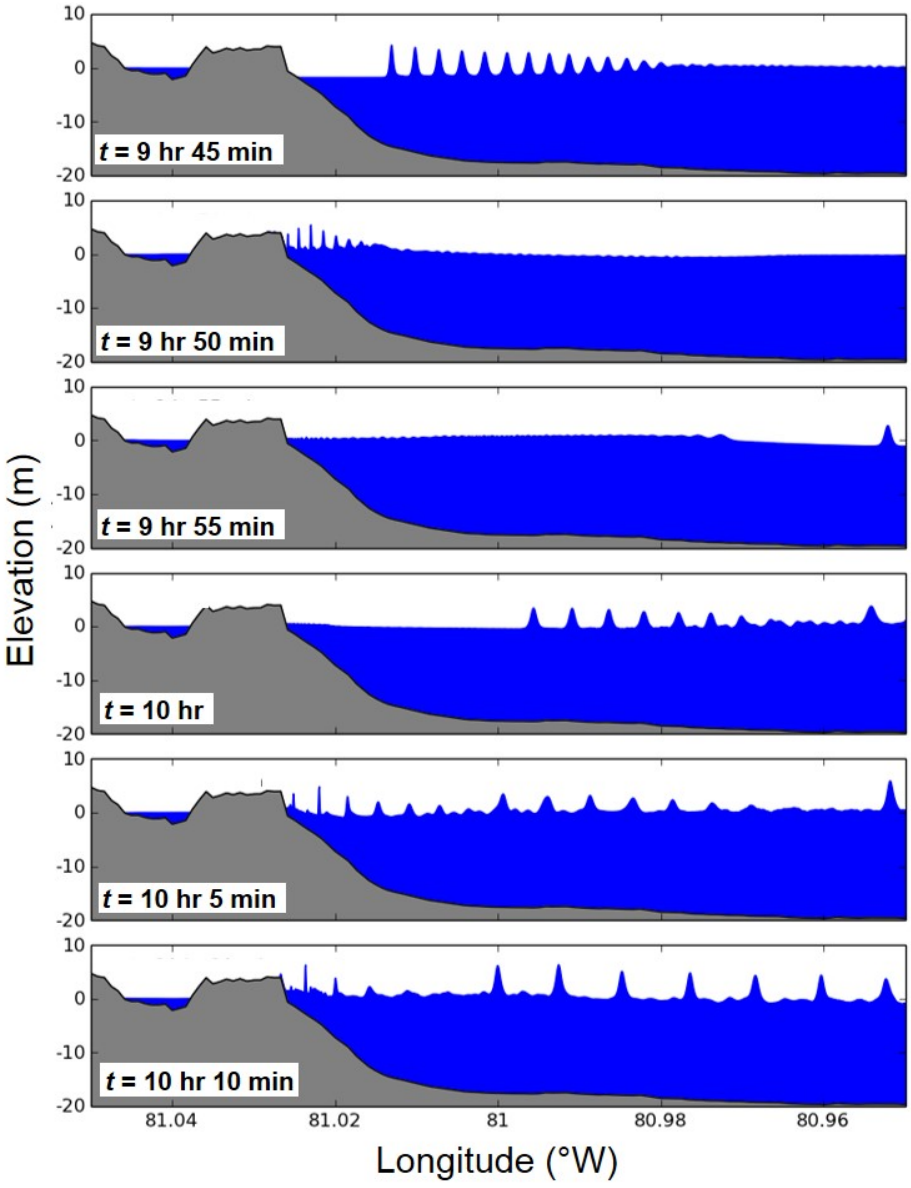

Figure 4.19: Boussinesq propagation results: water surface profiles over the coastal area. Maximum runup of 2.9 m is predicted in this simulation.

Of note, the near-shore wave heights in the present study are significantly lower, compared with those in the previous studies by Ward and Day (2001) who predicted 20 to 25 m high waves on Florida beaches, and Løvholt et al. (2008), who predicted wave amplitudes of 3.0 to 9.6 m offshore the U.S. East Coast. Ward and Day (2001) employed a linear theory, which is a credible approximation in deep ocean but may be insufficient for wave shoaling in shallow water. Because of the in viscid assumption of landslide materials, Løvholt et al. (2008) predicted significantly higher initial wave heights than those in this study which explains most of the difference.

Geist et al. (2009) demonstrated that the runup of waves on the U.S. East Coast is highly sensitive to the bottom friction. In the present study, a Manning's coefficient of n of 0.025 is used to represent bottom friction. This value is within the range commonly employed in coastal environments.

4.5 Inundation Phase: MOST

While the wave dynamics in the far-field propagation phase can be approximated using linear theory, it is apparent that wave propagation close to the U.S. territory is greatly affected by the continental slope and shelf, particularly because the landslide-generated tsunamis have a much shorter wavelength than those generated seismically. Other studies of the effect of extreme landslide events from La Palma on the U.S. Atlantic coast (Løvholt et al., 2008; Ward and Day, 2001) have avoided running inundation models completely, and instead used a Green's law scaling technique to estimate coastal runup. This technique gives very poor estimates of runup and does not take into account important nonlinear effects and bathymetric features. Unfortunately, it has been these inaccurate studies that have been given significant amounts of media attention.

The inundation phase of this study used the 2HD finite-difference MOST model (Titov and Gonzalez, 1997; Titov and Synolakis, 1998) based on the nonlinear long-wave approximation. The NOAA Center for Tsunami Research (NCTR) has extensively bench-marked (Synolakis et al., 2009) this code as part of its ongoing development of an operational tsunami forecasting system known as Short-term Inundation Forecasting for Tsunamis (SIFT). In the development of SIFT, many high resolution grids have been developed for U.S. coastal communities.

The methodology for modeling these coastal areas is to develop a set of three nested grids (A, B, and C) each of which is successively finer in resolution, until the near shore details can be resolved to the point that tide gauge data from historical tsunami in the area match reasonably well with the modeled results. It has been shown that under-resolving the wave can lead to grossly underestimated runup, and that 1/3 arcsec (10 m) horizontal resolution in the finest grid (C-grid) is generally appropriate for accurate runup estimates.

In this study, for comparison purposes the possible impacts are assessed at two communities conveniently located within the propagation grid-- Daytona Beach, Florida, and Myrtle Beach, South Carolina. These sites were chosen because well-vetted high-resolution community models are already developed at these locations as part of the operational SIFT forecast system, and so they can provide examples of high-quality sample simulation results at the coastlines. Future work will extend the propagation grid to include the entire eastern seaboard, and results will be presented for other communities as well, including Cape Hatteras, North Carolina, Montauk, New York, and Nantucket Island, Massachusetts.

4.5.1 Inundation at Daytona Beach, Florida

The Daytona Beach Standby Inundation Model (SIM) was developed as part of the NOAA tsunami forecasting system, and consists of three nested grids centered on Daytona Beach, Florida (Figure 4.20). The largest grid (A-grid) extends beyond the continental slope, into deep water (~1000 m).

The A-grid wave amplitude is shown in Figure 4.21a (time = 8 hrs 24 min after event), just as the wave front reaches the shelf, and in Figure 4.21b (time = 10 hrs 35 min after event), after the wave front reaches the shoreline. The shelf shortens the wavelength, and the wave reflects off the shoreline, creating a complicated reflection pattern.

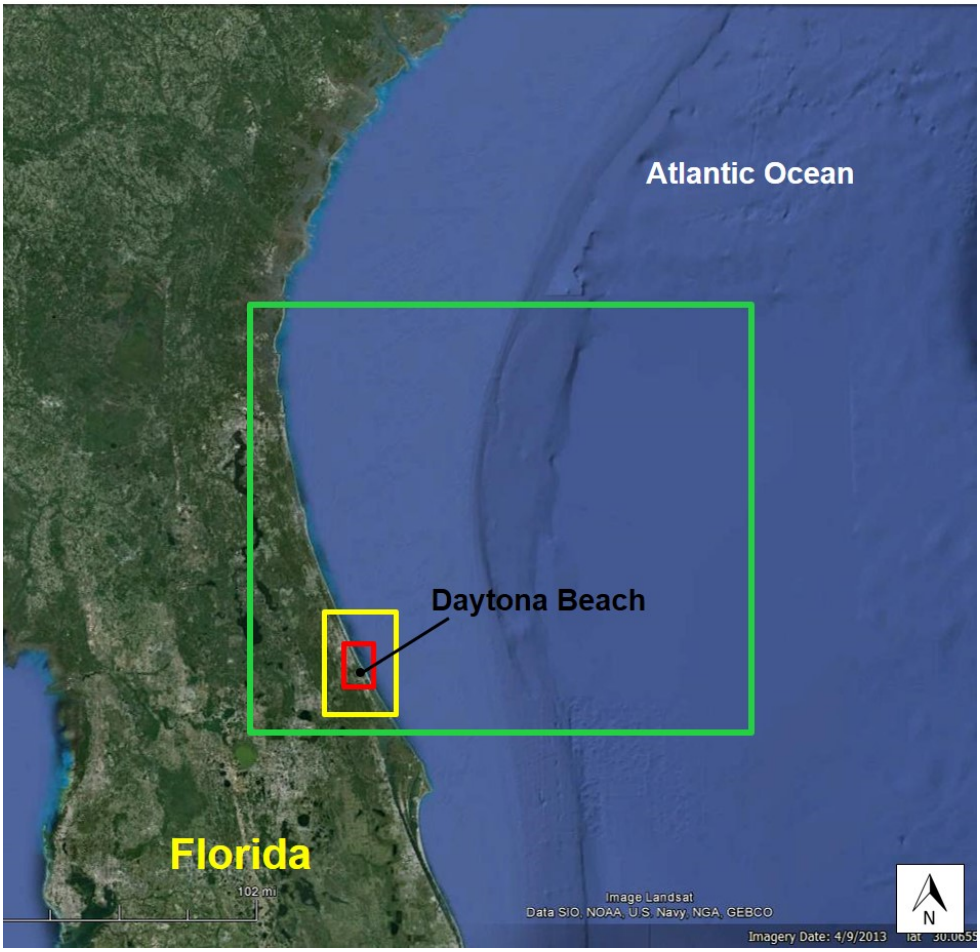

Figure 4.20: Overview of the Daytona Beach, Florida MOST inundation run, showing A-grid (green), B-grid (yellow), and C-grid (red) extents.

The C-grid results show both the incoming wave and the reflected wave superimposed at model time step 132 (event time = 10 hrs 00 min). The first (positive) wave arrives at the entrance to the Ponce de Leon channel (marked by a star in Figure 4.22a) at 9 hours and 40 minutes after the landslide impact. The amplitude at this location reaches approximately 1 to 2 m right at the coast, but the maximum over the entire model run (3.15 m) occurs in an isolated region just south of the channel entrance right at the shoreline. The only discernible inundation is expected to occur at this beach area, and is predicted to be nearly negligible (Figure 4.23), though damage to harbors in the Intracoastal Waterway due to high currents cannot be ruled out because wave amplitudes of nearly a meter are seen in the harbor areas.

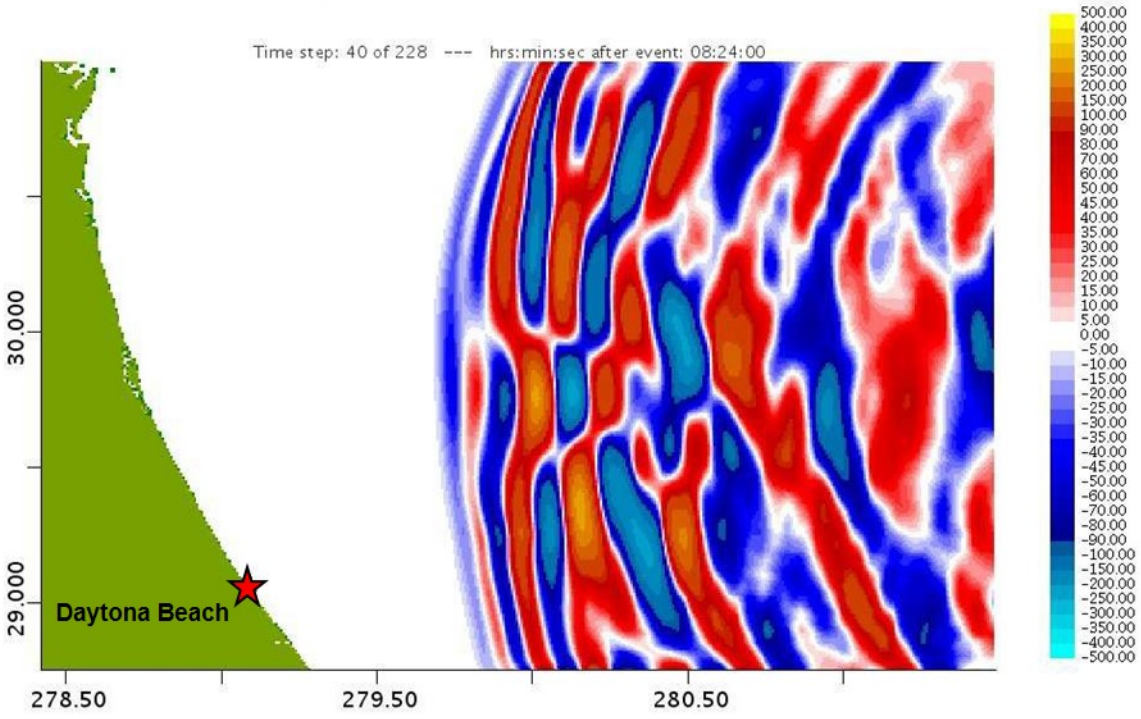

(a) Wave amplitude (cm) at T = 8 hrs 24 min

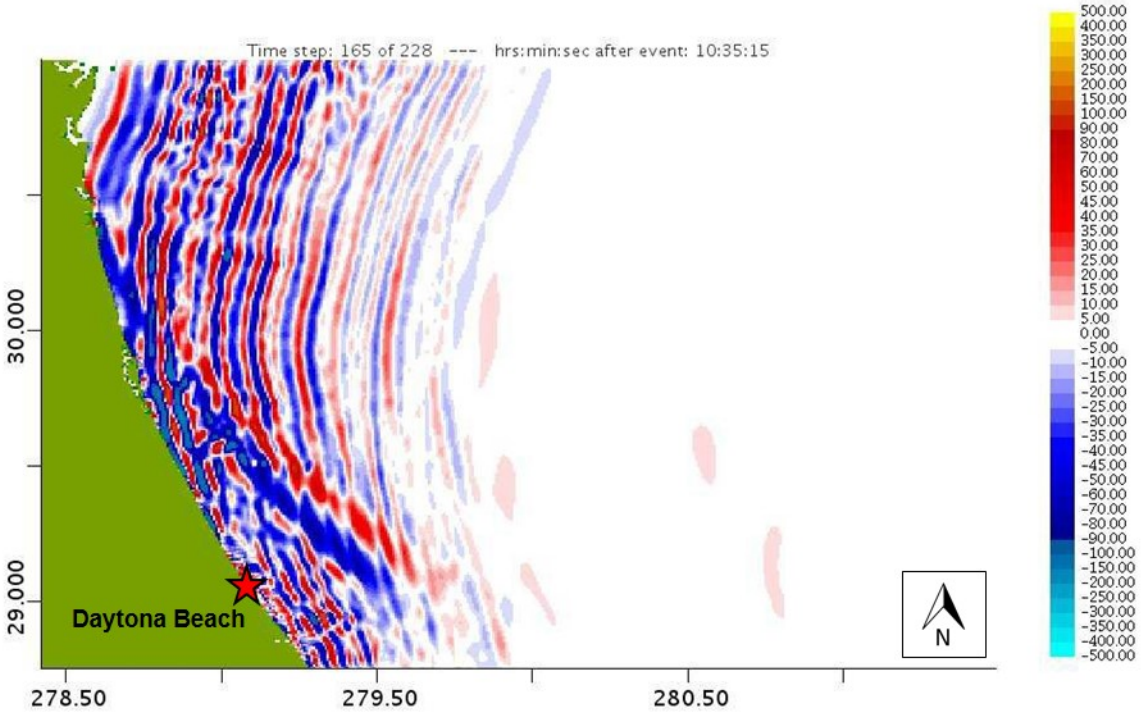

(b) Wave amplitude (cm) at T = 10 hrs 35 min

Figure 4.21: MOST inundation results for Daytona Beach, Florida (A-grid)

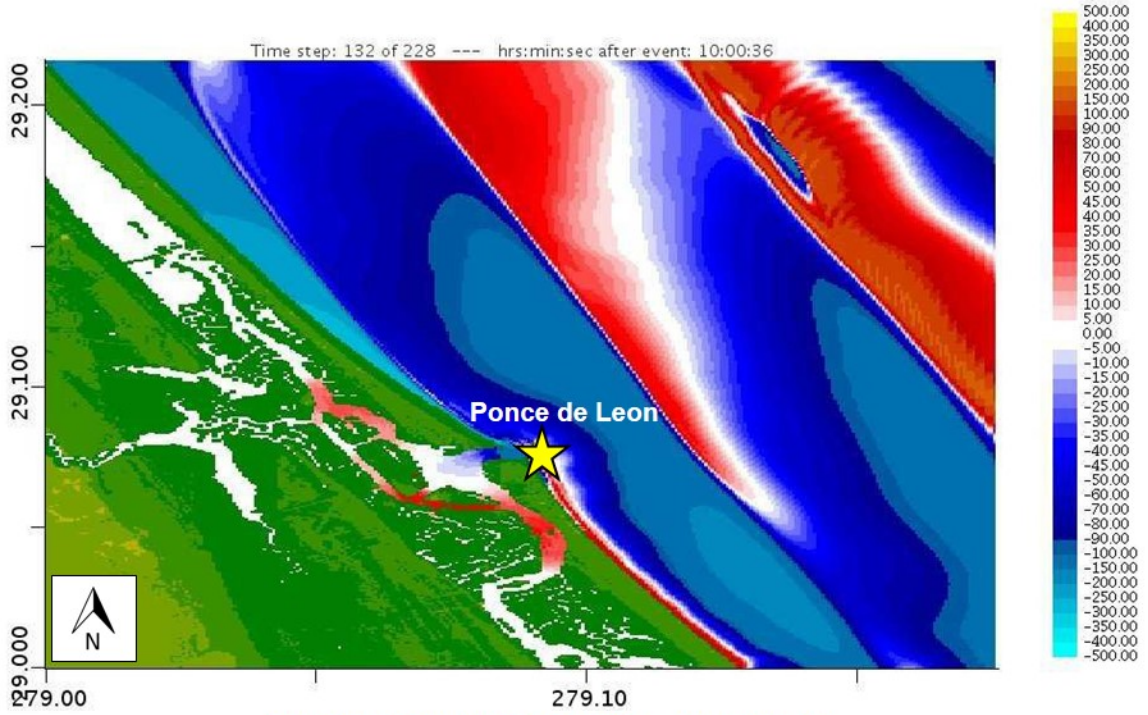

(a) Wave amplitude (cm) at T = 8 hrs 24 min

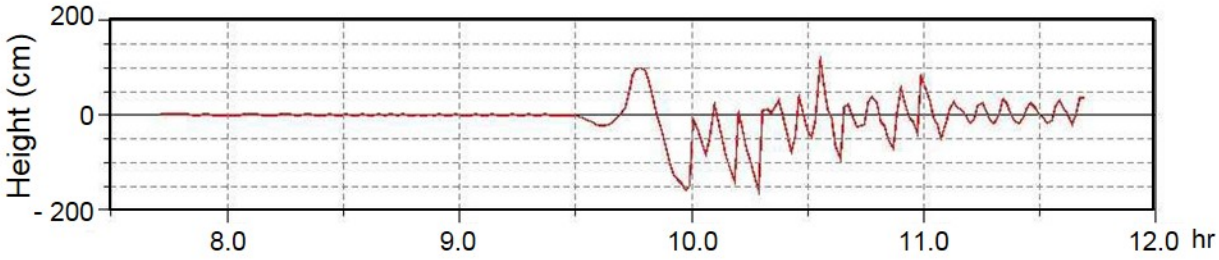

(b) Time series of wave amplitude (cm) at the gauge

Figure 4.22: MOST inundation results for Daytona Beach, Florida (C-grid). Tide gauge location at the mouth of the Ponce de Leon marked by star in (a).

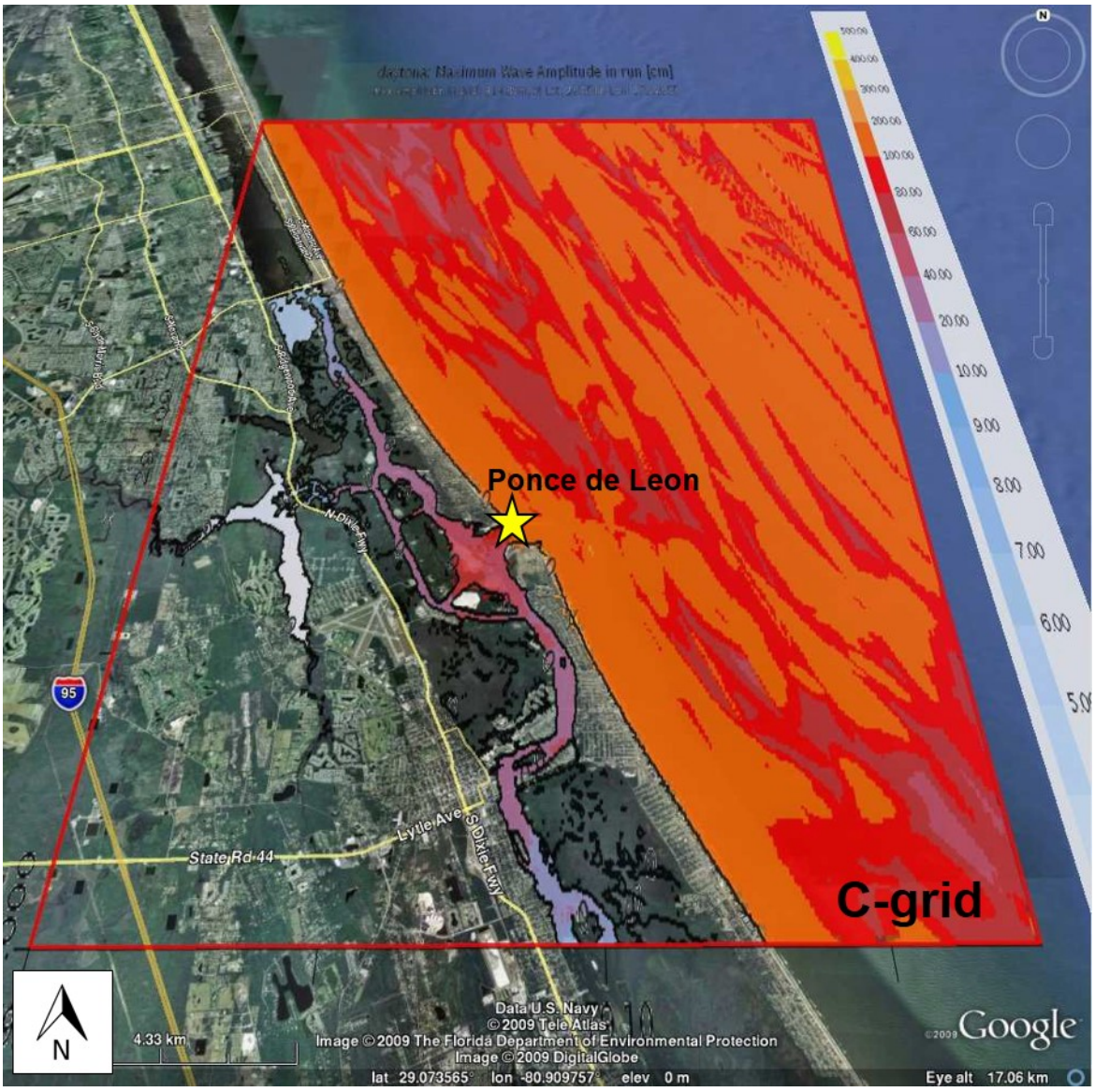

Figure 4.23: Maximum wave amplitude (cm) for Daytona Beach, Florida (C-Grid).

Figure 4.24 shows maximum amplitudes over a cross-section of the continental slope and shelf. The figure indicates the characteristic peak amplitude over the shelf break and gradual attenuation across the shallow shelf. Amplitudes of only about a meter occur near the shoreline, in agreement with Figure 4.23.

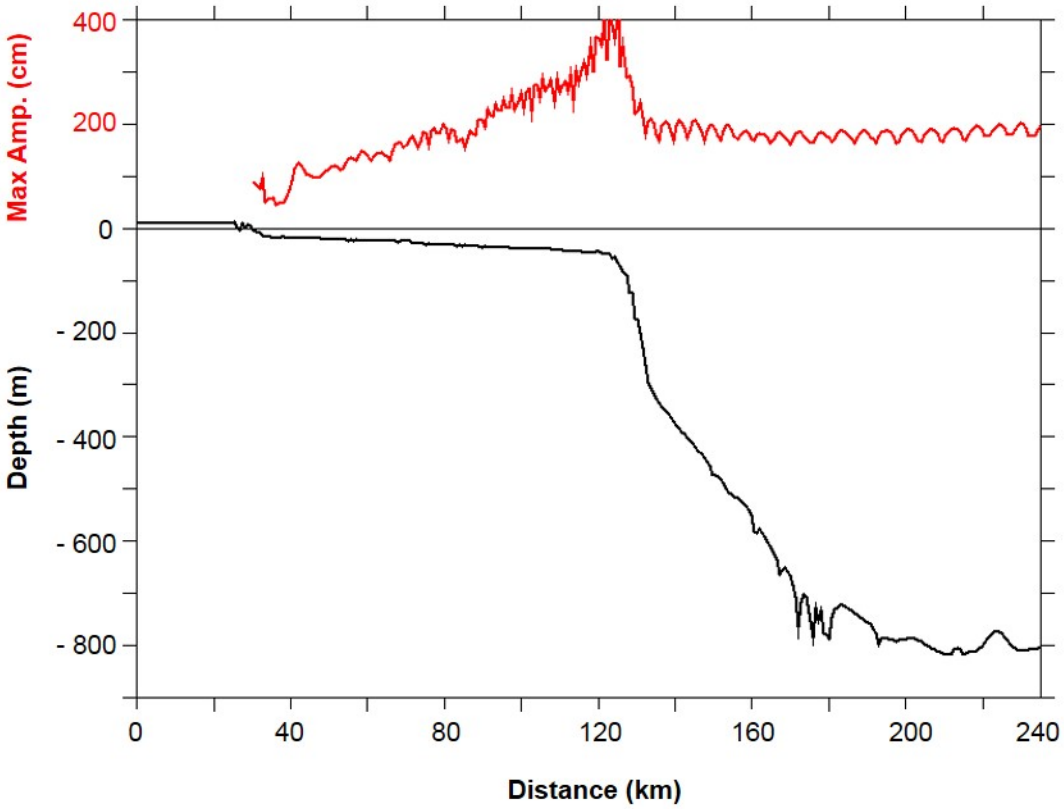

Figure 4.24: Daytona Beach inundation results: maximum wave amplitude (red) over the slope and shelf along a longitudinal section at 29.87° N. Note the different scales for amplitude and depth.

4.5.2 Inundation at Myrtle Beach, South Carolina

The Myrtle Beach SIM is the second region studied using this coupled scenario. Figure 4.25 shows the grid extents and bathymetry of the region. Due to the directionality of the wave energy of the deep-ocean propagation (Figure 4.1), the total wave amplitudes predicted to occur at this location are lower than at Daytona Beach.

The wave front in the A-grid dissipates considerably as it travels over the wide, shallow shelf. The wavelength also decreases drastically, as can be seen in the difference between the wave at the shelf break (Figure 4.26a) and the wave at the beach (Figure 4.26b).

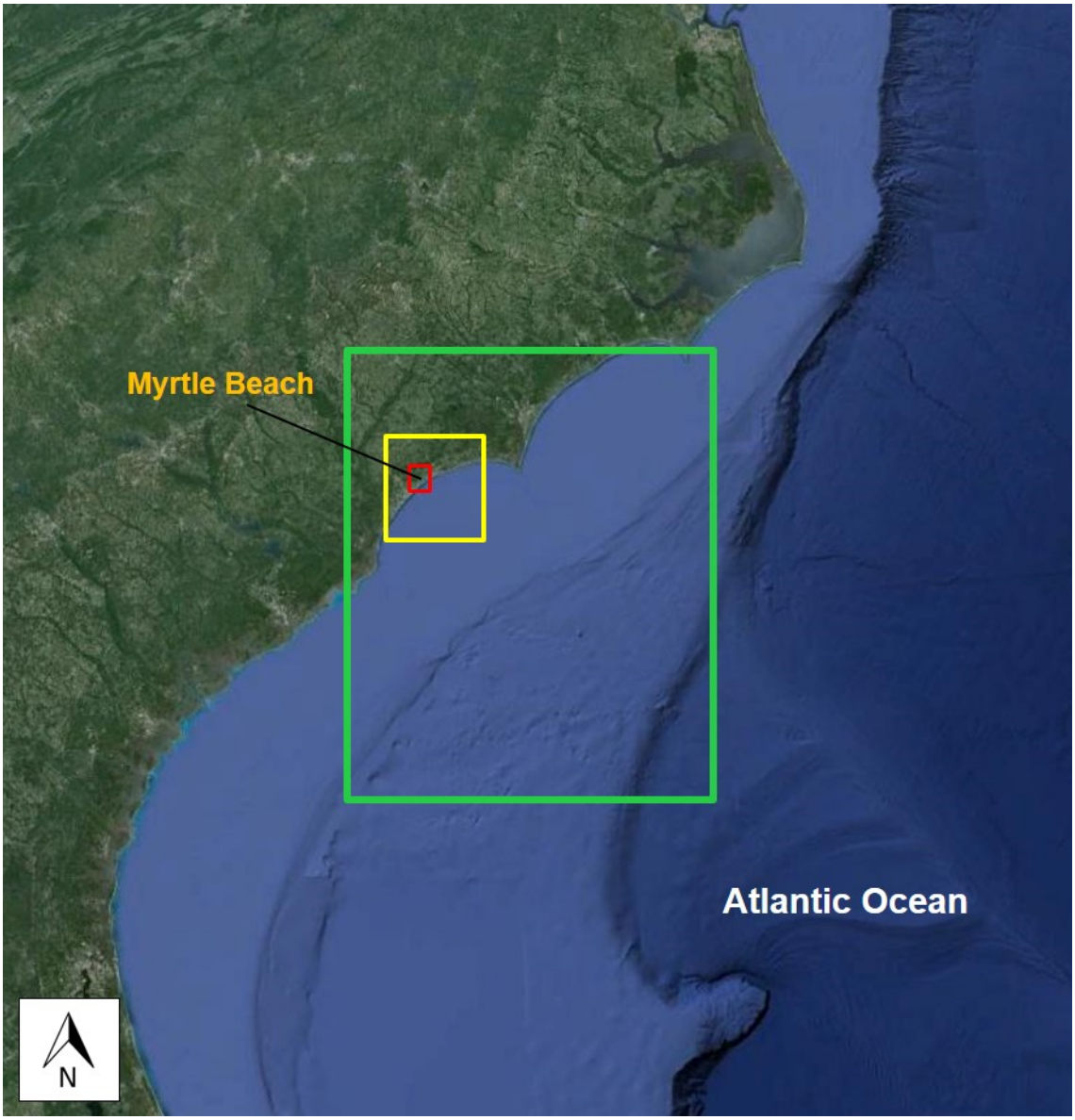

Figure 4.25: Overview of the Myrtle Beach, South Carolina, MOST inundation run, showing A-grid (green), B-grid (yellow), and C-grid (red) extents.

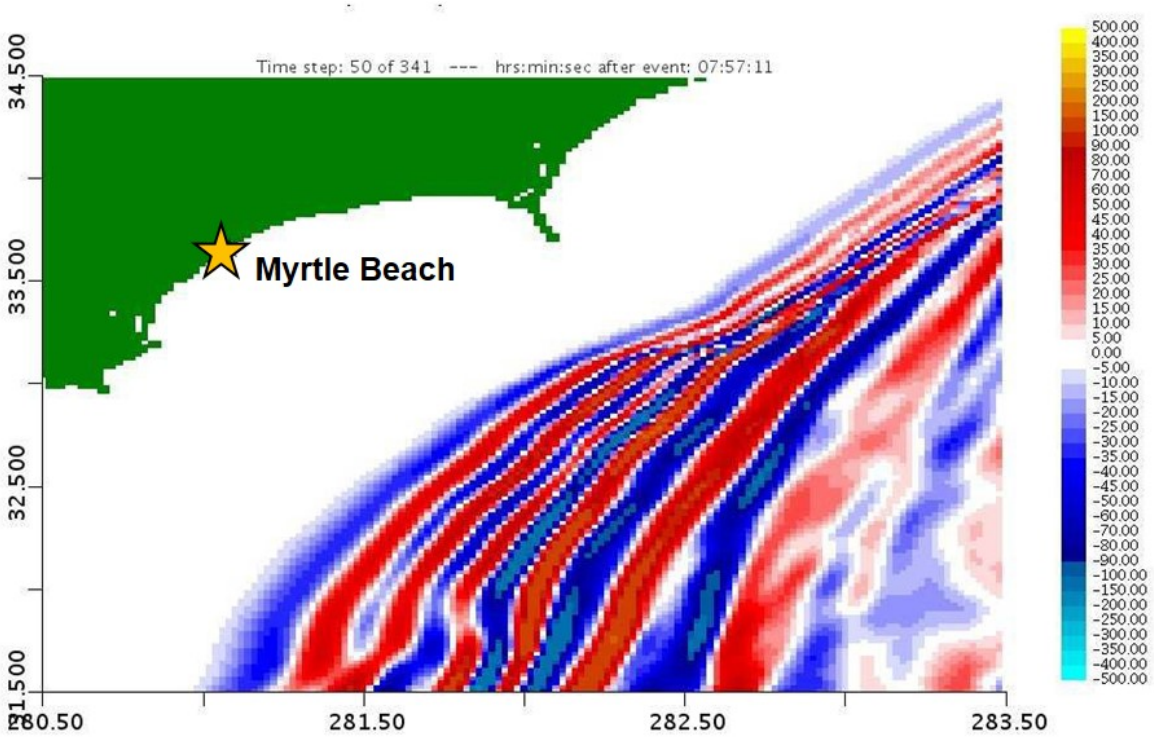

(a) Wave amplitude (cm) at T=07:57 (hh:mm)

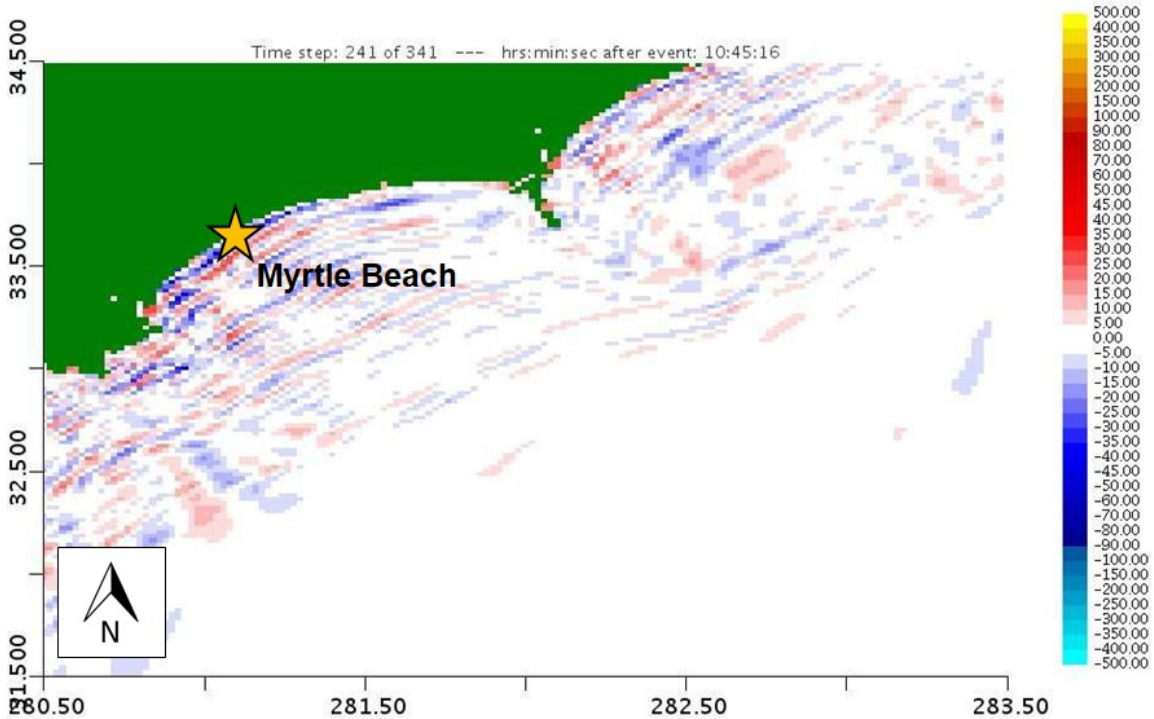

(b) Wave amplitude (cm) at T=10:45 (hh:mm)

Figure 4.26: MOST inundation results for Myrtle Beach, South Carolina (Grid-A).

Figure 4.27 shows the wave as it arrives at the beach at 10 hours 14 minutes after the landslide. The wave has an amplitude of 55 cm all along the shoreline. The maximum runup value observed in the simulation is 71 cm at the southernmost point in the grid. No inundation is predicted in this simulation (Figure 4.28).

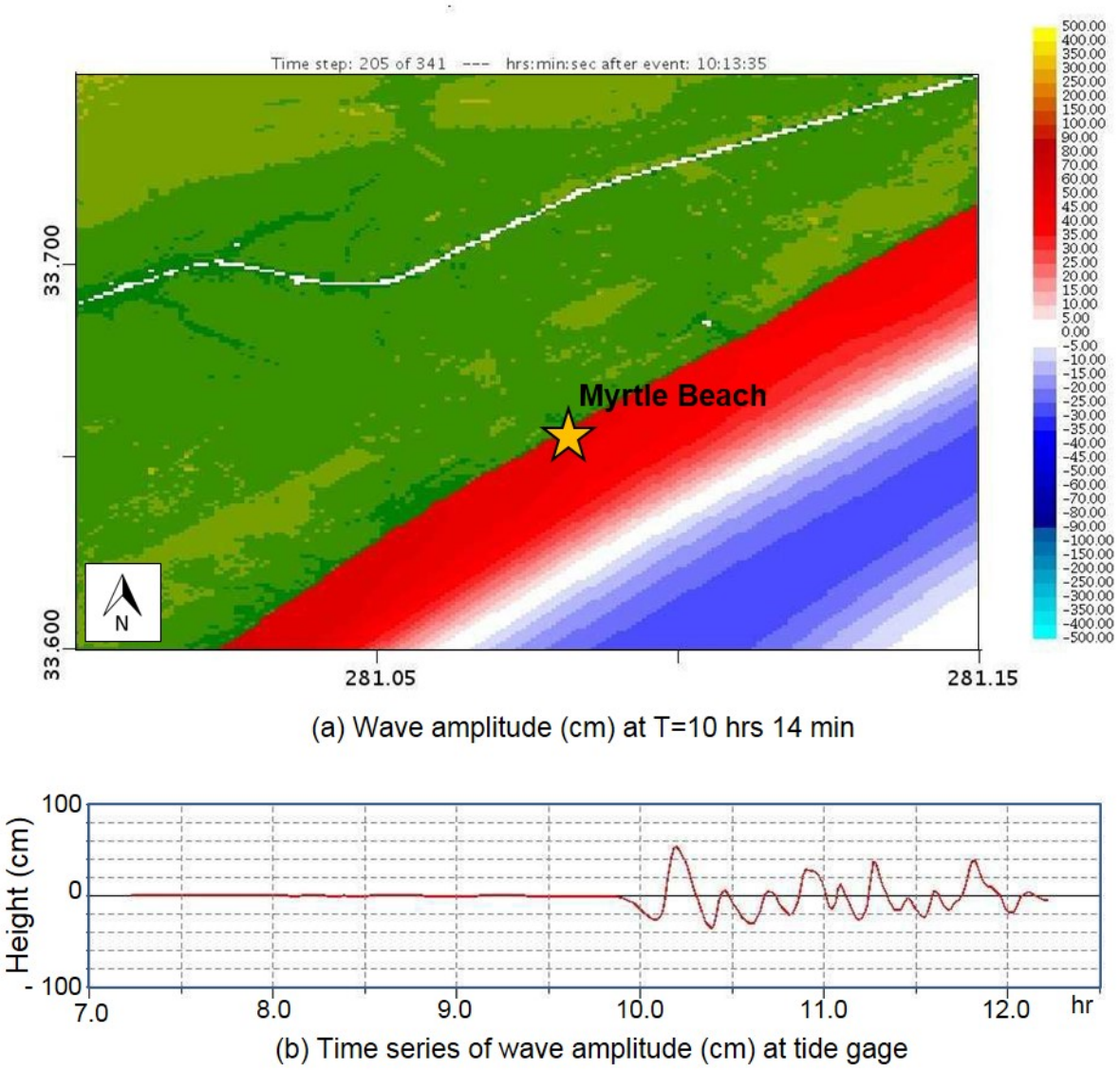

(a) Wave amplitude (cm) at T=10 hrs 14 min

(b) Time series of wave amplitude (cm) at tide gage

Figure 4.27: MOST inundation results for Myrtle Beach, South Carolina (C-grid). Tide gauge location is marked by star in (a).

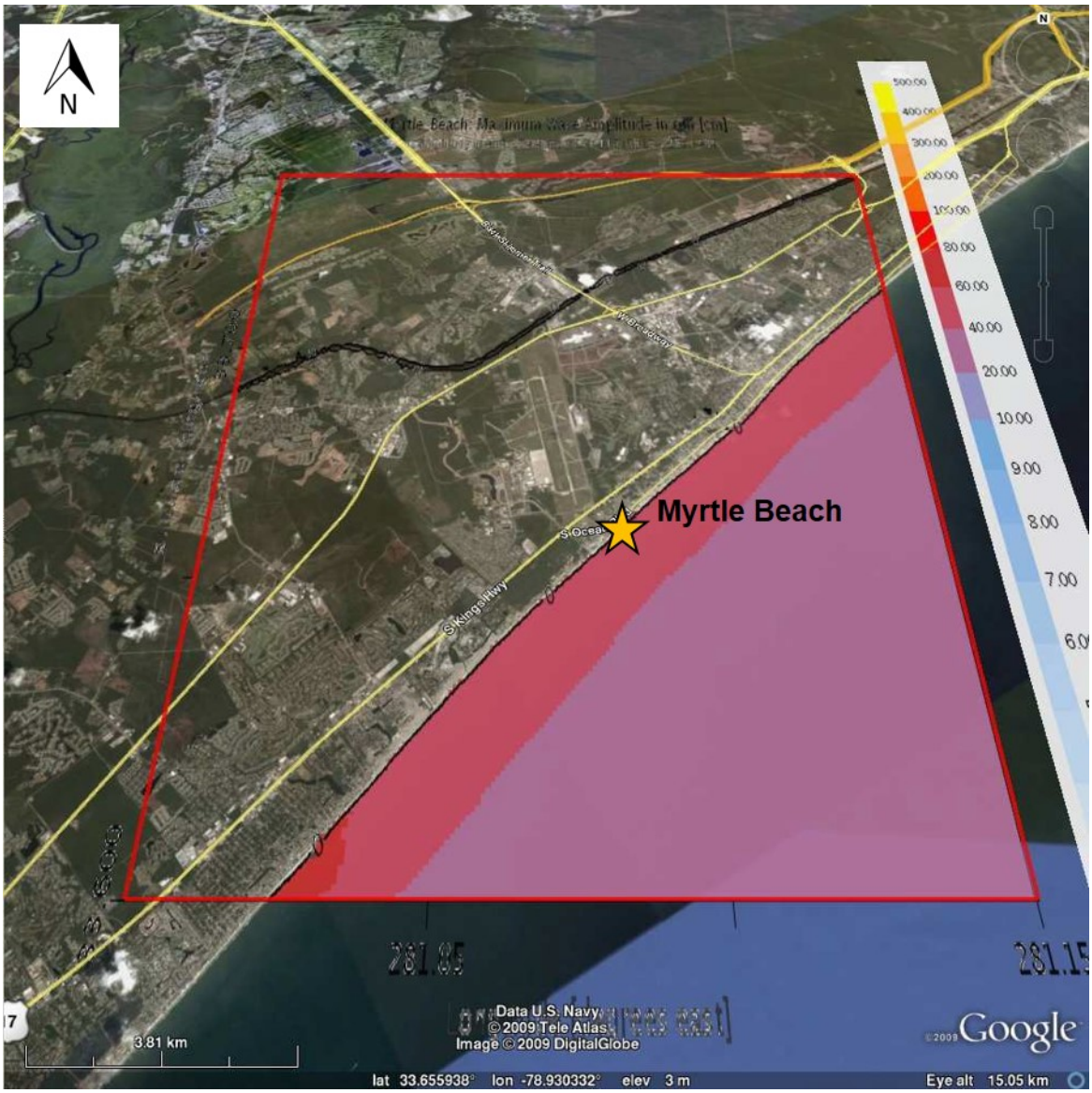

Figure 4.28: Maximum wave amplitude (cm) for Myrtle Beach, South Carolina.

Figure 4.29 shows an even more marked degree of amplitude attenuation over the shelf than at Daytona Beach, with peak amplitude again occurring at the shelf break. The lower peak amplitude predicted at this location is due to the fact that the energy of the wave is focused away from Myrtle Beach, possibly due to the blocking effect that Bermuda Island has on the incoming wave (Figure 4.1).

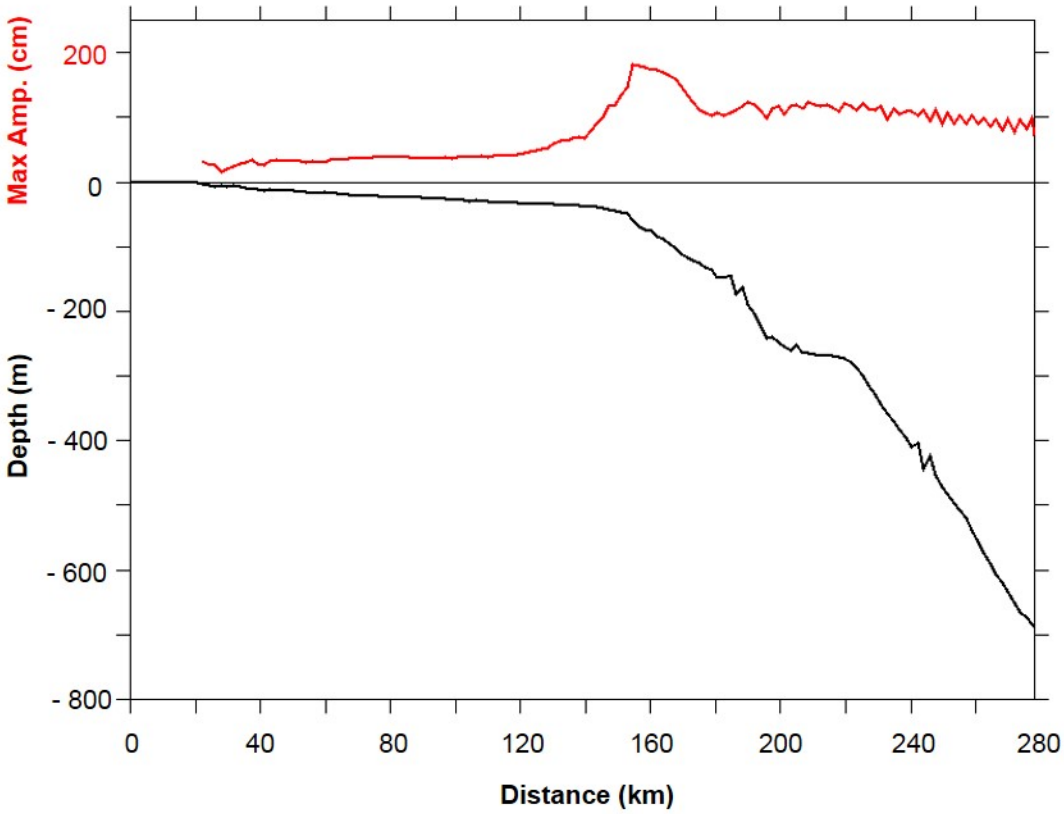

Figure 4.29: Myrtle Beach inundation results: maximum wave amplitude (red) along a longitude section at 32.0° N latitude over the slope and shelf. Note different scale for amplitude and depth.

4.6 Conclusions

The iSALE advection scheme is currently being refined to match the past landslide deposition patterns more closely in the region west of La Palma. This work is being undertaken because the results of the current iSALE run do not match observed runup data as well as Løvholt et al. (2008) has achieved using the Los Alamos National Laboratory SAGE hydrocode. However, the porosity model in iSALE should give us more accurate slide velocities than SAGE as the benchmarking section has shown, and their simulations take no account of interaction between the slide body and the basement.

Because the assumptions of linear theory break down over the shallow shelf for the shorter wavelengths characteristic of landslide waves, and wave dispersion is not explicitly simulated, using even the non-linear version of MOST for the propagation phase may be a possible source of uncertainty. This comparison with the Boussinesq model on the narrow propagation grid used in this report shows that MOST tends to over-estimate wave amplitudes across deep ocean basins, while modeling wave evolution fairly well over shallow continental shelves.

The inundation locations in this report (Myrtle Beach, Daytona Beach, Virginia Beach) were chosen because they are near the latitude of the landslide sources chosen for study, and because these grids were among the first to be developed in the NOAA forecast system.

As discussed, these locations show little inundation due to wave amplitude attenuation over the shelf. However, other U.S. East Coast locations might show a much higher level of impact because the shelf is significantly narrower in other regions, particularly Cape Hatteras, as it tends to lie in the path of high-amplitude waves from La Palma and Currituck, and because the shelf is at its narrowest at this location.

For the La Palma simulation, wave amplitudes at Myrtle Beach were less than 1 m, as compared to the 1 to 2 m amplitudes at Daytona Beach, because of the directionality of the propagating wave, and possibly due to blocking by Bermuda Island (Figure 4.1). The incoming waves are short, less than 1 km, and steep, with amplitudes off-shelf of almost 2 m, rising to a peak amplitude of about 2 m off Myrtle Beach and about 4 m off Daytona Beach, at the location of the shelf break (Figure 4.24). However, these amplitudes drop quickly as the waves cross the shelf. Time aliasing in Figure 4.24 indicates that the limit of resolving these short waves has been reached, and the new coupling run will go to the higher-resolution SIFT ”reference” grids when modeling the inundation phase.

4.7 Bibliography

Amsden, A. A., H. M. Ruppel, and C. W. Hirt (1980), Simplified ALE computer program for fluid flow at all speeds: Technical report la-8095, *Tech. rep.*, Los Alamos National Laboratory, Los Alamos, NM.

Carracedo, J. (1994), The Canary Islands: an example of structural control on the growth of large oceanic-island volcanoes, *Journal of Volcanology and Geothermal Research*, *60*, 225–241.

Chen, Q., J. Kirby, A. Dalrymple, R.A., and Kennedy, and A. Chawla (2000), Boussinesq modeling of wave transformation, breaking, and runup. ii: 2d, *Journal of Waterway, Port, Coastal, and Ocean Engineering*, *126(1)*, 48–56.

Fritz, H., W. Hager, and H.-E. Minor (2003), Landslide generated impulse waves: part 1: Instantaneous flow fields, *Exp. Fluids*, *35*, 505–519.

Fritz, H., W. Hager, and H. Minor (2004), Near field characteristic of landslide generated impulse waves, *Journal of Waterway, Port, Coast, and Ocean Engineering*, *130 (6)*, 287–302.

Fuhrman, D., and P. Madsen (2009), Tsunami generation, propagation, and run-up with a high-order Boussinesq model, *Coastal Engineering*, *56*, 747–758.

Geist, E., P. Lynett, and J. Chaytor (2009), Hydrodynamic modeling of tsunamis from the Currituck landslide, *Marine Geology*, *264*, 41–52.

Gisler, G., R. Weaver, and M. Gittings (2006), SAGE calculations of the tsunami threat from La Palma, *Science of Tsunami Hazards*, *24*, 288–301.

Grilli, S., and P. Watts (2005), Tsunami generation by submarine mass failure. i: Modeling experimental validation, and sensitivity analyses, *Journal of Waterway, Port, Coastal, and Ocean Engineering*, *131(6)*, 283–297.

Grue, J., E. Peliovsky, D. Fructus, T. Talipova, and C. Kharif (2008), Formulation of undular bores and solitary waves in the Strait of Malacca caused by the 26 December 2004 Indian Ocean tsunami, *Journal of Geophysical Research*, *113*(C05008), doi: 10.1029/2007JC004343.

Ioualalen, M., J. Asavanant, N. Kaewbanjak, S. Grilli, J. Kirby, and P. Watts (2007), Modeling the 26 December 2004 Indian Ocean tsunami: Case study of impact in Thailand, *Journal of Geophysical Research*, *112*(C07024), doi:10.1029/2006JC003850.

Kennedy, A., Q. Chen, J. Kirby, and R. Dalrymple (2000), Boussinesq modeling of wave transformation, breaking, and runup. i: 1d, *Journal of Waterway, Port, Coastal, and Ocean Engineering*, *126(1)*, 39–47.

Løvholt, F., G. Pedersen, and G. Gisler (2008), Oceanic propagation of a potential tsunami from the La Palma Island, *J. Geophys. Res.*, *113*(C09026), doi:10.1029/2007JC004603.

Lynett, P., and P.-F. Liu (2002), A numerical study of submarine-landslide-generated waves and run-up, pp. 2885–2910.

Masson, D., C. Harbitz, R. Wynn, and F. Pedersen, G., and Løvholt (2006), Submarine landslides – processes, triggers and hazard prediction, *Philosophical Transactions of the Royal Society*, *A 364*, 2009–2039.

Nwogu, O. (1993), Alternative form of Boussinesq equations for nearshore wave propagation, *Journal of Waterway, Port, Coastal, and Ocean Engineering*, *119(6)*, 618–638.

P., W., S. Grilli, J. Kirby, G. Fryer, and D. Tapin (2003), Landslide tsunami case studies using aB model and a fully nonlinear tsunami generation model, *Natural Hazards and Earth System Sciences*, *3*, 391–402.

Synolakis, C., E. Bernard, V. Titov, U. Kaˆnogˇ lu, and F. Gonza´lez (2007), Standards, criteria, and procedures for NOAA evaluation of tsunami numerical models. NOAA Technical Memorandum OAR PMEL-135, *Tech. rep.*, NOAA Pacific Marine Environmental Laboratory, Seattle, WA.

Synolakis, C., E. Bernard, V. Titov, U. Kaˆnogˇ lu, and F. Gonza´lez (2009), Validation and verification of tsunami numerical models, *Pure Appl. Geophys*, *165*((11-12)), 2197–2228.

ten Brink, U.S., D. Twichell, E. Geist, J. Chaytor, J. Locat, H. Lee, B. Buczkowski, R. Barkan, A. Solow, B. Andrews, T. Parsons, P. Lynett, J. Lin, and M. Sansoucy (2008), Evaluation of tsunami sources with the potential to impact the U.S. Atlantic and gulf coasts– an updated report to the Nuclear Regulatory Commission, *Tech. rep.*, U.S. Geological Survey.

Titov, V., and F. Gonza´lez (1997), Implementation and testing of the Method of Splitting Tsunami (MOST) model. NOAA Technical Memorandum ERL PMEL-112, *Tech. rep.*, NOAA Pacific Marine Environmental Laboratory, Seattle, WA.

Titov, V., and C. Synolakis (1998), Numerical modeling of tidal wave runup, *J. Waterw. Port Coast. Ocean Eng.*, *124*(4), 157–171.

Ward, S. N., and S. J. Day (2001), Cumbre Vieja volcano; potential collapse and tsunami at La Palma, Canary Islands, *Geophys. Res. Lett.*, *28*(17), 3397–3400.

Watts, P. (1998), Wavemaker curves for tsunamis generated by underwater landslides, *Journal of Waterways, Port, Coastal, and Ocean Engineering*, *124(3)*, 127–137.

Watts, P. (2000), Tsunami features of solid block underwater landslides, *Journal of Waterway, Port, Coastal, and Ocean Engineering*, *126 (3)*, 144–152.

Wei, G., J. Kirby, S. Grilli, and R. Subramanya (1995), A fully nonlinear Boussinesq model for surface waves. part 1. highly nonlinear unsteady waves, *Journal of Fluid Mechanics*, *294*, 71–92.

Wei, Y., E. Bernard, L. Tang, R. Weiss, V. Titov, C. Moore, M. Spillane, M. Hopkins, , and U. Kaˆnogˇ lu (2008), Real-time experimental forecast of the Peruvian tsunami of August 2007 for U.S. coastlines, *Geophys. Res. Lett.*, *35* (L04609), doi:10.1029/2007GL032250.

Weiss, R., H. Fritz, and K. Wu¨ nnemann (2009), Hybrid modeling of the mega-tsunami runup in Lituya Bay after half a century, *Geophysical Research Letters*, *36*(L09602), doi: 10.1029/2009GL03714.

Whelan, F., and D. Kelletat (2003), Submarine slides on volcanic islands - a source for mega-tsunamis in the Quaternary, *Progress in Physical Geography*, *27*, 198–216.

Zhou, H., and M. Teng (2010), Extended fourth-order depth-integrated model for water waves and currents generated by submarine landslides, *Journal of Engineering Mechanics*, 136(4), 516-517.

Zhou, H., C. W. Moore, Y. Wei, and V. V. Titov (2011), A nested-grid Boussinesq-type approach to modeling dispersive propagation and runup of landslide-generated tsunamis, Natural Hazards and Earth System Sciences, 11, 2677-2697.

5. LANDSLIDE HAZARDS FROM THE CONTINENTAL SLOPE

5.1 Introduction

The coupled iSALE/MOST model system was used to simulate the effect of the Currituck landslide on the continental slope and possible inundation at the coastline near Currituck and the surrounding area from Cape Hatteras, North Carolina, to Virginia Beach, Virginia. Critical differences exist between the SAGE results modeled in Geist et al. (2009) and this work, including, but not limited to, the inclusion of interaction between the slide body and the underlying basement, and the explicit modeling of the slide body and resulting hydrodynamics. The geomorphology of the slide was studied in ten Brink et al. (2008) and Prior et al. (1986), and guides us in choosing the modeling geometry as well as critical parameters for the multi-material iSALE code. The critical findings from these studies are the geometry of the slide (with a volume of approximately 150 km^3), the fact that it took place as a single event lasting less than 10 minutes with peak velocities between 30 and 40 m/s, and that the yield strength of the slide material was on the order of 2,000 Pa. The iSALE parameters and grid were selected from these estimates, and use the MOST model and the NOAA forecast methodology to couple the landslide results to an inundation model to look at wave evolution on the continental slope and inundation at the coast.

Figure 5.1 shows the extent of the region used for modeling the Currituck slide. The slide axis (shown in slate) represents the location of the iSALE landslide grid, while the slide debris field is outlined in yellow. The bathymetry data used is from the U.S. East Coast (Atlantic) medium-resolution dataset developed by the National Geophysical Data Center. This 9 arc-second grid was obtained from a variety of sources. In the Currituck region, the main dataset was a multibeam survey collected by the Center for Coastal and Ocean Mapping/Joint Hydrographic Center. The shelf is approximately 40 m deep, dropping to 100 m right at the shelf break. The Currituck slide is centered at 36.44° N latitude, and the width of the shelf at this latitude is 93 km.

Figure 5.2a shows a simple slide geometry, with a single slide body with a volume of 157.6 km^3 and a shallow shelf from 0–100 m deep. The second, more complicated geometry shown in Figure 5.2b shows two slide bodies of thickness 200 m and 300 m, respectively, and better reflects the true geometry as estimated by Prior et al. (1986). In order to better match the total volume of the simple geometry, the shelf slope angle was kept at 6 degrees and extend the slope distance to 3000 m deep. The figure exaggerates the extended depth because the vertical axis is stretched by a factor of 50:1 for visual clarity.

The landslide model was coupled with the MOST, as shown in Figure 5.3, with the shoreward-propagating trough and oceanward propagating crest input into the outer-most of the three nested grids at a point two minutes into the iSALE simulation. This profile was used to force the Virginia Beach high-resolution reference forecast model using the fully nonlinear MOST code.

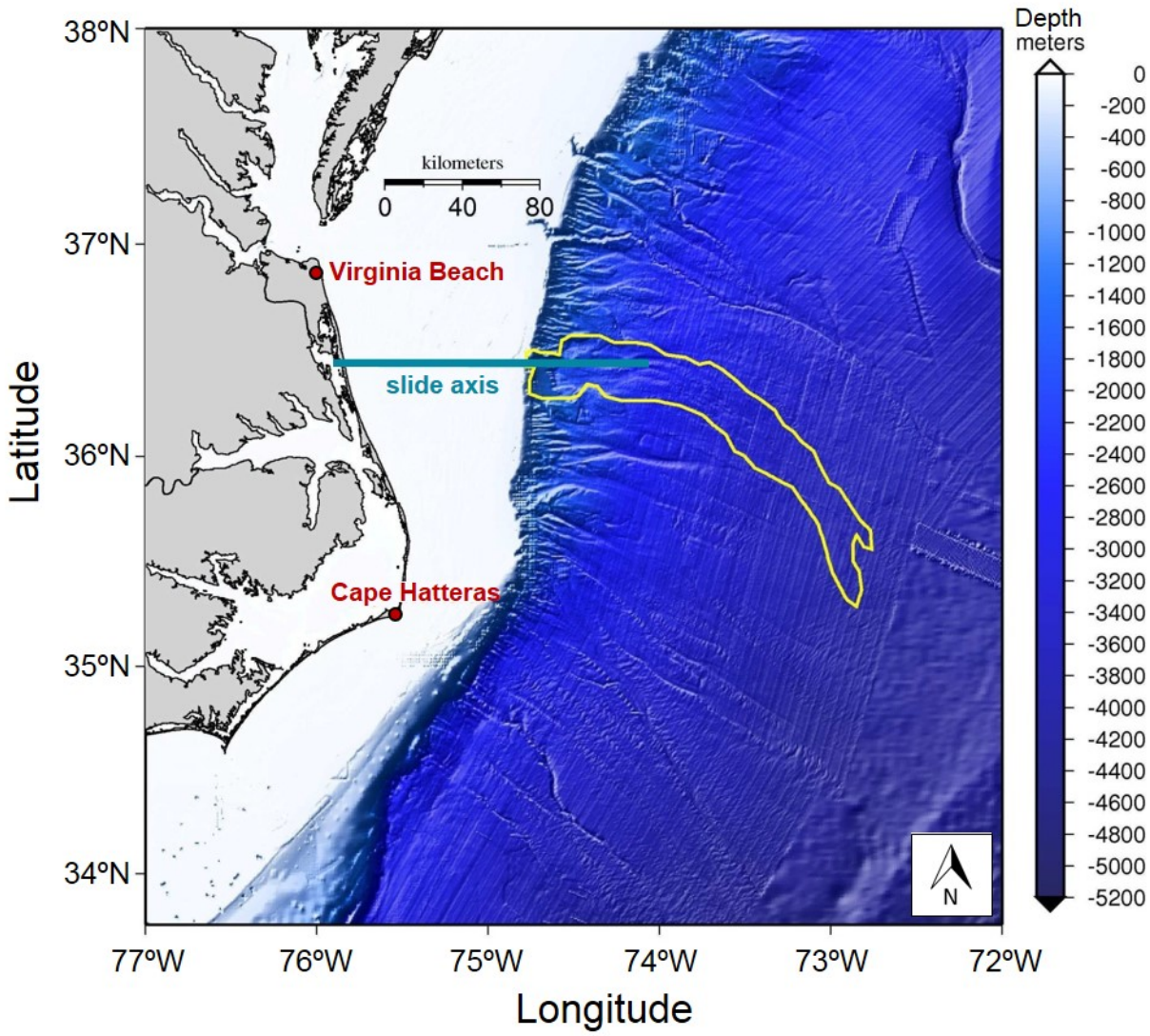

Figure 5.1: Overview of the Currituck region used for modeling MOST, including the slide axis for the 1HD iSALE model (slate), and measured historical debris field (yellow).

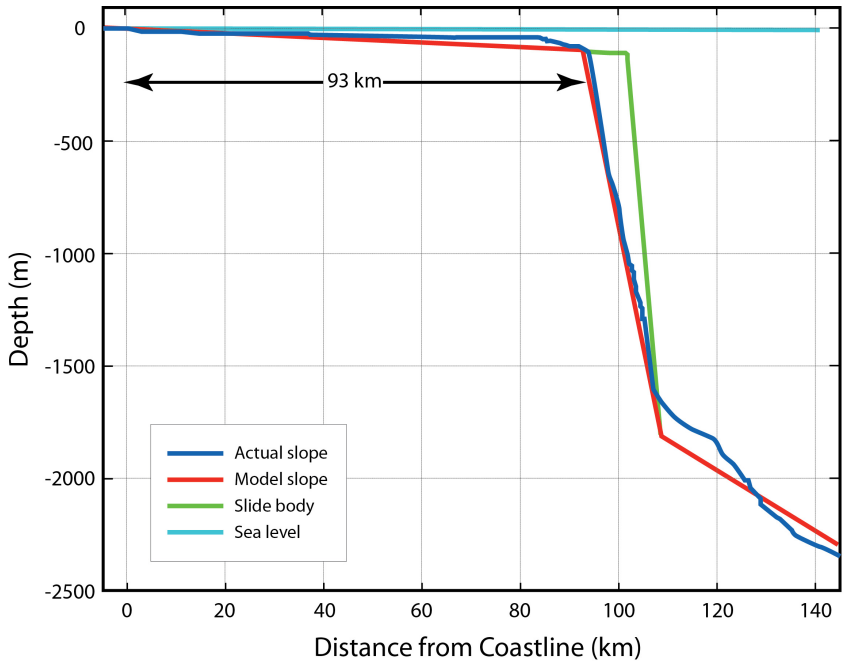

(a) Simple geometry of slope and slide body. The actual slope (darker blue) is shallower than the model slope (red) over the shelf. The slide body (green) is modeled as a single body with a volume of 157.6 km^3 (assuming a 20 km slide body width).

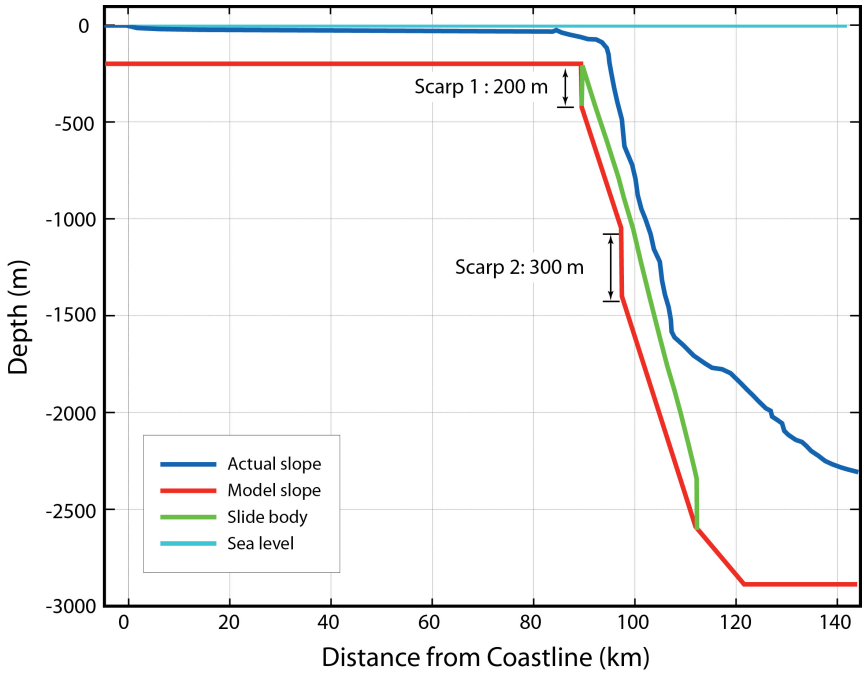

(b) More complicated slide body consisting of two scarps. Notice the much deeper model shelf (200 m, red) compared to the actual shelf (darker blue). The combined slide bodies (green) have a total volume of 154.7 km^3.

Figure 5.2: The Currituck slope and slide body geometries (from Prior et al. (1986))

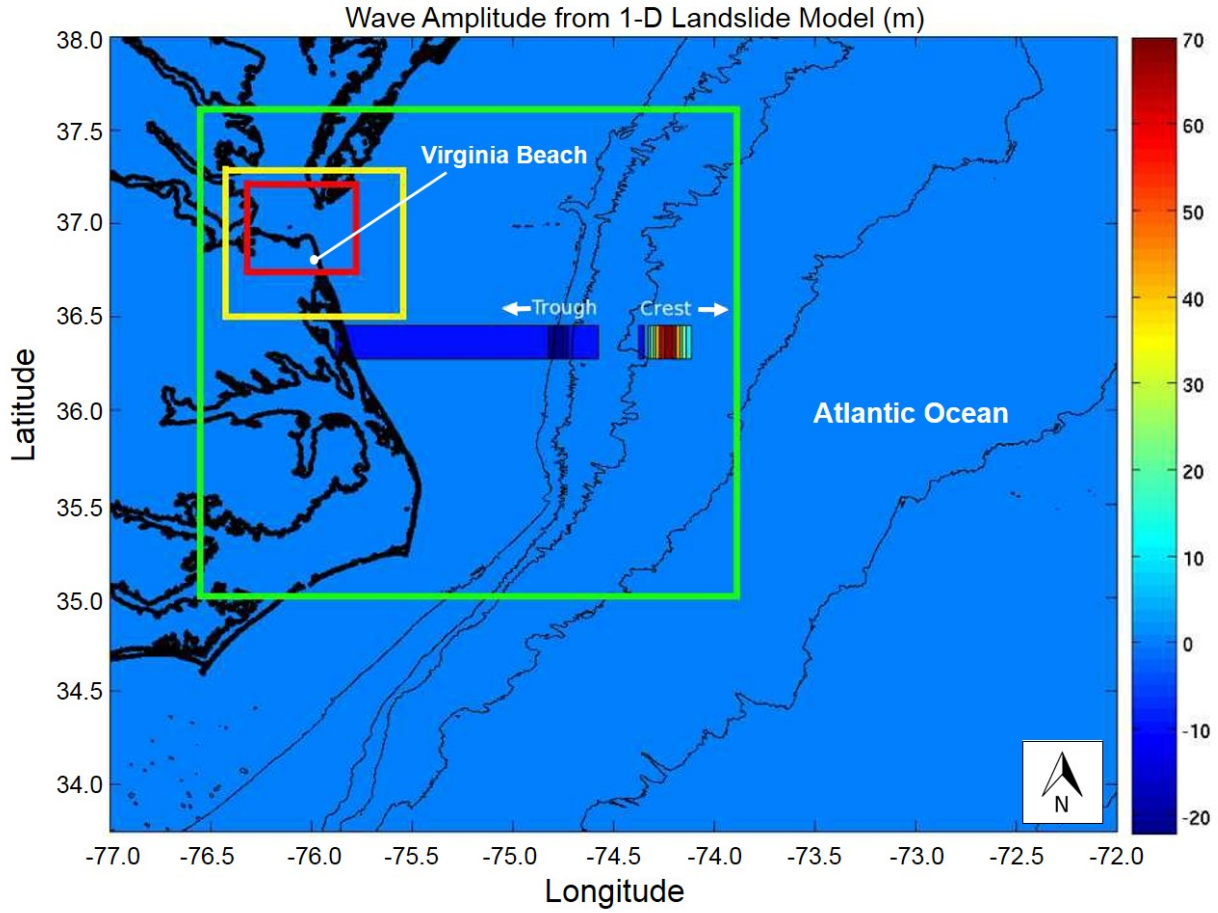

Figure 5.3: The coupling region showing ocean-going crest and shoreward propagating trough generated by the iSALE model. The three nested grids for the Virginia Beach forecast model are shown in green (A-grid), yellow (B-grid), and red (C-grid).

5.2 Initial Results

5.2.1 Landslide Results

Varying Geometry

Preliminary sensitivity runs suggested that slide body composition (as implied by iSALE's parameterized equation of state), slide volume, shelf depth, and slide velocity were controlling factors in the resulting wave amplitude and propagation distance over the shelf. Guided by Prior et al. (1986) and ten Brink et al. (2008), a mixed sedimentary slide body composition, and an initial slide velocity of 15 m/s was chosen. The debris runout of 30 km and slide body volume of 165 km^3 was closely matched, and output of the wave profile at 30 s, 2 min, and 15 min are shown in Figure 5.4.

As the slide body starts to move, it leaves a trough behind it and forces a crest at the toe of the slide. The crest propagates towards deep water, and the trough propagates shoreward. As shown in Figure 5.4b, the trough minimum reaches 200 m deep at time $t = 2$ min. As the trough propagates onto the shelf, the amplitude drops to less than 100 m deep (Figure 5.4c). This attenuation continues as the wave propagates shoreward.

The more complex, two-body slide simulation was run with the same initial conditions, but a deeper continental shelf. Figure 5.5a shows initial trough development at the scarp for each slide body (two troughs) that combine to form one by time $t = 2$ min (Figure 5.5b). The maximum trough amplitude is about 100 m, and attenuates to almost half this value at time $t = 2$ min, 75 km from the coastline.

For both geometries, runout distances are about 30 km, and a distinctive wedge-like trough forms and amplitudes attenuate by 100 percent within 20 km of the shelf break. The velocity profile at $x = 100$ km and time $t = 2$ min is shown in Figure 5.6, with the *x*-component of velocity in blue and the *y*-component in red. The slide body velocity is approximately 25 m/s at this point, and the free surface water particle vertical velocity is -25 m/s, indicating that, at this point, the wave is still being forced by the slide body.

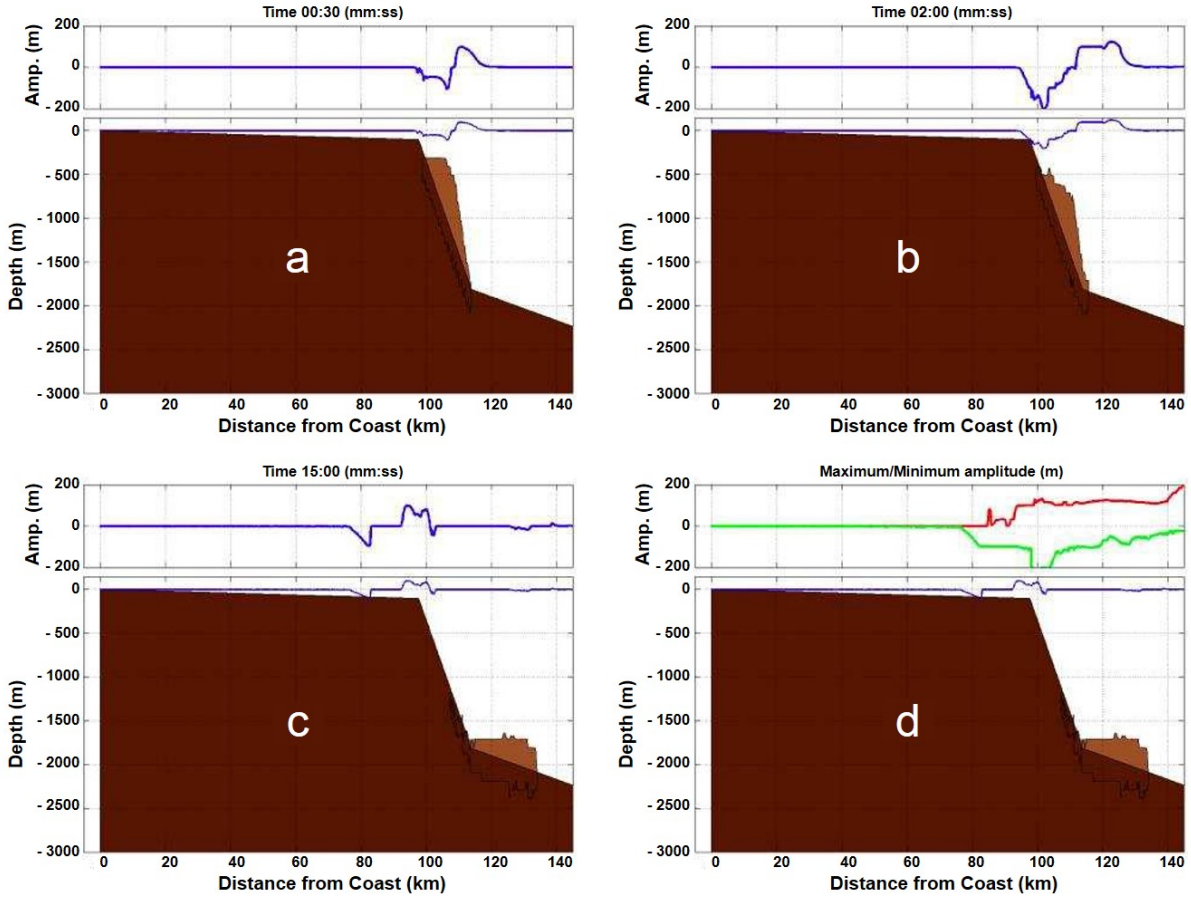

Figure 5.4: Simple geometry iSALE landslide simulation at (a) 30 seconds, (b) 2 minutes, (c) 15 minutes, and (d) maximum/minimum amplitude.

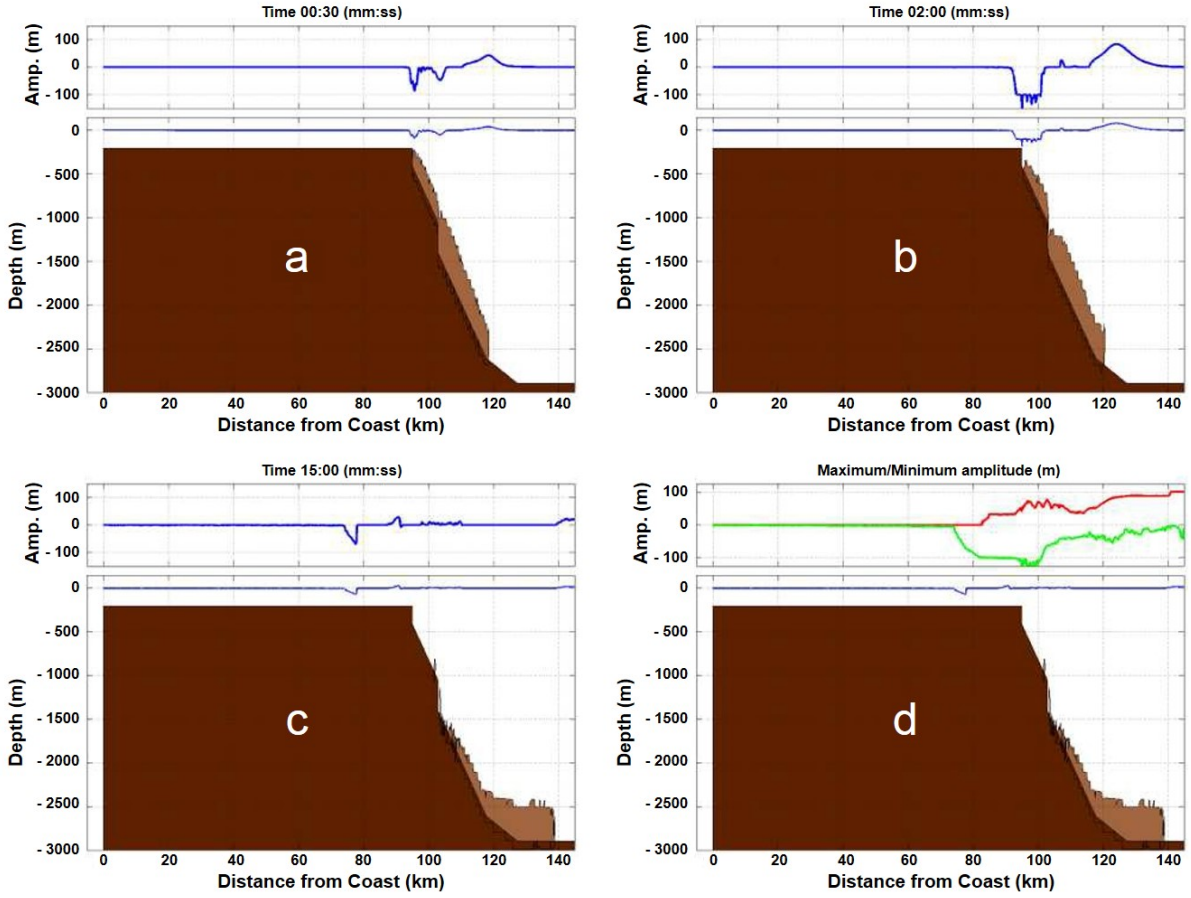

Figure 5.5: Complex geometry iSALE landslide simulation at (a) 30 seconds, (b) 2 minutes, (c) 15 minutes, and (d) maximum/minimum amplitude.

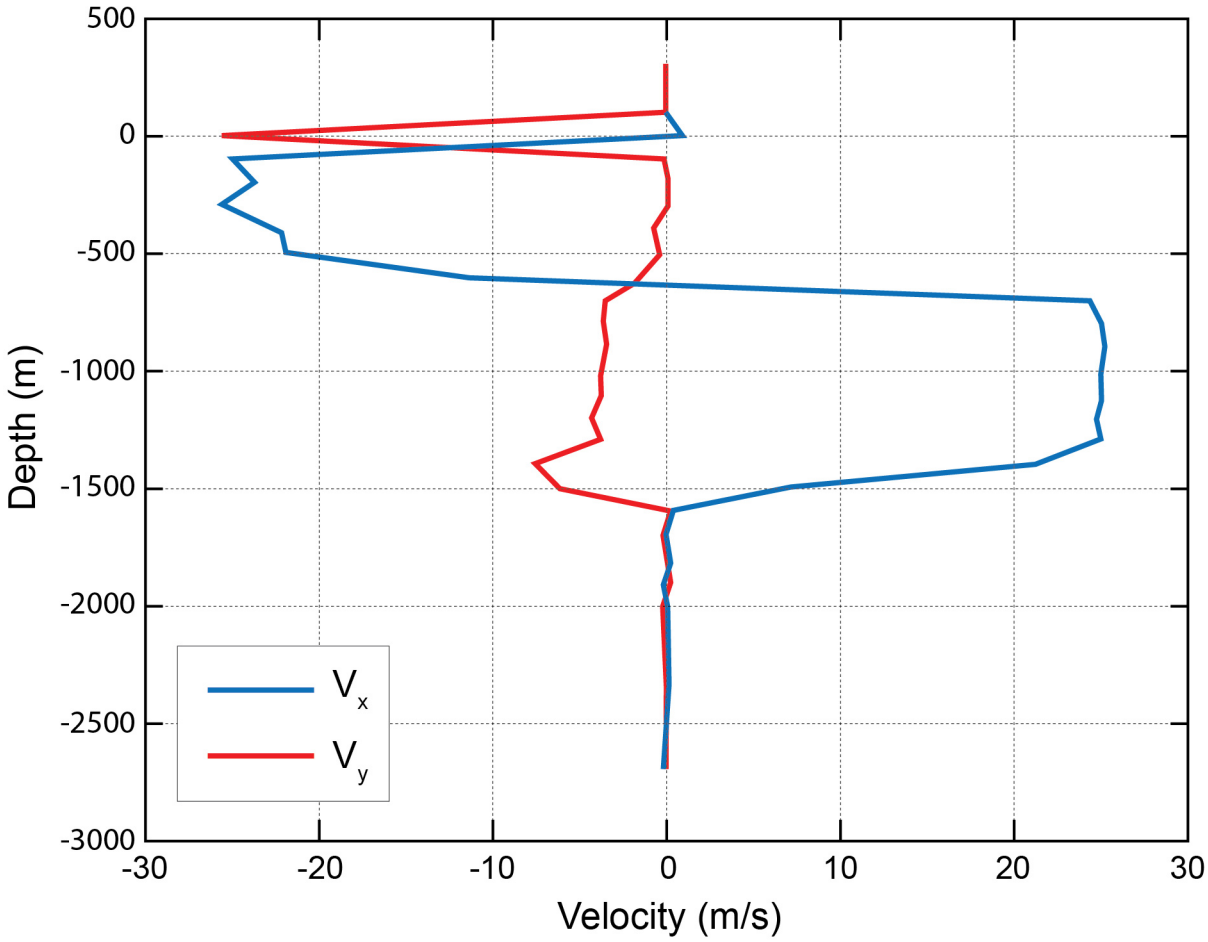

Figure 5.6: Velocity profile of complex geometry iSALE landslide simulation and time t = 2 min, with x-component in blue and y-component in red.

5.3 Inundation Results

The waveform at the maximum wave amplitude of the trough for the complex geometry case was used to force the fully-nonlinear inundation MOST model using the highest resolution forecast model for Virginia Beach, using the technique described in Section 1 of this report and in Titov and González (1997). The waveform is interpolated onto the outermost of the three nested grids as shown in Figure 5.3. The resulting waveform at time $t = 5$ min (red) and $t = 10$ min (green) are shown in Figure 5.7. The wedge-shaped trough is followed by a mirrored wedge-shaped crest exhibiting wave fission, or the creation of very short wavelength waves along the steep leading edge of the crest as described by Geist et al. (2009). The breaking of these waves is the sink to the energy cascade, and the subsequent lessening of trough amplitude and overall crest amplitude. Note that the trough depth measures 32 m at $t = 5$ min and drops to 25 m at $t = 10$ min.

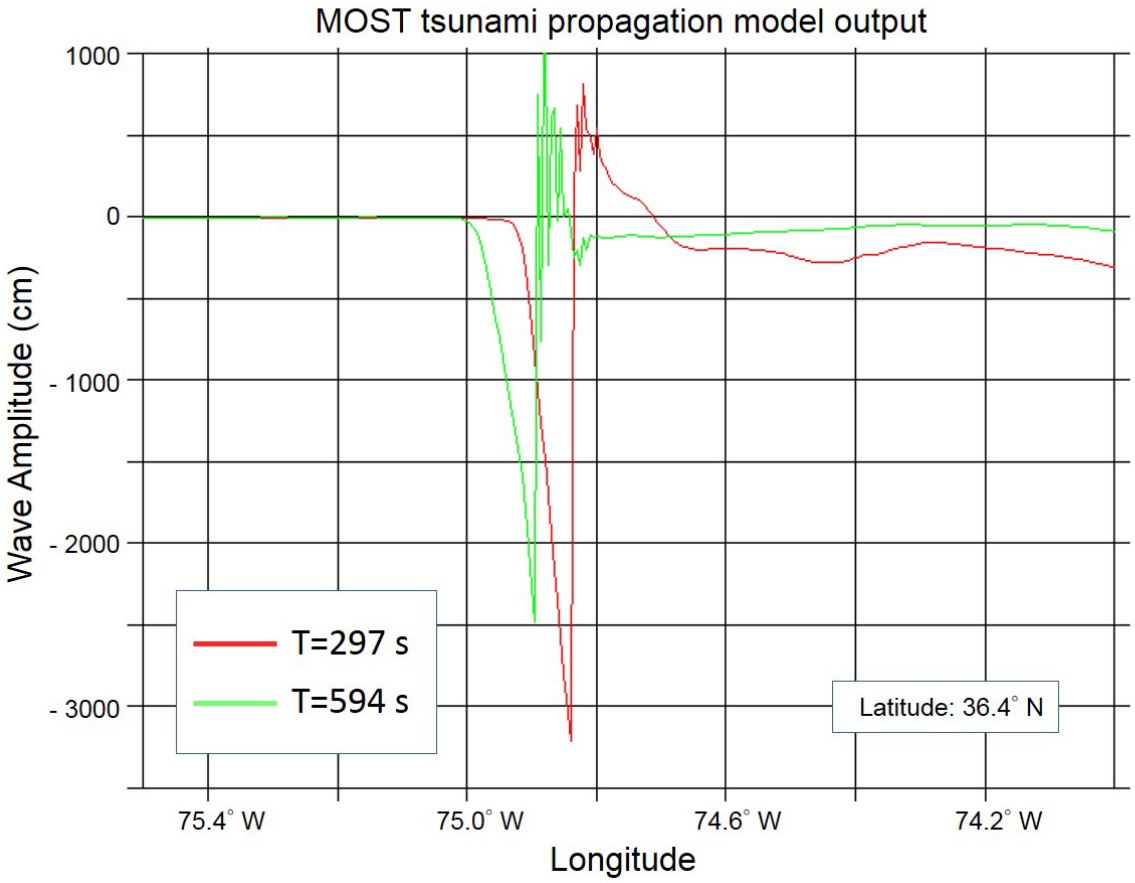

Figure 5.7: Wave amplitude of the Virginia Beach MOST run at time t = 5 min (red) and t = 10 min (green) along the slide axis.

The slide-axis maximum amplitude of the Virginia Beach MOST run is shown in Figure 5.8. An overall maximum of 24.5 m occurs 86 km from the coast, which agrees well with the maximum of 27 m amplitude occurring 75 km from the coast in Geist et al. (2009). The maximum amplitude at the coast (on the slide axis) is just over 3 meters while Geist et al. (2009) obtained 5 m. The overall maximum amplitude of the run is shown in Figure 5.9, which shows the maximum dominated by the growth of the outward-propagating wave. The shoreward-propagating trough creates a following crest, too, which has a maximum just inside the shelf break (red, dashed).

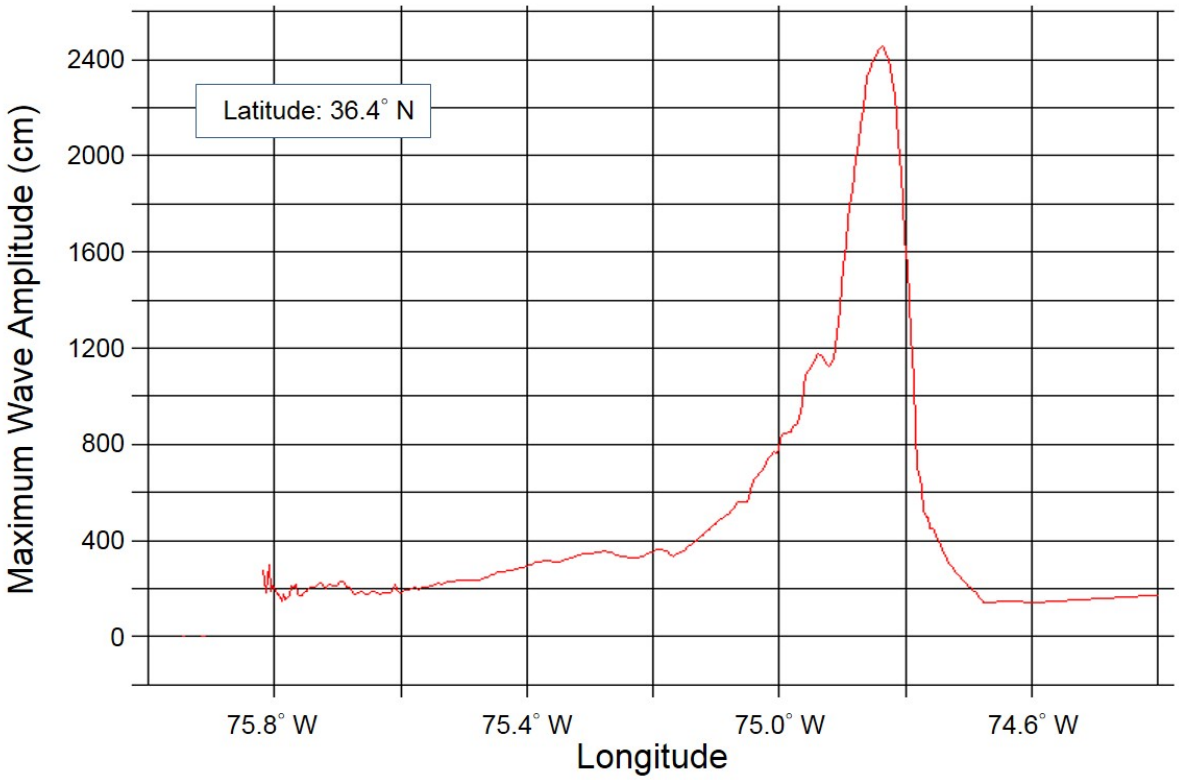

Figure 5.8: Maximum wave amplitude of the Virginia Beach MOST run along the slide axis.

An interesting result, pointed out by Geist et al. (2009), is that the outward-propagating wave refracts at the continental slope, becoming shoreward-propagating both north and south of the slide axis, so that maximum wave amplitude at the coastline occurs not along the slide axis, but north and south of it. Figure 5.10 shows the waves refract in a time sequence illustrating how this off-axis maximum at the coast occurs. In the Virginia Beach run, the coastline maximum occurs to the north within the smallest of the three nested grids (the C-grid) with a maximum amplitude of 4.1 m, and is shown in Figure 5.11.

5.4 Conclusions

Geist et al. (2009) show SAGE simulations of Currituck using an in viscid slide body consisting of granular material, possibly over-estimating slide velocities, and hence wave amplitude. While the strength model present herein tends to over-emphasize cohesion, and interaction with the slope basement tends to under-estimate velocities. This inundation model, while neglecting the Boussinesq approximation, captures the wave fission and attenuation and utilizes the advanced runup scheme of the NOAA MOST forecast model. Even with these different approaches, the overall maximum on the shelf and at the coast, and the wave refraction effects, agree fairly well.

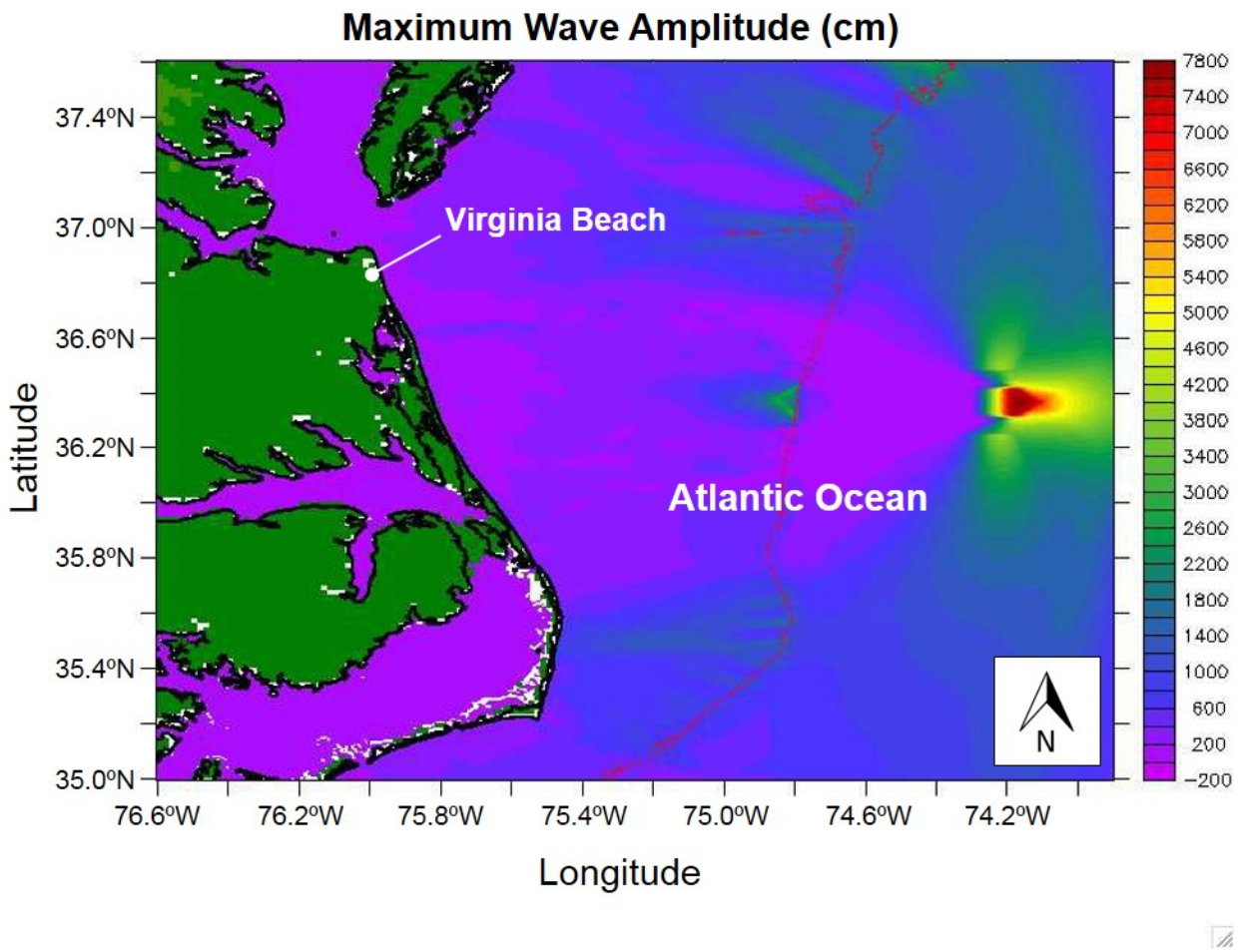

Figure 5.9: Maximum wave amplitude of the Virginia Beach MOST run in the outer-most of the nested grids (A-grid).

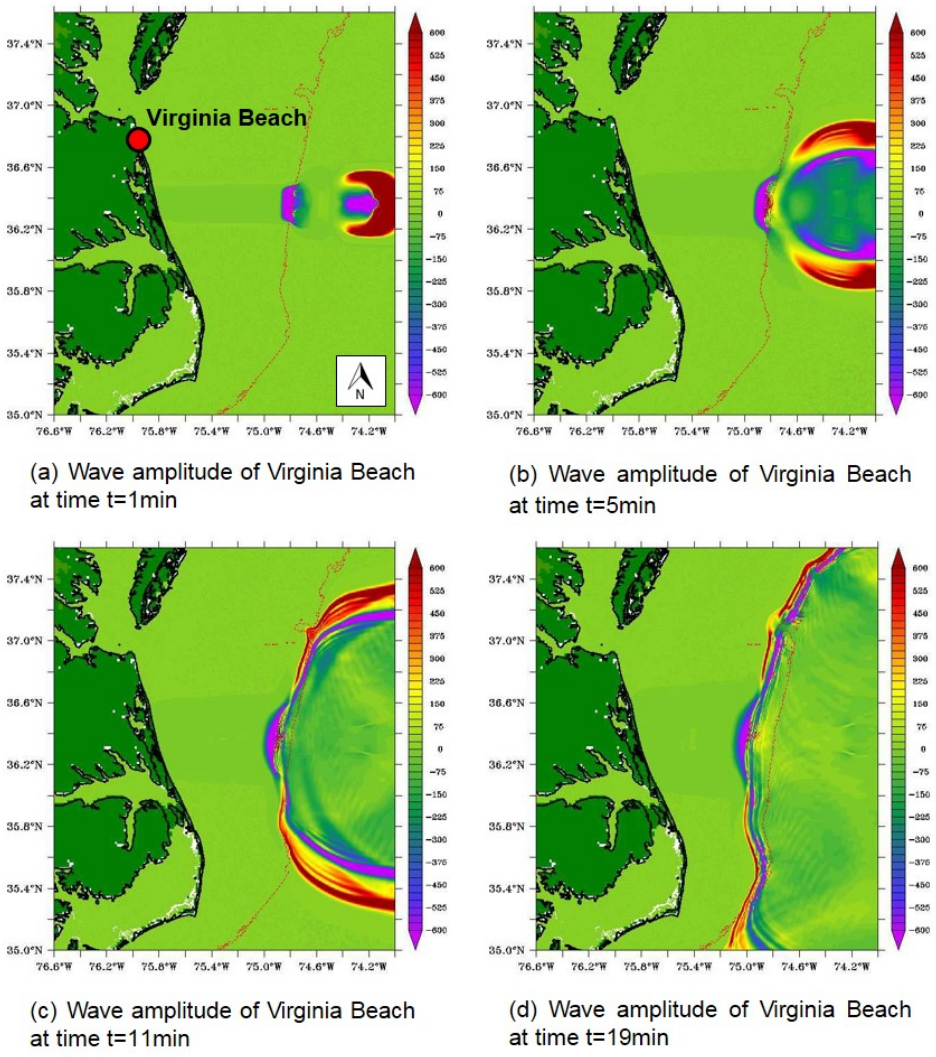

(a) Wave amplitude of Virginia Beach at time t=1min

(b) Wave amplitude of Virginia Beach at time t=5min

(c) Wave amplitude of Virginia Beach at time t=11min

(d) Wave amplitude of Virginia Beach at time t=19min

Figure 5.10: Time sequence of wave amplitude at Virginia Beach.

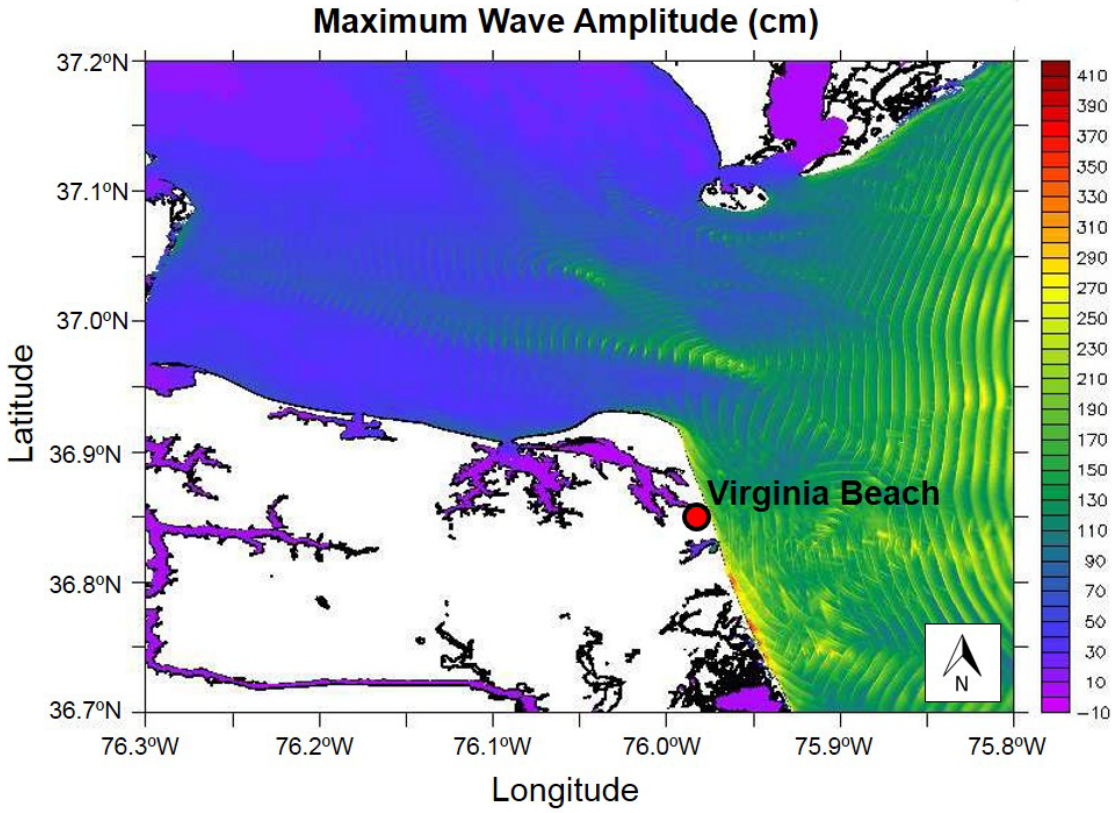

Figure 5.11: Maximum Wave amplitude of the Virginia Beach MOST run in the middle of the nested grids (C-grid), showing maximum in the run.

5.5 Bibliography

Geist, E., P. Lynett, and J. Chaytor (2009), Hydrodynamic modeling of tsunamis from the Currituck landslide, *Marine Geology*, *264*, 41–52.

Prior, D., E. Doyle, and T. Neurauter (1986), The Currituck slide, mid-Atlantic continental slope; revisited, *Marine Geology*, *73*, 25–45.

ten Brink, U.S., D. Twichell, E. Geist, J. chaytor, J. Locat, H. Lee, B. Buczkowski, R. Barkan, A. Solow, B. Andrews, T. Parsons, P. Lynett, J. Lin, and M. Sansoucy (2008), Evaluation of tsunami sources with the potential to impact the U.S. Atlantic and Gulf coasts – an updated report to the Nuclear Regulatory Commission, *Tech. rep.*, U. S. Geological Survey (ADAMS Accession No. ML082960196).

Titov, V., and F. González (1997), Implementation and testing of the Method of Splitting Tsunami (MOST) model. NOAA Technical Memorandum ERL PMEL-112, Tech. rep., NOAA Pacific Marine Environmental Laboratory, Seattle, WA.

Cornell, C.A. (1968). Engineering seismic risk analysis. *Bull. Seism. Soc. Am.,* **58**(5), 1583-1606.

6. GLOSSARY

Arrival time — The time when the first tsunami wave is observed at a particular location, typically given in local and/or universal time but also commonly noted in minutes or hours relative to time of earthquake.

Bathymetry — The measurement of water depth of an undisturbed body of water.

Current speed — The scalar rate of water motion measured as distance/time.

Current velocity — Movement of water expressed as a vector quantity. Velocity is the distance of movement per time coupled with direction of motion.

Deep-ocean Assessment and Reporting of Tsunamis — (DART®) Tsunami detection and transmission system that measures the pressure of an overlying column of water and detects the passage of a tsunami.

Digital Elevation Model (DEM) — A digital representation of bathymetry or topography based on regional survey data or satellite imagery. Data are arrays of regularly spaced elevations referenced to a map projection of the geographic coordinate system.

Epicenter — The point on the surface of the earth that is directly above the focus of an earthquake.

Far-field — Region outside of the source of a tsunami where no direct observations of the tsunami-generating event are evident, except for the tsunami waves themselves.

Flow depth – Depth, or height of the tsunami above the ground, at a specific location as indicated by flow markers such as piles of debris, impact scars on tree trunks, dead vegetation on trees or electric wires, or mud marks on building walls. The inundation height is the sum of the flow depth and local topographic height.

Focus — The point beneath the surface of the earth where a rupture or energy release occurs due to a build up of stress or the movement of earth's tectonic plates relative to one another.

Inundation — The horizontal inland extent of land that a tsunami penetrates, generally measured perpendicularly to a shoreline.

Marigram — Tide gauge recording of wave level as a function of time at a particular location. The instrument used for recording is termed marigraph.

Method of Splitting Tsunamis (MOST) — A suite of numerical simulation codes used to provide estimates of the three processes of tsunami evolution: tsunami generation, propagation, and inundation.

Moment magnitude (M_w) — The magnitude of an earthquake on a logarithmic scale in terms of the seismic moment, M_0, released ($M_w = \frac{2}{3}\log M_0 - 10.7$). Seismic moment, is defined as the product of the earth crust shear modulus, μ, fault rupture area, A, and average fault slip, d.

Near-field — Region of primary tsunami impact near the source of the tsunami. The near-field is defined as the region where non-tsunami effects of the tsunami-generating event have been observed, such as earth shaking from the earthquake, visible or measured ground deformation, or other direct (non-tsunami) evidences of the source of the tsunami wave.

Propagation database — A basin-wide database of pre-computed water elevations and flow velocities at uniformly spaced grid points throughout the world oceans. Values are computed from tsunamis generated by earthquakes with a fault rupture at any one of discrete 100×50 km^2 unit sources along worldwide subduction zones.

Runup or run-up — Vertical difference between the elevation of tsunami inundation and the sea level at the time of a tsunami. Runup is the elevation of the highest point of land inundated by a tsunami as measured relative to a stated datum, such as mean sea level.

Shoaling -- The effect by which surface waves entering shallower water increase in wave height to maintain a constant energy flux.

Short-term Inundation Forecasting for Tsunamis (SIFT) — A tsunami forecast system that integrates tsunami observations in the deep ocean with numerical models to provide an estimate of tsunami wave arrival and amplitude at specific coastal locations while a tsunami propagates across an ocean basin.

Subduction zone — A submarine region of the earth's crust at which two or more tectonic plates converge to cause one plate to sink under another, over-riding plate. Subduction zones are regions of high seismic activity.

Synthetic event — Hypothetical events based on computer simulations or theory of possible or even likely future scenarios.

Tidal wave — Term frequently used incorrectly as a synonym for tsunami. A tsunami is unrelated to the predictable periodic rise and fall of sea level due to the gravitational attractions of the moon and sun: the tide.

Tide — The predictable rise and fall of a body of water (ocean, sea, bay, etc.) due to the gravitational attractions of the moon and sun.

Tide gauge — An instrument for measuring the rise and fall of a column of water over time at a particular location.

Tele-tsunami or distant tsunami — Most commonly, a tsunami originating from a source greater than 1000 km away from a particular location. In some contexts, a tele-tsunami is one that propagates through deep ocean before reaching a particular location without regard to distance separation.

Travel time — The time it takes for a tsunami to travel from the generating source to a particular location.

Tsunameter — An oceanographic instrument used to detect and measure tsunamis in the deep ocean. Tsunami measurements are typically transmitted acoustically to a surface buoy that in turn relays them in real time to ground stations via satellite.

Tsunami — A Japanese term that literally translates to “harbor wave.” Tsunamis are a series of long-period shallow-water waves that are generated by the sudden displacement of water due to subsea disturbances such as earthquakes, submarine landslides, or volcanic eruptions. Less commonly, meteoric impact to the ocean or meteorological forcing can generate a tsunami.

Tsunami hazard assessment — A systematic investigation of seismically active regions of the world oceans to determine their potential tsunami impact at a particular location. Numerical models are typically used to characterize tsunami generation, propagation, and inundation and to quantify the risk posed to a particular community from tsunamis generated in each source region investigated.

Tsunami magnitude — A number that characterizes the strength of a tsunami based on the tsunami wave amplitudes. Several different tsunami magnitude determination methods have been proposed.

Tsunami propagation — The directional movement of a tsunami wave outward from the source of generation. The speed at which a tsunami propagates depends on the depth of the water column in which the wave is traveling. Tsunamis travel at a speed of 700 km/hr (450 mi/hr) over the average depth of 4,000 m in the open deep Pacific Ocean.

Tsunami source — Abrupt deformation of the ocean floor that generates series of long gravity waves propagating outward from the source area. The deformation is typically produced by underwater earthquakes, landslides, volcano eruptions, or other catastrophic geophysical processes.

Wall-clock time — The time that passes on a common clock or watch between the start and end of a model run, as distinguished from the time needed by a CPU or computer processor to complete the run, typically less than wall-clock time.

Wave amplitude — The maximum vertical rise or drop of a column of water as measured from a defined mean water level state.

Wave crest or peak — The highest part of a wave or maximum rise above a defined mean water level state, such as mean lower low water.

Wave height — The vertical difference between the highest part of a specific wave (crest) and its corresponding lowest point (trough).

Wavelength — The horizontal distance between two successive wave crests or troughs.

Wave period — The length of time between the passage of two successive wave crests or troughs as measured at a fixed location.

Wave trough — The lowest part of a wave or the maximum drop below a defined mean water level state, such as mean lower low water.

NRC FORM 335
(12-2010)
NRCMD 3.7

U.S. NUCLEAR REGULATORY COMMISSION

BIBLIOGRAPHIC DATA SHEET

(See instructions on the reverse)

1. REPORT NUMBER
(Assigned by NRC, Add Vol., Supp., Rev., and Addendum Numbers, if any.)
NUREG/CR-7222

2. TITLE AND SUBTITLE
Tsunami Hazard Assessment Based on Wave Generation, Propagation, and Inundation Modeling for the U.S. East Coast

3. DATE REPORT PUBLISHED

MONTH	YEAR
July	2016

4. FIN OR GRANT NUMBER

5. AUTHOR(S)
Vasily Titov, Christopher W. Moore, Mick Spillane, Yong Wei, Edison Gica, and Hongqiang Zhou

6. TYPE OF REPORT
Technical

7. PERIOD COVERED (Inclusive Dates)

8. PERFORMING ORGANIZATION - NAME AND ADDRESS (If NRC, provide Division, Office or Region, U. S. Nuclear Regulatory Commission, and mailing address; if contractor, provide name and mailing address.)
Pacific Marine Environmental Laboratory
Office of Oceanic and Atmospheric Research
National Oceanic and Atmospheric Administration
7600 Sand Point Way, N.E., Seattle, WA 98115

9. SPONSORING ORGANIZATION - NAME AND ADDRESS (If NRC, type "Same as above", if contractor, provide NRC Division, Office or Region, U. S. Nuclear Regulatory Commission, and mailing address.)
Structural, Geotechnical and Seismic Engineering Branch
Division of Engineering
Office of Nuclear Regulatory Research
U.S. Nuclear Regulatory Commission

10. SUPPLEMENTARY NOTES

11. ABSTRACT (200 words or less)
Subsequent to the 2004 and 2005 series of tsunamis in southeastern Asia, the U. S. Nuclear Regulatory Commission (NRC) conducted an in-depth review of past tsunami evaluations and guidelines for the Atlantic and Gulf coast nuclear power plants. NRC's previous tsunami design guidelines for these coastal facilities considered historical tsunami records but did not explicitly characterize design basis tsunamigenic sources including earthquakes, submarine landslides, and other potential sources for the Atlantic and Gulf coasts. This NUREG/CR describes a comprehensive study of tsunami hazard assessment for the Atlantic coast of the U.S. based on potential tsunami scenarios. The study makes use of the Pacific Marine Environmental Laboratory's (PMEL) pre-computed database of over a thousand synthetic tsunami sources to identify potentially hazardous tsunami events for the eastern U.S. coastline. This report should provide the NRC staff with the means and criteria to assess evaluations and analyses provided by the licensees on their tsunami design for nuclear facilities. This information will permit the NRC staff to: (1) confirm that adequate levels of safety are maintained; (2) improve the effectiveness and efficiency of the review processes; and (3) support the staff's technical decisions in a reasonably conservative and realistic manner and, thereby, increase public confidence in the staff's actions.

12. KEY WORDS/DESCRIPTORS (List words or phrases that will assist researchers in locating the report.)
Tsunami Hazard
Tsunami Source
Propagation
Inundation
Tsunami Scenarios

13. AVAILABILITY STATEMENT
unlimited

14. SECURITY CLASSIFICATION
(This Page)
unclassified
(This Report)
unclassified

15. NUMBER OF PAGES

16. PRICE

Federal Recycling Program

UNITED STATES
NUCLEAR REGULATORY COMMISSION
WASHINGTON, DC 20555-0001

OFFICIAL BUSINESS

NUREG/CR-7222

Tsunami Hazard Assessment Based on Wave Generation, Propagation, and Inundation Modeling for the U.S. East Coast

July 2016